Towards colloidal size control by precipitation

Jérôme George Joseph Louis Lebouille

Thesis committee

Promoters

Prof. Dr M.A. Cohen Stuart
Professor of Physical Chemistry and Colloid Science
Wageningen University

Prof. Dr F.A.M. Leermakers
Personal chair at the Laboratory for Physical Chemistry and Colloid Science
Wageningen University

Prof. Dr R. Tuinier
Professor by Special Appointment of Colloid-Polymer Mixtures at the Department of Chemistry
Utrecht University
Principal Scientist Colloids and Interfaces
DSM ChemTech R&D Geleen

Other members

Prof. Dr G. ten Brinke, University of Groningen
Dr G.M.H. Meesters, Delft University of Technology
Dr C.F. van Nostrum, Utrecht University
Prof. Dr J.T. Zuilhof, Wageningen University

This research was conducted under the auspices of the Graduate School VLAG (Advanced studies in Food Technology, Agrobiotechnology, Nutrition and Health Sciences).

Towards colloidal size control

by precipitation

Jérôme George Joseph Louis Lebouille

Thesis
submitted in fulfilment of the requirements for the degree of doctor
at Wageningen University
by the authority of the Rector Magnificus
Prof. Dr M.J. Kropff,
in the presence of the
Thesis Committee appointed by the Academic Board
to be defended in public
on Thursday 1 May 2014
at 11 a.m. in the Aula.

Jérôme G.J.L. Lebouille
Towards colloidal size control by precipitation,
160 pages.

PhD thesis, Wageningen University, Wageningen, NL (2014)
With references, with summaries in Dutch and English

ISBN: 978-94-6173-867-7

Voor Ilse, Lyzl en Lien

”In the warriors code, there’s no surrender, though his body says stop, his spirit cries, never, deep in our soul a quiet ember, know it’s you against you, it’s the paradox that drives us on, it’s a battle of wills, in the heat of attack it’s the passion that kills.”[1]

- Burning heart.

[1] Jim Peterik and Frankie Sullivan; Survivor (1985).

Table of Contents

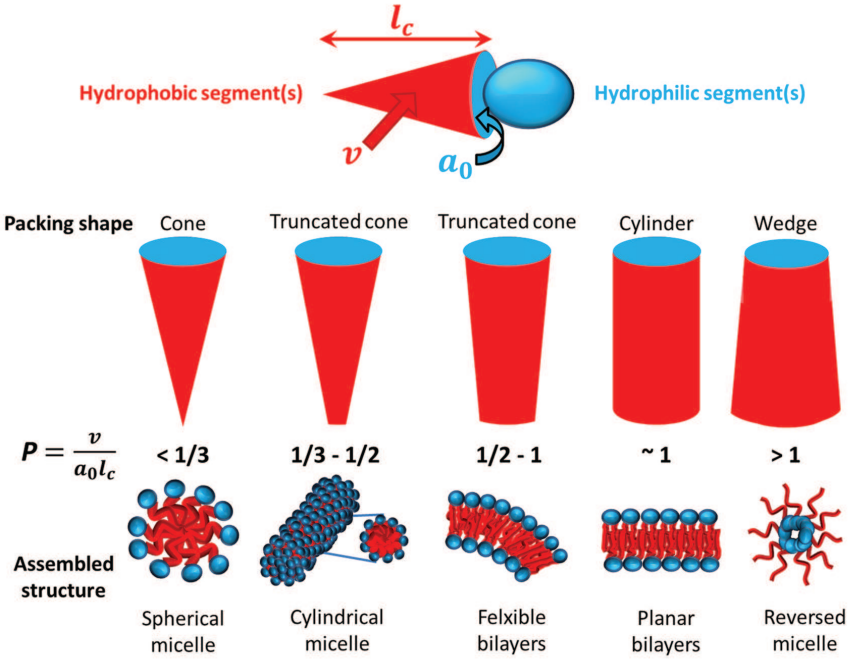
l_c
Hydrophobic segment(s)
Hydrophilic segment(s)
v
a_0
Packing shape
Cone
Truncated cone
Truncated cone
Cylinder
Wedge
$P = \frac{v}{a_0 l_c}$
< 1/3
1/3 - 1/2
1/2 - 1
~ 1
> 1
Assembled structure
Spherical micelle
Cylindrical micelle
Felxible bilayers
Planar bilayers
Reversed micelle

1 Introduction

1.1 Towards colloidal size control

Colloids are systems that contain particles in the size range between, say, a nanometer and a micrometer which are dispersed in another substance. Colloidal particles can have different geometries including rods, discs, spheres and cubes. In this thesis we focus on spherical colloidal particles. Colloids can be divided in two groups; lyophilic (made of soluble components) and lyophobic (made of insoluble components) ones.

Lyophilic colloids with water as the continuous medium are also referred to as hydrophilic (water loving) and lyophobic colloids as hydrophobic (water fearing). Hydrophilic colloids form spontaneously upon dispersing them into water and thus are reversible and dynamic. Well-known examples of hydrophilic colloids are particles composed of water soluble surfactants, such as micelles or vesicles. To predict their size and composition thermodynamic equilibrium theories can be employed.

In contrast, hydrophobic colloids are composed of non-water soluble components. These compounds aggregate or coalesce into colloidal structures. Hydrophobic colloids are only maintained in the colloidal size range if a stabilizer stops further aggregation or coalescence. These colloids are irreversible or metastable (implying that the current physical state is not the most stable state). Particles composed of hydrophobic components and stabilized by surfactants are here referred to as nanoparticles to make a clear distinction with reversible colloids, such as micelles. Often kinetic models are employed to predict the size and composition of hydrophobic colloids.

In this thesis also the term dead or frozen micelles is used. Dead micelles are a special case of hydrophobic colloids. Upon the formation their nature switches from lyophilic to lyophobic. Initially the molecules are dissolved, however, upon changing the nature of the solvent the molecules become gradually less soluble. During this solvent switch the molecules have short time frames to assemble into micellar structures. At some point the molecules become insoluble resulting in non-dynamic or static micelles; these are referred to as dead or frozen micelles. Since there is a (short) time that these micelles are dynamic, thermodynamic equilibrium theories might be employed to predict their size and composition.

Precipitation or spontaneous self-assembly is a powerful method to prepare colloids. The key example is the formation of surfactant micelles, that are assemblies the order of 10^2 am-

phiphiles that form spontaneously above a threshold concentration. The size control of these objects can directly be related to the structure of its constituents. Surfactants are molecules with two parts. One part is immiscible with water (hydrophobic) and forms the core and one block that is miscible with water (hydrophilic) and forms the corona of these micelles. These objects may have potential applications, for example as drug carriers, especially when the drug molecules are apolar and accumulate in the cores. However, the classical surfactants are extremely dynamic and typically too fragile for most drug delivery applications. This thesis deals with the use of copolymers, macromolecular analogues of surfactants, to make micellar-like nanoparticles with drug delivery as the key application. These colloids can be considered as being intermediate between lyophilic and lyophobic. The important selling point for using copolymer micelles is that these are much less dynamic in the sense that they do not immediately fall apart upon dilution. The same property presents a multitude of 'engineering' challenges: the properties of the particles (size, shape and composition) depend in a sensitive way on the preparation protocol. The focus was on the challenge to reproducibly make these particles. Directly coupled to this, it was investigated whether it is possible to predict the size characteristics, i.e., of the core and corona of these particles. The first question is essential and we show and discuss at length that the nanoprecipitation process can effectively be used for this. The second issue is important as well, because some understanding on how a particular outcome is expected may help to tune a particular system to the desired applications. More specifically the biological fate is mainly determined by their size and thus we need predictive tools for this quantity. We may view the nanoprecipitation as a guided self-assembly, in other words, the path for the formation of nanosized particles is strictly controlled. Knowledge of the formation process allowed us to predict the micellar characteristics using a polymer modeling toolbox.

The remainder of this introductory chapter is to sketch and introduce various essential concepts of my thesis. At the end of this chapter the reader may find in more detail the aim of this thesis and the outline of the work done.

1.2 Self-assembly

In order to make structures in the nano domain there are two routes which can be employed. The first is the top down approach, by dividing a certain macroscopic peice of material into smaller objects (after many division steps), eventually ending up in the nano domain. The presence of a stabilizer is needed to avoid that the smaller pieces will aggregate to bigger pieces again. Methods used are for instance milling, grinding, droplet breaking, etc. In general, these treatments give little control over the size and shape of the particles. The closer one approaches the nano domain the more difficult it becomes to further split small particles [1, 2]. The second approach is bottom up. Here one starts from a (dissolved) molecular state and by assembling molecules into supramolecular structures it is possible to prepare nanometer sized or mesoscopic structures, ordered structures of specific molecules. The mesoscopic structures are the result of so called co- or self-assembly, driven by non-covalent interactions. Nature creates such nanostructures spontaneously because the non-covalent interactions are attractive. Examples of non-covalent interactions are hydrogen bonding, ionic bonding, van der Waals forces, $\pi - \pi$-interactions and hydrophobic interactions. These interactions are the dominant driving forces in molecular systems; they make the 'bonds' in supramolecular

chemistry [3–7]. Although these bonds are individually weak, a large number of them will have a significant effect. The large variety of these interactions together with the enormous variation in molecular architectures leads to a rich spectrum of physical properties. An example is the organization of phospholipids in a biological membrane. A wide span of mesoscopic structures with different chemical compositions, shapes and functionalities can be formed via self-assembly processes. In nature the non-covalent interactions often lead to supermolecular complexes by self-assembly. DNA, RNA, cell membranes, proteins, crystals, monolayers, colloids in milk and partially digested fats are naturally occurring self-assembled complexes/structures held together by these interactions. Many medical treatments involving drugs rely on the non-covalent interactions of drugs and their targets, proteins, DNA, RNA and other chemical/ supermolecular entities.

Self-assembly can result in a large number of different structures. Here we will limit ourselves to the structures that can be formed by non-ionic, uncharged, amphiphilic molecules, with a head-tail architecture. These molecules are generically known as surfactants and we will discuss them and their uses below. We refer to the assembled structures as micelles. A remarkable property of micelles is that they are composed of an anisotropically ordered array of molecules that are densely packed such that the tails avoid the contact with water. Israelachvilli and coworkers realized that due to the close packing of the molecules it is the size and shape of the molecules that predominantly determine the form of the aggregates [8, 9]. From geometric considerations it seems reasonable that a limited number of structures such as spheres, rods and plates may be expected. The so-called surfactant packing parameter (P), see Fig. 1.1, is the leading quantity

$$P = \frac{v}{a_0 \times l_c} \tag{1.1}$$

to assess the capability of amphiphiles to form a certain nanostructure. Here v is the volume of the solvophobic block(s), l_c is the length of the tail(s) and a_0 is the surface area occupied by the solvophilic fragments at the critical micelle concentration (CMC). For $P < 1/3$ spherical micelles are preferred, whereas for $1/3 < P < 1/2$ cylindrical micelles form. In the range $1/2 < P < 1$ vesicles are the optimal structure, for $P \approx 1$ planar bilayers form and for $P > 1$ reversed spherical micelles are expected [8, 9]. The interesting point is that for short surfactants one can easily make educated guesses for l_c, v and a_0, so that an estimate for P is possible. Unfortunately for polymeric amphiphiles the corresponding guesses are less trivial.

1.3 Surfactants; stabilizers of colloidal particles

A surfactant is a surface active agent, i.e., a molecule that accumulates at interfaces. Surfactants can help to stabilize colloids consisting of apolar (e.g. oil based) components into a polar solvent (e.g. water based) as well as polar components into an apolar solvent. Without the aid of surfactants a colloidal system is not stable, in time the oil and water will separate into two phases. Surfactants typically combine two different polarities, polar referred to as head and apolar referred to as tail, in one molecule. The dual polarity in one molecule enables these compounds to accumulate interfaces between a polar and apolar phase (water and oil). As already discussed above, surfactants are also capable of forming different structures especially in the nano domain. Surfactants, mostly molecules with a low molar mass, are key elements in nature. In living cells phospholipids are the essential molecules in cell walls.

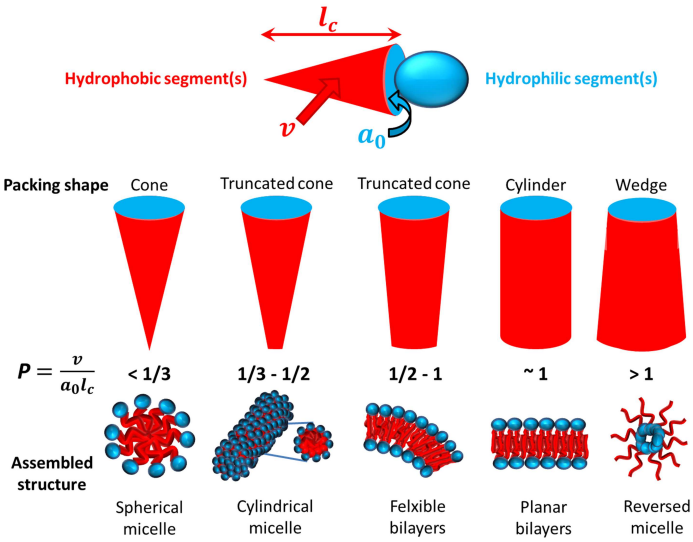

Figure 1.1: Schematic illustration of the relationship between a value for the surfactant packing parameter *P* and the preferred self-assembled structures, based on Ref. [9].

The cell wall phospholipids form a bilayer that separates the interior of a living cell from the environment. A specific phospholipid, dipalmitoylphosphatidylcholine (DPPC) [10, 11], is the most important surfactant which enables infants to take their first breath. Without the presence of DPPC the lungs of infants suffer from the infant (or neonatal) respiratory syndrome meaning that their lungs without external aid cannot supply the body with the needed oxygen. So one might argue that life as we know it would not exist without these surfactants.

In ancient days humans already noticed and exploited the special behavior of amphiphiles. The earliest recorded evidence of the manufacturing of surfactants was the use of soap (a salt of a fatty acid) for washing stones [12] found in ancient Babylon (2800 BC). On a Babylonian clay tablet (2200 BC) a formulation was written for preparing this soap, consisting of water, alkali and cassia oil. Later, the Egyptians refined the manufacturing and started using soap for bathing. Nowadays surfactants are abundantly used in many different applications and technologies. Companies such as Henkel and Procter and Gamble (mass-)produce surfactants as detergents and soaps [13–18]. The pharmaceutical industry uses surfactants for drug delivery purposes as solubilizing agents for non-water soluble drugs and as transfection agents for DNA-modification therapies [19, 20]. In multinational food and nutrition industries such as Unilever and Nestle, surfactants are being used as stabilizers for emulsions or dispersions in food applications [21–24]. Stabilizers for emulsions are called emulsifiers. The paint and coatings industry, e.g. Akzo Nobel and Rohm & Haas, utilize surfactants to stabilize and compatibilize their paint products [25–28]. Electronic companies such as ASML and Intel use surfactants as wetting agents in their chip manufacturing processes [29–32]. The metal mining industry employs surfactants as flotation agents to recover metals more easily from the ores [33]. In chemical industry (Dow and 3M) especially in polymer industry surfactants are used as stabilizers in emulsion polymerization [34–37]. The oil industry uses surfactants to recover more oil from oil wells; enhanced or tertiary oil recovery [38]. Personal care

applications, like make-up and many lotions are benefitting from the specific properties of surfactants [39–42]. Human health has been tremendously improved and extended by using soaps and detergents in personal and medical care and in food products by avoiding microbiologic contaminations. Many of these products are emulsions.

Many surfactants have to be optimized for their applications. Often, the functionality for a certain application evolved via a trial and error approach over many years. This approach does not demand an insight in the function of the surfactant. However, in order to develop predefined applications one needs to have an understanding of the structure-function relationship. Meeting higher technology requirements and expectations demands improved understanding so that newly developed compounds may outperform the standards of today. Several approaches may help to satisfy this growing demand for better surfactants. First, there is organic synthesis, aiming at making new compounds that perform better than existing ones. Secondly, there is the more natural approach of finding organisms that enable the large scale production of amphiphilic structures derived from naturally occurring organisms (plants and micro-organisms; bacteria, yeasts and molds). Thirdly, there is the approach that more or less combines the previous two. By using naturally occurring organisms and applying different ways of altering/mutating the genetic code aims to achieve optimum performance of the slightly altered compounds produced by these organisms. Finally, there is the possibility to optimize the physical properties. This approach focuses on a thorough understanding between the application/performance and the structure of the used compounds. The most powerful approach is utilizing models which enable to achieve a deeper understanding of the relation between the composition of the structures and their performance based on physical-chemical theories. Such knowledge could lead to insight into desired chemical structures based on optimized physical functionality.

Many new applications demand a profound knowledge and understanding about the way compounds act in different environments. For instance in drug delivery, especially in oncology treatments, control over chemistry, size and loading of carrier particles is of utmost importance. The chemical compounds employed need to be biocompatible. Mandatory requirements for drug delivery systems are that they i) should be tolerated by the human body, ii) being resorbable and/or excretable by the biologic pathways. These conditions should be met in order to avoid any undesired reactions of the human body. Certain drugs are more potent than others. when using less potent drugs drug delivery vehicles need to be more loaded to achieve the desired efficacy, than in case of more potent drugs. However, the desired size of the delivery vehicles remains the same. Many newly developed drugs are extremely potent, but are typically hydrophobic. The main disadvantage of these new drugs is their very low water-solubility which makes it difficult to administer them.

We focus on spherical nanoparticles, they exhibit excellent characteristics for usage in drug delivery [43]. Their size is characterized by a single length scale, their diameter (or radius). By tuning the micellar diameter carefully there is some ability to direct these micelles to certain places in the body, predetermining their biological fate. They can be made so small that they are capable of passing the blood-brain barrier [19, 44] or accumulating in tumor cells [45–49]. The outer part of a spherical micelle, termed corona, can be stealthy (is not recognized) for the immune system of most humans (but not all!) if made of polyethylene oxide (PEO) [50]. Again, the hydrophobic core enables the storage of hydrophobic drugs. These requirements imply that control over size and loading is demanded and therefore knowledge and understanding of the physical-chemical properties is essential.

1.4 Critical micelle concentration (CMC)

Micelles typically reach a well-defined size and the concentration of free amphiphiles remains constant at a value reached at the first appearance of well-defined, finite sized micelles (the critical micellisation concentration CMC). Micellar structures composed of surfactants are in equilibrium with free surfactant molecules (often denoted as monomers or unimers) in solution. Upon increasing the surfactant concentration relatively more surfactants enter the micelles. Above the CMC effectively all additional amphiphiles micelles [51–53].

The CMC value is of importance, because it indicates the concentration of free amphiphiles: the higher the CMC, the more amphiphiles are free in solution. At and above the CMC freely dissolved amphiphiles exchange with amphiphiles incorporated into the micelle. Thus a higher CMC will also lead to an increased rate of exchange of amphiphiles incorporated in a micelle with freely dissolved amphiphiles. The exchange of these amphiphiles has an impact on the cargo load, encapsulated hydrophobic compounds, incorporated in the micelles. When there is a high degree of exchange between amphiphiles incorporated in micelles and freely dissolved in the bulk the loaded cargo of a micelle is easier released from the micelles. The disadvantage of a high CMC is that, upon dilution, existing micelles fall apart in order to keep the freely dissolved amphiphile concentration constant, resulting in an instant release of their cargo. A low CMC implies less dynamic micelles. For drug-carriers, preferably non-dynamic micelles, often called dead or frozen micelles [54], are most desired because of a virtually non-detectable/existing CMC. These dead or frozen micelles show superior stability in time and delayed cargo release profiles due to the lack of exchange between amphiphiles incorporated in a micelle and freely dissolved in the bulk.

For extremely stable micelle formulations that do not alter upon dilution the CMC should be virtually zero. This implies that there is no exchange between surfactants incorporated in the micelle and dissolved surfactants, due to the lack of the latter. Stability of such formulations is superior upon dilution, which is one of the key requirements for drug delivery applications. In these kinds of applications only a small amount/volume of therapeutic active ingredient/drug encapsulated in micelles, the medicine, is injected in the human body. Upon injection of these small volumes in the human body a huge dilution occurs. If injected into the blood stream the volume is added to approximately 4 to 6 liters of blood. If the total water content of the human body is taken into account the dilution factor is even higher because 70 percent of the total weight of a human is water. Using non water-soluble surfactants to form micelles in aqueous systems enhances the stability of these structures upon dilution. This increased stability will also have a beneficial effect on the drug release profile. It will no longer be dependent on the micellar instability generated by dilution.

1.5 Block copolymers

Polymers are chain-like molecules composed of covalently bound repeating units (monomers). These chain-like molecules/polymers can for instance be linear, branched or ring-like. Polymers can be classified in different types. Homopolymers are made up of one single kind of monomers. Copolymers are composed of repeating units of two (or more) different chemical compositions. Random copolymers exhibit a random distribution of two (or more) repeating units along their chain. Block copolymers are composed of organized

'blocks' of polymers or copolymers along the chain. Block copolymer for which water is a selective solvent, good for one block and bad for the other, may be seen as macro-amphiphiles or macro-surfactants.

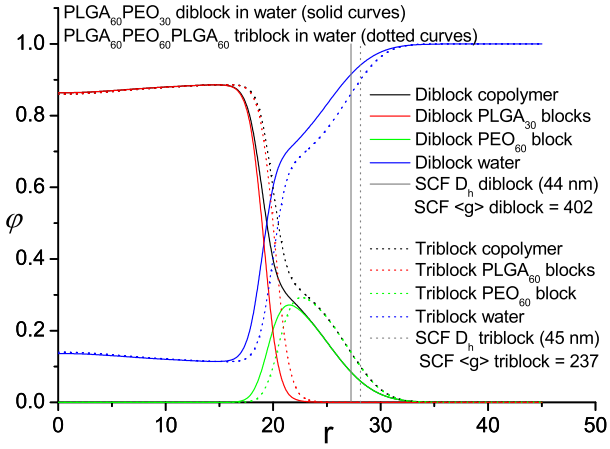

Figure 1.2: Equilibrium radial density profiles of water, total copolymer, PLGA block(s) and PEO block for diblock and triblock copolymer micelles. φ is the volume fraction of the different components and r is the distance to the center of a micelle. The diblock copolymer micelle, $PLGA_{60}PEO_{30}$; 7.5-3.0 kDa molar mass, has an aggregation number of 402 and a SF-SCF D_h of 44 nm. The triblock copolymer micelle, $PLGA_{60}PEO_{60}PLGA_{60}$; 7.5-6.0-7.5 kDa molar mass, has an aggregation number of 237 and a SF-SCF D_h of 45 nm. The diblock copolymer is exactly half of the triblock copolymer. Note the difference in PEO corona density profile. The PEO corona of the triblock is denser compared to the PEO corona of the diblock. (SF-SCF = Scheutjens-Fleer self-consistent field).

In the largest part of this thesis the focus is on triblock copolymers [61–63]. Triblock copolymers consist of three blocks, having two distinct different chemical compositions. Again, in order to prepare micelles of triblock copolymers at least one of these blocks should be hydrophilic and the other(s) should be hydrophobic. In this thesis triblock copolymers are considered that are made of as the hydrophilic block, polyethylene oxide (PEO) and the hydrophobic block consists of either poly(lactic-co-glycolic)acid (PLGA) or poly(ε-caprolactone) (PCL). The hydrophilic block, PEO, is the middle block and the other blocks, both equal in size, are either PLGA or PCL. The block lengths were chosen such that the triblock copolymer is non-water soluble. The triblock copolymer composition was chosen such that they self-assemble in spherical, flower-like, micelles [64]. We chose triblock copolymers instead of diblock copolymers because the PEO corona is more dense for triblock copolymers, see Fig. 1.2. This is beneficial for pharmaceutical applications. Drug release will be slowed down which decreases the required frequency of repeating the medical treatment. The polymeric PEO blocks are biocompatible, non-degradable and excretable via biologic pathway. The PLGA and PCL blocks are hydrolytically degradable polymers [65]. Their degradation products are molecules which occur naturally in the human body so their biocompatibility is assured.

The choice of these triblock copolymers is also practical from a synthetic point of view. Using the hydrophilic middle block as a starting precursor in a ring opening polymerization

of lactic-co-glycolic acid or ε-caprolactone it is possible to achieve molar mass control over the outer hydrophobic blocks of the triblock copolymer resulting in a narrow molar mass distribution of the synthesized triblock copolymers. Ring opening polymerization [66–68] is also a fairly easy, controllable and standard polymerization method.

Whether (block(co))polymers dissolve or not depends on the solvent quality. In a poor solvent the overall interactions between the segments and solvent molecules are unfavorable. This leads to an effective attraction between the polymer segments and phase separation between polymer molecules and solvent. In a good solvent there are favorable polymer segment-solvent interaction. This leads to an effective repulsion between the polymer segments. In a theta solvent the excluded volume interactions between the segments and the solvent induced attraction cancel and the polymer chains behave ideally. Lowering the solvent quality from theta to poor solvency leads to polymer chain collapse and phase separation for sufficiently long chains. Increasing the solvency from theta to good leads to swelling of the polymer chains.

Upon switching from a good to a poor solvent quality a polymer chain goes from the swollen state to the collapsed state. During this collapse the polymer chains will start coalescing resulting in the formation of a concentrated phase. If a surfactant is present during this collapse and subsequent coalescence the precipitation can be stopped at a certain point enabling the formation of finite sized colloidal polymeric (nano)particles. These surfactants act as a stabilizer to keep the finite sized particles separated. Whether or not they will settle under gravity is dependent on their size and density. If small enough and with a density close to that of water density the suspension remains homogeneous due to Brownian motion.

1.6 Nanoprecipitation

In order to prepare polymeric nanoparticles both water soluble and non-water-soluble amphiphiles can be employed. The easiest way to prepare nanoparticles is by dissolving a water soluble amphiphile in water at a concentration that significantly exceeds the CMC, whereupon the surfactants spontaneously self-assemble into micelles. To this surfactant solution a small volume of hydrophobic polymer dissolved in a water miscible good but non-aqueous solvent is added, see Fig. 1.3. As the polymers enter the aqueous solution the solvent quality for these hydrophobic polymers instantaneously turns from good to poor. As a consequence the polymers collapse and form very small particles which then coalesce. Meanwhile the water-soluble amphiphile adsorbs on the surface of the growing particles. This goes on until the surfactant covers the whole surface of these spherical particles. This stops the coalescing of these spherical particles resulting in a stable nanoparticle suspension.

In case of using non-water soluble amphiphiles a different approach is needed because initially dissolving in water is not possible. In order to prepare particles for these systems the solvent shift or precipitation method [69] was employed in a different fashion [70–72]. Now the amphiphilic copolymers are dissolved in a good solvent (e.g. acetone) and subsequently this solution is added to an excess of aqueous solution, see Fig. 1.4. The shift from good to poor solvent will force the copolymers to attempt to form spherical particles. Given the copolymer composition this can be successful (stable dead or frozen spherical micelles) or not (instability or other self-assembled structures). In case of non-water soluble amphiphilic triblock copolymers with appropriate length and solvencies of the different blocks this can be

successful. Then the hydrophobic outer ends of the triblock come into a hostile environment, water, they will join in the core that is protected by the corona of hydrophilic blocks that are solvated in the water environment.

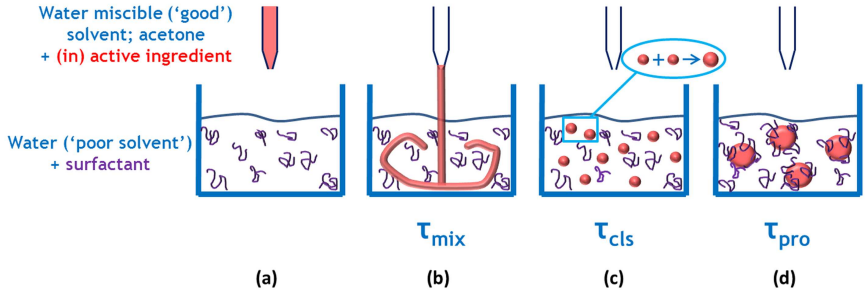

Figure 1.3: Different stages of a nanoprecipitation experiment for water soluble amphiphiles: (a) typically a polymer solution in good solvent is added to a water based solution of water soluble amphiphiles; (b) the macroscopic mixing step; (c) the initial state of the system considered: polymer spheres are homogeneously distributed within the experimental volume; (d) end of the experiment: polymer spheres have coalesced until a protective layer of surfactant protects the individual spheres against coalescence.

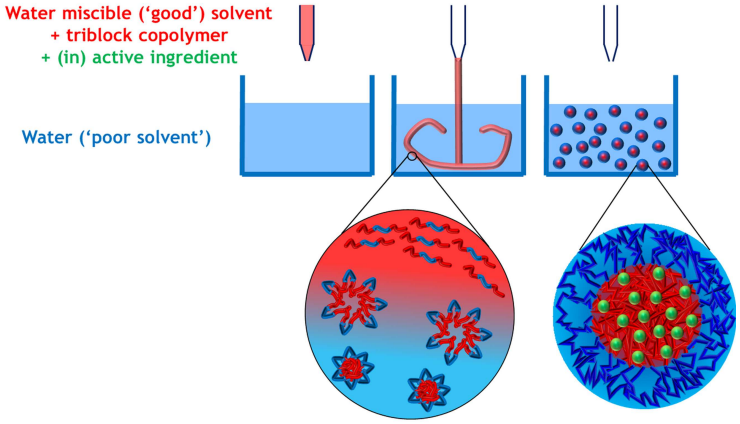

Figure 1.4: Cartoon of the nanoprecipitation process for non-water soluble triblock copolymer micelles. Typically a triblock copolymer solution in good solvent is added to water. Upon this mixing the triblock copolymer shifts from a good solvent to a poor solvent evoking the formation of micelles.

A hydrophobic polymer, a hydrophobic active ingredient or both can be initially co-dissolved with the triblock copolymers in the solvent which upon transfer to the aqueous solution will load the core of the micelle with hydrophobic polymer and/or hydrophobic active ingredient. This precipitation method is a fast and easy way to prepare spherical micelles using the triblock copolymers.

1.7 Aim of this thesis

Only a few polymer nanoparticle preparation methods that allow encapsulation of hydrophobic ingredients permit a high level of control of the particle size and particle size distribution [73]. Nanoprecipitation permits manufacturing nanoparticles in a very simple and reproducible way [69]. Despite the simplicity of this experimental method, a comprehensive theoretical understanding of nanoparticle formation using copolymers is still lacking. A rather limited understanding is yet developed on how the particle size depends on the materials and process parameters, in particular on concentrations of surfactant and precipitated compounds, and on copolymer chemistry and composition.

Therefore in many experimental situations investigators still resort to simple empirical correlations [74] or statistical methods such as design of experiments (DOE) [75]. More advanced theoretical methods, such as Brownian dynamics simulations [76] or population balance coupled to computational fluid dynamics simulation [77], do provide very valuable insights into the kinetics of mixing and rapid assembly upon quenching for non-equilibrium systems. However, these methods do not permit formulation of simple yet physically meaningful relationships between the experimentally relevant parameters and the nanoparticle size. Relationships between particle size (and loading) and types of compounds and the concentrations used would be extremely useful in designing nanoparticles with *a priori* determined size as it would allow one to avoid very laborious trial and error investigations and instead enable a rational design. Also for particles in thermodynamic equilibrium, or close to it, there is not a workable, quick method that enables a rational design.

The aim of this thesis is to study the possibility of a rational design by modeling of nanoparticles. Nanoprecipitation will be the chosen processing method for making these nanoparticles, since it is a fast and easy way to make these systems. The study focuses on the ability to tune the size and loading capacity of these systems and an assessment of their stability in time. We study the rational design, by size and loading, of nanoparticles made both in water-soluble, and non-water-soluble surfactants. Especially for pharmaceutical, drug delivery, applications a high control over size is of utmost importance [43, 78]. The size of the nanoparticles mainly determines the biological fate of these particles. For instance for oncology applications the size (and its distribution) is important for passive targeting of tumors. The enhanced permeation and retention (EPR) effect [45, 46], an accumulation of nanoparticles of specific size in tumor tissue, is an example of passive targeting. To further increase the efficiency of these drug delivery systems the method of active targeting is employed. Active targeting is achieved by particles which recognize (= bind preferably to) the recognized sites also referred to as receptors which should be preferably specific for the diseased tissue. Often diseased cells express receptors on their cell membrane surface which can be targeted by specific moieties. These targeting moieties are often peptide sequences, which will have a selective affinity for their receptors. Since many peptide sequences can invoke an immune response of the human body we theoretically study whether these targeting moieties can be incorporated within the micellar corona, and so remain invisible for the immune system but in such a way that they still can bind. We want to theoretically study if these targeting moieties will interact/bond with their specific receptors.

1.8 Outline of this thesis

This thesis consists of four chapters that report research investigations followed by a general discussion and an overall summary. First we focus on experimental and theoretical work that aims at rationalization of nanoparticle size for water soluble surfactants in **Chapter2**. In **Chapter 3** we will use Scheutjens-Fleer Self-Consistent Field (SF-SCF) theory to enable *a priori* size and loading predictions for non-water soluble triblock copolymer surfactants. Thereafter we investigate the relationship between experimental results and theoretical predictions in **Chapter 4**. Also in **Chapter 4** we give an insight in how to tune size and loading independently and we assess the stability of these systems in time. Finally, in **Chapter 5** we theoretically study the possibility of active and passive targeting simultaneously. The active targeting moieties will be put in the micellar corona, which possibly disables immune response of the human body, however, at the same time still enable active targeting of specific, diseased tissue. In the General discussion, **Chapter 6**, we will reflect on the overall results and their implications. The results will be put into perspective of drug delivery applications, focusing on oncology applications. We will discuss research needed in order to assess the true potential of *a priori* size prediction and loading tunable nanoparticle systems for active and passive targeting with respect to oncology applications.

The chapters in this thesis are written such that they can be read independently; each chapter has its own abstract, introduction, materials and methods, results and conclusion. At the end of this thesis a general summary is given for all chapters.

Bibliography

[1] S.L.A. Hennart, W.J. Wildeboer, P. van Hee, G.M.H. Meesters, Powder Technol., **199**, 226-231 (2010).
[2] S.L.A. Hennart, P. van Hee, W.J. Wildeboer, G.M.H. Meesters, Part. Part. Syst. Charact., **29**, 285-303 (2012).
[3] J.-M. Lehn, Science, **51227**, 849-856 (1985).
[4] J.-M. Lehn, *Supramolecular chemistry-concepts and perspectives* (VCH, Weinheim, 1995).
[5] J.-M. Lehn, Prog. Polym. Sci., **30**, 814-831 (2005).
[6] J.-M. Lehn, Science, **295**, 240-2403 (2002).
[7] J.-M. Lehn, Polym. Int., **51**, 825-839 (2002).
[8] J.N. Israelachvilli, D.J. Mitchell, B.W. Ninham, J. Chem. Soc., Faraday Trans. 2, **72**, 1525-1568 (1976).
[9] J.N. Israelachvilli, *Intermolecular and surface forces* (Academic press: London, First edition, 1985).
[10] A.H. Jobe, New England J. Med., **328**, 861-868 (1993).
[11] R.Veldhuizen, K. Nag, S. Orgeig and F. Possmayer, Biochim. Biophy. Acta, **1408**, 90-108 (1998).
[12] H. Butler, *Poucher's Perfumes, Cosmetics and Soaps*, **10**, Springer-Verlag (2000).
[13] R.U. Peter and U. Richarz-Barthauer, Brit. J. Dermatol., **132**, 441-445 (1995).
[14] R.G. Laughlin, Colloid. Surface. A, **128**, 27-38 (1998).
[15] S. Bandyopadhyay, J.C. Shelley, M. Tarek, P.B. Moore and M.L. Klein, J. Phys. Chem. B, **102**, 6318-6322 (1998).
[16] P.M. Holland and D.N. Rubingh, J. Phys. Chem., **87**, 1984-1990 (1983).
[17] W. von Rybinski and K. Hill, Angew. Chem. Int. Edit., **37**, 1328-1345 (1998).
[18] M.J. Schwuger, J. Colloid Interf. Sci., **42**, 491-498 (1973).
[19] J. Panyam and V. Labhasetwar, Adv. Drug Deliver. Rev., **55**, 329-347 (2003).
[20] O. Boussif, F. Lezoualc'h, M.A. Zanta, M.D. Mergny, D. Sherman, B. Demeneix and J-P. Behr, PNAS, **92**, 7297-7301 (1995).
[21] A.H. Clark, G.M. Kavanagh and S.B. Ross-Murphy, Food Hydrocolloids, **15**, 383-400 (2001).
[22] S. Tcholakova, N.D. Denkov and A. Lips, Phys. Chem. Chem. Phys., **10**, 1608-1627 (2008).
[23] A. Syrbe, W.J. Bauer and H. Klostermeyer, Int. Dairy J., **8**, 179-193 (1998).
[24] P. Duboc and B. Mollet, Int. Dairy J., **11**, 759-768 (2001).
[25] S. Creutz, R. Jrme, G.M.P. Kaptijn, A.W. Van Der Werf and J.M. Akkerman, J. Of Coating. Technol., **70**, 41-46 (1998).
[26] I. Johansson and M. Svensson, Curr. Opin. Colloid Interface Sci., **6**, 178-188 (2001).
[27] Q.T. Pham, W.B. Russel, J.C. Thibeault and W. Lau, Macromolecules, **3**, 5139-5146 (1999).
[28] G. Swift, Polym. Degrad. Stabil., **45**, 215-231 (1994).
[29] P. Zhang, M. Jaramillo, D. King, B. Ross, D. Witko, T. Paxton and T. Davis, Proceedings Of SPIE, **5039**, 1409-1415 (2003).
[30] P. Zhang, M. Jaramillo, D. King, T. Markley, Z. Zarkov, D. Witko, T. Paxton and T. Davis, Proceedings Of SPIE, **5039**, 1402-1408 (2003).

[31] J. Wang, Microelectron. Reliab., **42**, 293-299 (2002).
[32] S.J. Gokhale, J.L. Plawsky and P.C. Wayner Jr., Langmuir, **21**, 8188-8197 (2005).
[33] S. Manne and H.E. Gaubt, Science, **270**, 1480-1482 (1995).
[34] C.J. McDonald and M.J. Devon, Adv. Colloid Interface Sci., **99**, 181-213 (2002).
[35] C.J. McDonald, J. Kevin, A. Bouck, Bruce Chaput and Carl J. Stevens, Macromolecules, **33**, 1593-1605 (2000).
[36] J.R. Duke Jr., M.A. Hoisington, D.A. Langlois and B.C. Benicewicz, Polymer, **39**, 4369-4378 (1998).
[37] S. Dai, P. Ravi and K.C. Tam, Soft Matter, **4**, 435449 (2008). S. Dai, P. Ravi and K.C. Tam
[38] I.M. Banat, Bioresource Technol., **51**, 1-12 (1995).
[39] S. Gonzlez, M. Fernndez-Lorente and Y. Gilaberte-Calzada, Clin. Dermatol., **26**, 614-626 (2008).
[40] G.M. Eccleston, Colloids Surf. A, **123-124**, 169-182 (1997).
[41] C. Wibowo and K.M. Ng, AIChE Journal, **47**, 2746-2767 (2001).
[42] A.V. Rawlings, Int. J. of Cosmetic Sci., **25**, 63-95 (2003).
[43] N. Kamaly, Z. Xiao, P.M. Valencia, A.F. Radovc-Moreno and O.C. Farokhzad, Chem Soc Rev., **41**, 2971-3010 (2012).
[44] J. Kreuter, Adv. Drug Deliver. Rev., **47**, 65-81 (2001).
[45] Y. Matsumura, H. Maeda, Cancer Res., **6**, 6387-6392 (1986).
[46] H. Maeda, J. Wu, T. Sawa, Y. Matsumura and K. Hori, J. Control. Release, **65**, 271-284 (2000)
[47] H. Maeda and Y. Matsumura, Crit. Rev. Ther. Drug, **6**, 193-210 (1989).
[48] H. Maeda and J. Fang, Adv. Polym. Sci., **193**, 103-121 (2006).
[49] H. Maeda and J. Daruwalla, Eur. J. Pharm. Biopharm, **71**, 409-419 (2009).
[50] D.E. Owens and N.A. Peppas, Inter. J. Pharm., **307**, 93-102 (2006).
[51] L. Liebler, H. Orland and J.C. Wheeler, J. Chem. Phys., **79**, 3550-3557 (1983).
[52] P.D.T. Huibers, V.S. Labanov, A.R. Katritzki, D.O. Shah and M. Karelson, Langmuir, **12**, 1462-1470 (1996).
[53] A. Dominguez, A Fernandez, N. Gonzales, E. Iglesias and L. Montenegro, J. Chem. Educ., **74**, 1227-1231 (1997).
[54] T. Nicolai, O. Colombani and C. Chassenieux, Soft Matter, **6**, 3111-3118 (2010).
[55] Z. Tuzar and P. Kratochvil, Adv. Colloid Interface Sci., **6**, 201-232 (1976).
[56] D.J. Kinning, E.L. Thomas and L.J. Fetters, Macromolecules, **24**, 3893-3900. (1991)
[57] M. Malmsten and B. Lindman, Macromolecules, **25**, 5440-5445 (1993).
[58] S. Förster, M.Zisenis, E. Wenz and M. Antonietti, J. Chem. Phys., **104**, 9956-9970 (1996).
[59] K.J. Hanley and T.P. Lodge, Macromolecules, **33**, 5918-5931 (2000).
[60] G. Riess, Prog. Polym. Sci., **28**, 1107-1170 (2003).
[61] R. Xu, M.A. Winnik, F.R. Hallet, G. Riess and M.D. Croucher, Macromolecules, **24**, 87-93 (1991).
[62] P. Alexandridis, J.F. Holzwarth and T.A. Hatton, Macromolecules, **27**, 2414-2425 (1993).
[63] B. Chu, Langmuir, **11**, 414-421 (1995).
[64] N.P. Balsara, M. Tirrell and T.P. Lodge, Macromolecules, **24**, 1975-1986 (1990).
[65] R. Peters, J.G.J.L. Lebouille, B. Plum, P. Schoenmakers and S. van der Wal, Pol. De-

grad. Stabil., **96**, 1589-1601 (2011).
[66] R. Ravichandran, Int. J. green nanotech., **1:2**, 72-96 (2010).
[67] C.C. Chen and G. Wagner, Trans. IChemE A, **82**, 1432-1437 (2004).
[68] N.S. Sozer and L. Kokini, Trends in Biotechnology, **27**, 82-89 (2009).
[69] T. Niwa, H. Takeuchi, T. Hino, N. Kunou, Y. Kawashima, J. Control. Release, **25**, 89-98 (1993).
[70] J.G.J.L. Lebouille, R. Tuinier, L.F.W. Vleugels, M.A. Cohen Stuart and F.A.M. Leermakers, Soft Matter, **9**, 7515-7525 (2013).
[71] J.G.J.L. Lebouille, L.F.W. Vleugels, A. Dias, F.A.M. Leermakers, M.A. Cohen Stuart and R. Tuinier, Eur. Phys. J. E, **36**, 107 (2013).
[72] J.G.J.L Lebouille, T. Kockelkoren, L.F.W. Vleugels, R. Tuinier, **US 0223206 A1** (2011).
[73] S. Galindo-Rodriguez, E. Alleèmann, H. Fessi and E. Doelker, Pharm. Res., **21**, 1428-1439 (2004).
[74] S. Stainmesse, A.-M. Orecchioni, E. Nakache, F. Puisieux and H. Fessie, Colloid Polym. Sci., **273**, 505-511 (1995).
[75] J. Molpeceres, M. Guzman, M.R. Aberturas, M, Chacon and Y. Kawashima, J. Control. Release, **85**, 206-213 (1996).
[76] T. Chen, A.-P. Hynninen, R.K. Prud'homme, I.G. Kevrekidis, and A.Z. Panagiotopoulos, J. Phys. Chem. B, **112**, 16357-16366 (2008).
[77] J.C. Cheng and R.O. Fox, Ind. Eng. Chem. Res., **49**, 10651-10662 (2010).
[78] K. Kataoka, G.S. Kwon, M. Yokoyama, T. Okano and Y. Sakurai, J. Control. Release, **24**, 119-132 (1993).

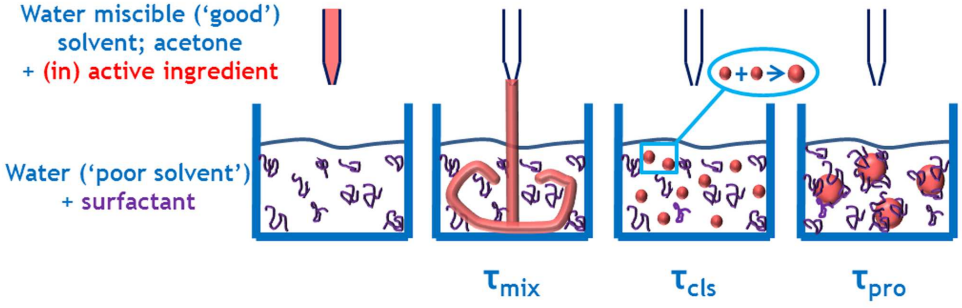
Water miscible ('good')
solvent; acetone
+ (in) active ingredient
Water ('poor solvent')
+ surfactant
τmix
τcls
τpro

Nanoprecipitation of polymers in a poor solvent

2

This chapter was published as:
J.G.J.L. Lebouille, R. Stepanyan, J.J.M. Slot, M.A. Cohen Stuart and R. Tuinier , Nanoprecipitation of polymers in a bad solvent, Colloids and Surf. A, Accepted (2013).
A short version was published as: R. Stepanyan, J.G.J.L. Lebouille, J.J.M. Slot, R. Tuinier and M.A. Cohen Stuart, Controlled nanoparticle formation by diffusion limited coalescence, Phys. Rev. Lett., **109**, 138301 (2012).

Abstract

Nanoparticles (NPs) composed of polymers are of great interest since they can add a functionality in many applications, ranging from food and pharma to plastics and electronics. A key factor that determines the functionality of NPs is their size. Nanoprecipitation [T. Niwa *et al.*, J. Control. Release, **1993**, *25*, 89-98] is a commonly used technique to prepare NPs. We have performed a combined experimental and theoretical study on the size of NPs formed by precipitation of polymers into a poor solvent in the presence of a stabilizing surfactant. Upon quenching a hydrophobic polymer solution in an aqueous solution of surfactant, coalescence of polymeric particles sets in. It competes with adsorption of surfactant onto the surface of the polymeric particles, which leads to a protective corona layer that finally stops the coalescence and brings the system in a kinetically frozen state.

We propose an extension of the theoretical framework put forward by Lannibois *et al.* [J. Phys. II France, **7**, 318-342 (1997)] for nanoparticle formation via nanoprecipitation. This theory is based upon a kinetic model for diffusion limited coalescence (DLC) in which the relevant transport and diffusion mechanisms are quantified. We find that the macroscopic mixing time and the diffusivity of the polymer and surfactant are the main parameters determining the final particle size. The DLC model shows that, at given polymer concentration and mixing time, the smallest particles can be obtained in the excess of surfactant. This situation corresponds well to the experimentally used conditions. The mixing efficiency is predicted to have a profound influence on the final particle diameter: faster mixing results in smaller particles. The final particle size in the slow mixing regime, which is the typical situation in experiments, turns out to be independent of the molar mass of the polymer and scales as a power $1/3$ with the initial polymer concentration. An increase of the surfactant molar mass is predicted to lead to larger particles, because of longer mixing time and lower surfactant mobility.

We have performed systematic experimental investigations on nanoparticles formation using various systems but focused on polycaprolactone (PCL) polymers in acetone precipitated in aqueous solutions containing polyvinyl alcohol as surfactant. The PCL molar mass and concentration and mixing time were varied. We show that both our experimental results as well as literature data are in good agreement with our theoretical DLC predictions. This work therefore provides a solid framework for tailoring nanoparticles with a desired size.

keywords: Nanoparticles, (nano)precipitation, particle size, encapsulation, surfactant, polymer, block copolymers, diffusion limited coalescence.

2.1 Introduction

Nanoprecipitation [1, 2] is a promising technique for encapsulation hydrophobic species in nanoparticles (NP) dispersed in aqueous systems [3, 4]. Although the method itself is quite versatile and can be used for a broad range of hydrophobic polymers [5], until now it has mainly been applied for the preparation of poly-(lactic-co-glycolic) acid (PLGA) and polycaprolactone (PCL) particles for drug delivery. The main promise of the technique has been a possibility to encapsulate a hydrophobic drug in a submicron particle and thereby effectively increase its water solubility. For a short overview of applications in physics, medicine and chemistry, see [6–9].

A typical set up of a nanoprecipitation experiment is depicted in Fig. 2.1. Hydrophobic species (a polymer such as PLGA in this example and/or drug) are dissolved in acetone. Note that PLGA can be replaced with polymers such as PCL. At room temperature, the acetone solution is injected into an aqueous solution of (polymeric) surfactant such as polyvinyl alcohol (PVA). After some short period of time a suspension of submicron particles is obtained.

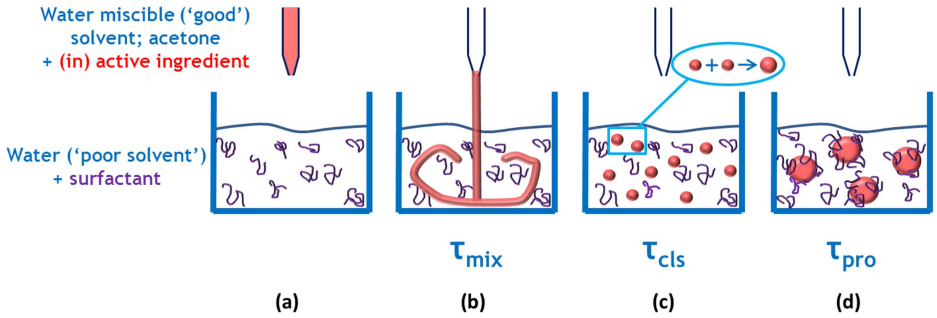

Figure 2.1: Different stages of a nanoprecipitation experiment: (a) typically 1 mL of a 10 mg/mL PLGA or PCL solution in acetone is to be added to 10 mL of 1 wt% surfactant (for instance PVA or Pluronic F127) solution in water; (b) the macroscopic mixing step; (c) the initial state of the system considered: polymer spheres are homogeneously distributed within the experimental volume; (d) end of the experiment: polymer spheres have coalesced until a protective layer of surfactant (PVA or Pluronic F127) protects the individual spheres against coalescence.

Although seemingly quite straightforward, applying the technique for practical applications is not free of difficulties. For drug delivery applications, the nanoparticles have to fulfill strict dimensional criteria and should be stable over sufficiently long times [10]. Although some particular methods, such as nanoprecipitation, have been studied experimentally quite thoroughly, there is limited correlation with the underlying physics that determines the final particle size. A physical picture of the nanoprecipitation process of hydrophobic molecules in water and the role of stabilizing surfactants was described by Lannibois *et al.* [11, 12], and was being extended to high concentrations of polymeric hydrophobic compounds [13] and applied to obtain rather narrow size distributions [14]. Knowledge of the physics that governs the nanoprecipitation process could help to rationalize how various experimental parameters, such as mixing efficiency/time, surfactant and polymer concentration and molar masses, affect the final particle size. This tremendously facilitates the design of a smarter preparation protocol.

For pharmaceutical applications a hydrophobic polymer (drug carrier) is typically used in combination with a polymeric surfactant to form water-suspendable particles. Alternatively, (di)block copolymers can be used that offer the advantage of a stronger interaction with the carrier polymer. A vast amount of research has been devoted to this topic, especially experimentally [15–18], see also the reviews [19, 20]. Particle formation using nanoprecipitation has also been studied using computer simulations and numerical methods, see for instance [11, 16, 21–23], whereas a simple theoretical model with explicit analytical expressions or at least a computationally 'cheap' numerical model for the size is much more helpful in steering the experimental research. The final size of block copolymer micelles in water, that apparently approaches equilibrium after a solvent switch [24], can be predicted very well by equilibrium self-consistent field computations [25, 26]. For the systems studied here dynamics however plays a role.

From an application point of view, the polymeric surfactant system is strongly preferable compared to using copolymers. Therefore it is key to develop insight into the processes that are operational during micellar precipitation in a polymer/surfactant suspension. Lannibois *et al*. [11] have made a first step in understanding the main physics of particle formation, by realizing that the competition between coalescence of hydrophobic material and adsorption of surfactants at the water-hydrophobic droplet interface governs the final size.

The goal of this work is to further quantify the relevant diffusion processes during nanoparticle formation. Although the realistic applications of the nanoparticles always involve at least three components – surfactant, carrier polymer, and drug – we restrict ourselves to a system without any drug present. The main question to be answered is 'what (process as well as polymer and surfactant) parameters determine the end size of the nanoparticles?' As an example, one can think of the mixing intensity and temperature as typical process parameters, and molar masses and concentrations of the components as typical system parameters, and how these determine the final result.

The outline of this manuscript is as follows. First, we introduce the theoretical approach that considers diffusion limited coalescence in a quenched polymer solution in a poor solvent. The aim of this part is to identify the relevant coalescence rate of polymer particles in the absence of any stabilization. Then, we proceed by incorporating the surfactant into the system and show that in the limit of strong polymer-surfactant interaction the system arrives at a kinetically frozen state, in which each polymer particle is surrounded by a surfactant corona. The size of the particles is shown to depend on the interplay between the particle coalescence and the surfactant adsorption rates. Secondly, we report our systematic experimental results and literature data on nanoprecipitation in the light of the proposed theoretical model. This is followed by discussions on the combined experimental and theoretical results followed by the conclusions.

2.2 Theoretical framework

In this section we formulate a theoretical model to describe the nanoprecipitation process. Our goal is to provide a simple analytical expression for the NP size as a function of the mixing intensity and the surfactant and polymer properties while accounting for the essential features of the process. For the sake of simplicity, we restrict ourselves to a bi-component system and consider the case that a dilute solution of a hydrophobic polymer is injected into

a water/surfactant solution. Both polymers and surfactants are subject to Brownian motion. Solvent and water are assumed to be well miscible which implies that a rapid quench of the hydrophobic polymer in water takes place. The polymers are now dispersed in a poor solvent so they form collapsed spheres, and these polymer particles start to coalesce upon encounter, to form larger particles. Simultaneously, the surfactant molecules adsorb onto the surface of the newly formed polymeric particles. This adsorption progressively hampers the coalescence process; steric repulsion between the surfactants prevents coalescence. Adsorption finally fully stabilizes the individual polymer particles against further coalescence and a stable situation is reached. The NPs formed represent a system in a kinetically frozen state. Therefore the NP size will depend strongly on the system kinetics, which includes at least three processes:

- mixing polymer plus solvent with the aqueous surfactant solution on a time scale τ_{mix};
- coalescence of the hydrophobic polymer particles (nanodroplets) in a hostile water environment, characterized by a time scale τ_{cls} (we suppose that the collapsed polymer molecules represent a lquid rather than a solid state);
- protection of the polymeric NPs by surfactants on a time scale τ_{pro}. This last step brings the system into a kinetically frozen state.

Below we address these three processes in more detail.

2.2.1 Diffusion limited coalescence in a polymer suspension

Before considering the process for the multicomponent system sketched in Fig. 2.1, let us address a somewhat simpler problem. Imagine a suspension of Brownian polymer particles (collapsed polymer chains) homogeneously distributed in a poor solvent. Such a situation actually corresponds to the limit of 'very fast mixing' or $\tau_{\text{mix}} \to 0$, i.e. a very rapid quench of a polymer solution.

The initial situation is similar to the one depicted in Fig. 2.1 (c) with one major difference – there is no surfactant. Apparently, in the course of time, the particles, subject to Brownian motion, will meet each other, collide and stick, forming larger particles. If they were hard (solid) particles, this would lead to fractal aggregates, for which well-known growth laws have been developed. This case is commonly known as 'diffusion limited aggregation' (DLA), leading to fractal clusters. Such an aggregation proceeds until the clusters meet and a space-spanning gel forms [27–29].

As our particles are liquid-like, they will coalesce to homogeneous spherical particles rather than forming fractal aggregates, so that we are dealing with 'diffusion limited coalescence' (DLC) [30, 31]. The purpose of this section is to calculate the average particle size as a function of time.

We assume that the coalescence rate in such a process is only limited by the diffusion time – the average time needed for particles to cover the interparticle distance to meet each other – and not by the 'particle fusion' itself. Then the problem is reduced to a diffusion limited second order 'reaction' [32]. Such diffusion limited kinetics were already addressed by von Smoluchowski [33, 34], who argued that the observed reaction rate constant for this process reads

$$K = 4\pi D' R' \quad , \tag{2.1}$$

where $D' = D_A + D_B$ is the sum of the diffusion coefficients of the reacting species and $R' = R_A + R_B$ is their interaction radius. In the one-component case of coalescing polymers, species A and B both refer to coalescing polymers and an equation for the polymer concentration as a function of time can be readily written as

$$\frac{dc_p}{dt} = -K_{pp} h c_p^2 = -\frac{8}{3}\frac{k_B T}{\eta} h c_p^2 \quad , \tag{2.2}$$

where K_{pp} is the rate constant for polymer-polymer coalescence. In Eq. (2.2), $D_p = k_B T/(6\pi\eta R_p)$ is the Stokes-Einstein equation for the diffusion coefficient of a sphere with a radius R_p in a fluid with viscosity η. The subscript 'p' refers to 'polymer'. The factor h equals the probability that a collision leads to a coalescence event. We assume $h = 1$ in the absence of surfactant. The coalescence time scale immediately follows from (2.2)

$$\tau_{\mathrm{cls}} = \frac{3}{8 c_{p0}} \frac{\eta}{k_B T} \quad . \tag{2.3}$$

Since we are dealing with a coalescence process, there is a direct relation between particle mass and particle radius R_p via the mass conservation law in the form

$$c_p(t) R_p^3(t) = c_{p0} R_{p0}^3 \quad .$$

Here, R_{p0} and c_{p0} are the size and the number concentration of the polymer particles immediately after mixing took place. The solvent is assumed to be poor enough not to penetrate inside the polymer particles, so $m = 4\pi\rho R_{p0}^3 c_{p0} V/3$. When a certain mass m of a polymer with density ρ has been initially 'suspended' in a volume V, Eq. (2.2) can be rewritten in terms of the average polymer particle radius

$$\frac{dR_p(t)}{dt} = \frac{2}{3\pi}\frac{k_B T}{\eta}\frac{m}{\rho V}\frac{1}{R_p^2(t)} \tag{2.4}$$

leading to the solution

$$R_p^3(t) = R_{p0}^3 + \frac{2}{\pi}\frac{k_B T}{\eta}\frac{m}{\rho V} t \quad , \tag{2.5}$$

or

$$R_p = R_{p0}\left(1 + \frac{t}{\tau_{\mathrm{cls}}}\right)^{1/3} \quad . \tag{2.6}$$

Here R_{p0} is the initial size of the polymer particles, i.e. the size just after the mixing step has been completed. We have neglected the size distribution and derived an equation for the mass averaged radius, $\langle R_p^3 \rangle^{1/3}$.

In order to quantify the time scale τ_{cls} involved, let us take an example with the following numerical values of the parameters: polymer mass m=10 mg with density of approximately $\rho \sim 1$ g/cm^3 is initially suspended in V=10 mL of water with viscosity $\eta \sim 1$ mPa·s at T=300 K. After substituting the numerical values in Eq. (2.5), we obtain

$$R_p^3(t) = R_{p0}^3 + 2.6 \cdot 10^6 \left[\frac{nm^3}{s}\right] \cdot t\,[s] \quad .$$

The resulting time evolution of the particle size is depicted in Fig. 2.2 for different initial values of the polymer particle size. Clearly, the initial radius is important only at the very

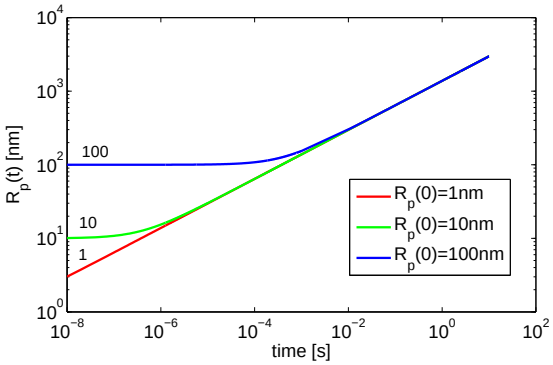

Figure 2.2: Size evolution after a quench of Brownian polymer chains in a poor solvent for different initial polymer particle sizes.

early stages of evolution. Beyond the initial stage a quite universal behavior is observed where the size is solely governed by the mobility and the total amount of polymer. It is also apparent that the coalescence times involved are in the subsecond region. Indeed, it is observed that when one starts with an optically clear suspension, $R_{p0} \lesssim 100$ nm, within less than a second the suspension will become turbid, $R_p(1\text{ s}) \sim 1\ \mu$m.

One more important feature of Eq. (2.5), also reflected in Fig. 2.2, is that the upper particle size is unbound. In other words, the polymer particles will continue to coalesce until one big (in terms of the current model, big means infinite) particle is formed. This is indeed, what one should expect for a phase separation process in a thermodynamic limit. The situation will dramatically change in the presence of surfactant as explained in the following section.

2.2.2 Coalescence in the presence of surfactant

Based on the above consideration, a qualitative picture about polymer coalescence *in the presence of surfactant* also emerges. Parallel to coalescence of polymer particles, surfactant adsorption on the polymer particles takes place. Although 'hairy-particle' interaction [35] is quite a complex topic in itself, one point is clear: a surfactant layer on the particle surface hinders coalescence because two densely covered particles cannot approach closely enough to fuse. Steric repulsion between (polymeric) surfactants then leads to a repulsive interaction between two polymer particles.

Thus, in the early stages of the process, polymer particles are 'bald' and easily fuse leading to coarser particles (h is 1 is Eq. (2.2)). At the same time, the polymer droplets get covered by surfactant and above a certain degree of surfactant surface coverage the coalescence process slows down and stops when the surfaces get saturated with surfactant. This final state leads to a finite polymer particle size, which is purely kinetically determined.

To develop a simple quantitative theoretical model, we make use of the following assumptions:

1. The solvent in the big vessel in Fig. 2.1 is good for the surfactant molecules (in fact, the surfactant is also a polymer in our experiments). We shall neglect surfactant micellization by assuming that the surfactant molecules present in surfactant micelles behave similarly to the dissolved ones, at least in what concerns their agglomeration with polymeric NPs.
2. Polymer particles and surfactant molecules are both subject to Brownian motion.
3. There is a strong favorable interaction between the polymer and the surfactant. So, when a polymer particle and a surfactant molecule meet, the surfactant 'sticks' to the surface and never desorbs.
4. Polymer particles coalesce when they meet each other, unless they are 'protected' by the surfactant molecules (we shall elucidate this assumption more further on). There is no particle break up.
5. Each surfactant molecule occupies some fixed surface area a^2 when adsorbed. Thus, for a given polymer particle with radius R_p only a limited number of surfactant molecules, $4\pi R_p^2/a^2$, can adsorb on its surface.
6. We use the mean-field continuum approximation.

In what follows, the surfactant effect will be incorporated in the coalescence model of section 2.2.1.

2.2.2.1 Smoluchowski's reaction rate

Now, as we have two 'reacting' species, the reaction rates for a polymer-polymer and polymer-surfactant reactions have to be determined.

The expression for the polymer-polymer rate constant remains unchanged [see Eq. (2.2)] and a similar expression for the polymer-surfactant case can be written [11, 13]

$$K_{ps} = 4\pi(D_p + D_s)(R_p + R_s) \quad , \tag{2.7}$$

where K_{ps} is the rate constant that describes surfactant to polymer adsorption. Here R_s is the radius of gyration of the surfactant in solution and the diffusion coefficients are calculated according to the Stokes-Einstein laws

$$D_p = \frac{k_B T}{6\pi\eta R_p} \quad \text{and} \quad D_s = \frac{k_B T}{6\pi\eta R_s} \quad . \tag{2.8}$$

To be precise, using the Zimm expression [36] for the diffusion coefficient of the surfactant molecules in the solvent would be more appropriate. However, it differs from Eq. (2.8) only by a numerical prefactor, which is not important given the level of accuracy of the present model.

2.2.2.2 Surfactant concentration

An equation for the concentration of the unadsorbed *free* surfactant molecules can be written using the rate constant from Eq. (2.7)

$$\frac{dc_s^{\text{free}}}{dt} = -K_{ps} h_s c_s^{\text{free}} c_p = -\frac{2}{3}\frac{k_B T}{\eta}\left(\frac{1}{R_p}+\frac{1}{R_s}\right)(R_p+R_s)\, h_s c_s^{\text{free}} c_p \quad . \tag{2.9}$$

The factor h_s appearing in (2.9) expresses a probability for a surfactant molecule to adsorb upon encountering a polymer particle and is analogous to the factor h in Eq. (2.2) (for more details see [32]). An interesting observation from Eq. (2.9) and (2.2) is that $\tau_{\text{pro}} \sim \tau_{\text{cls}}$ and, hence, the collision rate of the polymer particles and their protection by the surfactant go at approximately the same pace.

2.2.2.3 Influence of surfactant on the coalescence rate

Kinetic Eq. (2.2) and (2.9) could be readily solved if the functions h and h_s were specified, which we will do next. Let us first address the probability of particle fusion upon encounter h. The surfactant adsorbed on the particle surface influences h, as it reduces the probability of a coalescence event to occur. Hence, h is a function of the fraction of the particle surface protected by the surfactant, $h \equiv h\left\{(n(t)a^2)/((4\pi R_p^2(t)))\right\}$, where $n(t)$ denotes the average number of surfactant molecules adsorbed on a polymer particle with radius R_p at time t, each surfactant molecule covering a surface area a^2.

Computing the exact form of $h(\cdot)$ can be quite involved [37], although it is clear that $h(0) \simeq 1$ and $h(1) \simeq 0$. As a simple approximation we assume h and h_s are the same. Such a choice does not change the scaling of the most relevant quantities but implies that the coalescence process is hindered by surfactant adsorption, and stops abruptly at full coverage when $n = 4\pi R_p^2/a^2$. Hence the coalescence probability is slowed down as the surfactant adsorption increases. It will follow that the exact form of h and h_s do not influence the final result when these functions are identical. It then also follows the coalescence of particles continues until the particles are saturated with the surfactant.

2.2.2.4 Final set of equations and solution

Let us recapitulate the theoretical model so far. Based on the considerations above, we have arrived at a set of two equations. One equation describes the evolution of the number concentration of the polymer particles c_p during coalescence via Eq. (2.2) and the other quantifies the free surfactant concentration c_s^{free} given by Eq. (2.9). For further consideration, it is convenient to recast the expressions in terms of the particle size $R_p = R_{p0}(c_{p0}/c_p)^{1/3}$ and the concentration of the attached surfactant molecules $c_s^{\text{att}} = c_{s0} - c_s^{\text{free}}$:

$$\frac{dR_p}{dt} = \frac{8}{9}\frac{k_{\text{B}} T}{\eta} h(x) \frac{R_{p0}^3 c_{p0}}{R_p^2} \quad , \tag{2.10}$$

$$\frac{dc_s^{\text{att}}}{dt} = \frac{2}{3}\frac{k_{\text{B}} T}{\eta}\frac{(R_p+R_s)^2}{R_p R_s} h_s(x)(c_{s0} - c_s^{\text{att}}) c_p \quad , \tag{2.11}$$

where $x = na^2/(4\pi R_p^2) = (a^2 R_p/R_{p0}^3)(c_s^{\rm att}/c_{p0})$. The set is ompleted by the initial conditions $c_s^{\rm att}(0) = 0$ and $R_p(0) = R_{p0}$.

Solving Eq. (2.10) and (2.11) simultaneously yields the time evolution of the particle size. However, we are interested in the final size of the polymer particles only. Upon dividing Eq. (2.11) by Eq. (2.10) and assuming identical functional forms for h and h_s, we arrive at

$$\frac{dc_s^{\rm att}}{dR_p} = \frac{3}{4}\frac{(R_p+R_s)^2}{R_p^2 R_s}(c_{s0} - c_s^{\rm att}) \quad , \tag{2.12}$$

$$\frac{a^2 R_p}{R_{p0}^3}\frac{c_s^{\rm att}}{c_{p0}} \leq 1 \quad , \tag{2.13}$$

where an extra inequality is added to the differential equation to fulfill the boundary conditions imposed by the functions h and h_s.

Eq. (2.12) has a simple solution

$$c_s^{\rm att}(t) = c_{s0}\left\{1 - \exp\left[-\frac{3}{4}\left(\ln\frac{R_p(t)}{R_{p0}} + \frac{R_p(t)-R_{p0}}{R_s} - \frac{R_s}{R_p(t)} + \frac{R_s}{R_{p0}}\right)\right]\right\} \quad . \tag{2.14}$$

Enforcing the extra condition of Eq. (2.13) onto Eq. (2.14) leads to the inequality

$$1 - \exp\left\{-\frac{3}{4}\left[\ln\zeta(t) + \alpha(\zeta(t)-1) + \frac{1}{\alpha}\left(1 - \frac{1}{\zeta(t)}\right)\right]\right\} \leq \frac{\kappa}{\zeta(t)} \quad , \tag{2.15}$$

where some dimensionless quantities have been introduced: $\zeta(t) = R_p(t)/R_{p0}$ is the dimensionless radius of the polymer particles, $\alpha = R_{p0}/R_s$ is the ratio between the initial polymer particle size and the gyration radius of the surfactant molecules, and $\kappa = 4\pi R_{p0}^2 c_{p0}/(a^2 c_{s0})$ is the ratio of the total initial surface area of the polymer particles and the maximum area surfactant molecules can occupy and block.

It can be shown that the largest value of ζ fulfilling inequality (2.15) corresponds to the equal sign. Hence, solving the corresponding transcendental equation for ζ gives the final particle size. Although Eq. (2.15) cannot be solved analytically in the general case, explicit solutions can be derived for the final particle size in the asymptotic limit of excess surfactant, $\kappa \ll 1$,

$$R_p^{\rm end} = R_{p0}\left(1 + \frac{\kappa}{3/4 + \alpha + \alpha^{-1}}\right) \quad . \tag{2.16}$$

If surfactant is scarce, $\kappa \gg 1$, an even simpler analytical formula for the end particle size $R_p^{\rm end} \equiv \zeta R_{p0}$ can be found:

$$R_p^{\rm end} = R_{p0}\kappa \quad . \tag{2.17}$$

The approximate solutions of Eq. (2.16) and (2.17) are surprisingly close to the exact one, as shown in Fig. 2.3 (a), where the asymptotic limits are compared to the numerical results of Eq. (2.15). It is also interesting to point out that the solution is not very sensitive to the variations in α, the ratio between the initial polymer particle size and the gyration radius of surfactant. Indeed, as Fig. 2.3 (b) shows, only slight variations in the end size values can be observed even if α is changed by two orders of magnitude. The interpolation

$$R_p^{\rm end} = R_{p0}(1+\kappa) \tag{2.18}$$

smoothly connects the above asympotic limits and actually describes the numerical results

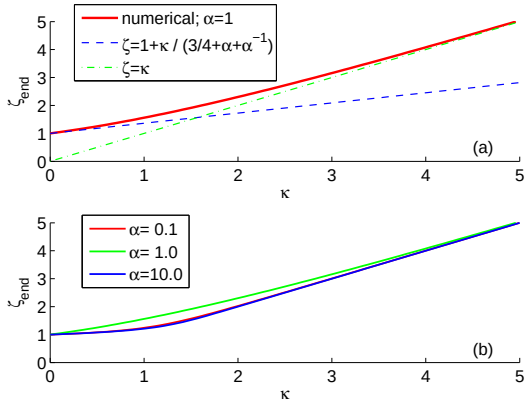

Figure 2.3: (a) Comparison between the exact (numerical) solution of Eq. (2.15) and the approximation of Eq. (2.16) for $alpha = 1$. (b) Sensitivity of the solution of the approximate Eq. (2.16) to the parameter α.

that can be obtained from Eq. (2.15). The fact that $\tau_{\rm cls} \sim \tau_{\rm pro}$, as pointed out above, implies that the final NP size is independent of the mobility of polymer or surfactant molecules. In the 'fast mixing' limit ($\tau_{\rm mix} \ll \tau_{\rm cls}$) the final size depends mainly on the surfactant concentration.

2.2.2.5 'Slow mixing' limit

There is also another limit, $\tau_{\rm mix} \geq \tau_{\rm cls}$, which is characterized by fast particle coalescence on the time scale shorter than the typical mixing time followed by stabilization of the NPs, thereby setting their final size, at times $t \geq \tau_{\rm mix}$. At the onset of the coarsening process, the polymers are present as isolated chains in a good solvent. As the solvent quality steeply drops the polymers collapse instantaneously. Subsequent collision of collapsed chains leads to coalescence following the kinetics prescribed by Eq. (2.10) with $h \equiv 1$. At this stage ($t < \tau_{\rm mix}$) the surfactants cannot yet adsorb onto the polymer droplets. After full mixing ($t \simeq \tau_{\rm mix}$), the particle size has evolved to

$$R_{\rm mix} \simeq R_{p0}\,(1 + \tau_{\rm mix}/\tau_{\rm cls})^{1/3} \quad ,$$

as follows from Eq. (2.6). At longer times, $t > \tau_{\rm mix}$, there is sufficient time for the surfactant to adsorb onto the surface of the coalescing polymer-rich particles. As a result the system then has arrived at a well mixed state and its kinetics obeys the set of Eq. (2.10) and (2.11) as discussed above, with the constraint that $R_{\rm mix}$ must be used as the 'initial' particle size in Eq. (2.14). This two-step process leads to a final expression for the polymer particle radius in a kinetically frozen state

$$R_p^{\rm end} = R_{p0}(1+\kappa)\left(1 + \frac{\tau_{\rm mix}}{\tau_{\rm cls}}\right)^{1/3} \quad , \tag{2.19}$$

which is depicted in Fig. 2.4. In Eq. (2.19) we have used a simple interpolation $(1+\kappa)R_{p0}$ of Eq. (2.18) for the size after mixing. The final particle radius (2.19) is characterized by

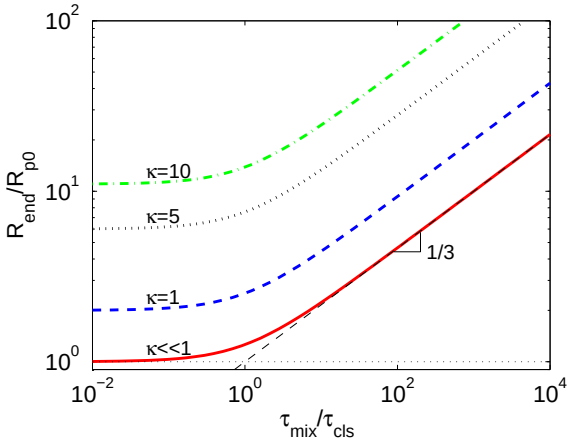

Figure 2.4: Particle size as a function of the ratio between mixing and coalescence times for various amounts of surfactants present expressed via κ.

a plateau at small $\tau_{\rm mix}/\tau_{\rm cls}$, where the NP diameter is independent of mixing or encounter and coalescence time and is totally governed by the surfactant concentration (parameter κ) with the smallest particles obtained for large excess of surfactant ($\kappa \ll 1$). The other regime, $\tau_{\rm mix}/\tau_{\rm cls} > 1$, shows a typical $1/3$ power law behavior and is dominated by the mixing efficiency. This power law follows from the limit of large $\tau_{\rm mix}$ in Eq. (2.19),

$$R_p^{\rm end} = R_{p0}(1+\kappa)\left(\frac{\tau_{\rm mix}}{\tau_{\rm cls}}\right)^{1/3} \quad .$$

In the practical case of small κ and large $\tau_{\rm mix}$ this provides the scaling result

$$R_p^{\rm end} \sim (c_{p0}\tau_{\rm mix})^{1/3} \quad , \tag{2.20}$$

where we used Eq. (2.3) for $\tau_{\rm cls}$.

2.2.3 Implications of the model for experiments

Let us first recapitulate the qualitative model behind the calculation presented so far. The nanoprecipitation can be divided into two important stages: the mixing shown in Fig. 2.1 (b) and the polymer/surfactant diffusion shown in Fig. 2.1 (c) and Fig. 2.1 (d). Clearly, such a division is a bit artificial as there is no clear border between the mixing and the diffusion 'regimes', but we will use it for the sake of simplicity.

At the very beginning of the mixing the polymer 'particles' have the size of a single swollen polymer coil because the polymer is initially dissolved in a good solvent. As soon as the individual polymer chains are solvated by the poor solvent, they collapse to the size of R_{p0} and start coalescing with each other as they are yet not mixed well with the aqueous surfactant solution. When the time $\tau_{\rm mix}$ is elapsed, acetone and water are mixed and also some coalescence has taken place leading to the particle size $R_{\rm mix}$.

Further coalescence is accompanied by protection of the polymer particles by surfactant.

As in the experimentally relevant regime there is a large excess of surfactant, $\kappa << 1$, the final particle size $R_p^{\rm end}$ is expected to be close to the size at the beginning of the diffusion driven coalescence process, $R_p^{\rm end} \simeq R_{\rm mix} \simeq R_{p0}(1+\tau_{\rm mix}/\tau_{\rm cls})^{1/3}$. Thus, the final polymer particle size in a typical experimental situation is mainly determined by the coalescence during the mixing process and not by the stage after mixing has been completed. The coalescence time expressed via experimentally measurable quantities reads

$$\tau_{\rm cls} = \frac{3}{8}\frac{\eta}{k_{\rm B}T}\frac{M_p}{N_A c_{mp}} \quad . \tag{2.21}$$

M_p is the polymer molar mass, N_A is the Avogadro's constant and c_{mp} is the *mass* concentration of polymer in solution. We have used here the initial polymer particle size $R_{p0} = (3M_p/(4\pi N_A \rho))^{1/3}$, where ρ is the polymer density.

The final particle size is plotted in Fig. 2.4 as a function of the mixing and the coalescence times. Two regimes can be distinguished in Fig. 2.4: one for large and one for small ratios $\tau_{\rm mix}/\tau_{\rm cls}$. For very fast mixing, $\tau_{\rm mix}/\tau_{\rm cls} \ll 1$, the final radius is of the order of R_{p0} and does not depend on $\tau_{\rm cls}$. Hence, the final particle size does not depend on the polymer concentration in the limit of very fast mixing, but does depend on the molar mass. In the slow mixing regime, $\tau_{\rm mix}/\tau_{\rm cls} > 1$, a power law scaling of the final polymer particle size with an exponent of $1/3$ is predicted: $R_p^{\rm end} \sim R_{p0}(\tau_{\rm mix}/\tau_{\rm cls})^{1/3} \sim \tau_{\rm mix}^{1/3}[k_{\rm B}Tc_{mp}/(\eta\rho)]^{1/3}$. Here the final size will increase if $\tau_{\rm cls}$ is decreased, e.g. due to higher concentration.

Let us finally summarize the conclusions and the theoretically predicted trends, which can be used to control the particle size experimentally:

1. Under the currently used experimental conditions – excess of surfactant – the particle size at the end of the mixing phase determines the final size of the surfactant stabilized NPs. The particles are stabilized by the surfactant corona and the system is in a kinetically frozen state.
2. In the slow mixing regime, the size of the micelles formed is proportional to the polymer concentration to power $1/3$: $R_p^{\rm end} \sim c_{mp}^{1/3}$ [11, 13]. So, the lower the concentration, the smaller particles can be formed.
3. Fast mixing is essential: smaller particles are obtained when $\tau_{\rm mix}$ is reduced.
4. In case of relatively slow mixing, as typically encountered in experiment, the end size is independent of the initial size of the polymer particles. This implies, that the final size will be insensitive to the molar mass of the polymer.
5. There is no explicit dependence on the molar mass of the surfactants. However, the mixing time will probably increase if higher molar mass of the surfactant is added at constant surfactant concentration ϕ. Indeed, the (shear) viscosity of the aqueous solution of surfactant (in our experiments PVA) will scale as $\eta_{\rm m}(1+\phi[\eta])$, with medium viscosity $\eta_{\rm m}$ and where the intrinsic viscosity increases with the molar mass $[\eta] \sim M_s^{0.8}$ (we have used the Zimm model in a good solvent, [36]). A higher shear viscosity of the solution implies longer mixing times and, hence, larger NPs.
6. Another parameter, which possibly plays a role, is the temperature. As many model parameters (weakly) depend on it, explicitly and implicitly, it is hardly possible to elucidate what the exact effect of the temperature should be. Apparently, the higher the

temperature, the lower the coalescence time τ_{cls}, see Eq. (2.21). But also the mixing time τ_{mix} will probably be decreasing upon temperature rise. Although it is hard to predict what the net effect on the ratio τ_{mix}/τ_{cls} will be, we mention it as a tool to adjust the particle size to a limited degree.

2.3 Materials and methods

2.3.1 Materials

Polycaprolactone (PCL) of different molar masses (CAPA 2203; 2 kDa, 2403; 4 kDa, 2803; 8 kDa, 6250; 25 kDa, 6400; 37 kDa, 6500; 50 kDa and 6800; 80 kDa) were purchased from Solvay (Oudenaarde, Belgium). Poly-(lactic-co-glycolic) acid (PLGA; 1/1 molecular ratio for lactic and glycolic acid) 20 kDa was purchased from Boehringer Ingelheim (Ingelheim am Rhein, Germany). Acetone and Pluronic F127 (NF prill polaxamer 407) were purchased from BASF (Bayern, Germany). Polyvinylalcohol (PVA) of different molar masses (13-23 kDa, 31-50 kDa and 85-124 kDa; all three with a hydrolyzation percentage of 87-89% and 9-11 kDa 80% hydrolyzed) were purchased from Sigma (St. Louis, USA). Rapamycin was obtained from Oscar Tropitzsch (Germany).

2.3.2 Particle size analysis

2.3.2.1 Dynamic light scattering

The final hydrodynamic diameter of the particles was determined by Dynamic Light Scattering (DLS) (Zetasizer Nano ZS, Malvern Instruments Ltd., Malvern, UK) at 25°C at a scattering angle of 173°. Ideally the number of photon counts is large enough to get a good signal to noise ratio and yet small enough to prevent multiple scattering effects. In dynamic light scattering the fluctuations in the scattered intensity are analyzed and the resulting autocorrelation function is related to an averaged diffusion coefficient of the particles that undergo Brownian motion. Via the Stokes-Einstein relation the diffusion coefficient is converted to a hydrodynamic particle size diameter, D_h. We note that this diameter is the *z*-average of the size distribution. We also report the measured polydispersity index (PdI) that describes the width of the particle size distribution. The polydispersity index is a parameter calculated from the cumulant analysis of the DLS measured intensity autocorrelation function. In the cumulants analysis, a single particle size is assumed and a single exponential fit is applied to the autocorrelation function. All samples were measured as processed (undiluted). Size distributions of the prepared NPs measured with DLS were unimodal.

2.3.2.2 Cryo-TEM

For a few samples we also studied the size using cryo transmission electron microscopy (cryo-TEM) at the TU Eindhoven in the Netherlands. The aqueous samples were prepared with a vitrification robot from FEI; Vitrobot Mark III. The used cryo-TEM equipment was a cryoTITAN from FEI, a 300kV FEG microscope, optimized for both resolution and contrast. Two samples containing particles made of only active ingredient and a combination rapamycin and PLGA were analyzed using cryo-TEM. The first sample was pure rapamycin; 1.00

mL of 60 mg rapamycin/mL acetone. The second sample was a rapamycin and PLGA (20 kDa) (1/1 mass ratio); 15 mg rapamycin and 15 mg of PLGA/mL acetone. The samples were added to an aqueous solution with a volume of 10.00mL (containing 1wt%) PVA (9-11 kDa 80% hydrolyzed) according to the nanoprecipitation procedure followed by cryo-TEM and DLS analysis were performed.

2.3.3 Rheology of PVA solutions

The shear stress of solutions with PVA were measured as a function of shear rate in order to investigate the influence of the viscosity on the NP size. We studied solutions containing three different molar masses of PVA (13-23 kDa, 31-50 kDa and 85-124 kDa; all three with a degree of hydrolysis of 87-89%). The polymer solutions were analyzed at five different weight concentrations (2.50, 1.00, 0.50, 0.25 and 0.10% (wt%)). The viscosity measurement was performed on an Anton Paar MCR 300 Rheometer at 25°C with a double gap cylinder (DG 26.7). The shear rate was varied between 30 and 300 s^{-1}. At these concentrations the solutions appeared Newtonian.

2.3.4 Nanoprecipitation / nanoparticle preparation method

Typically, 25.0 mg of polymer (PCL) was weighed and dissolved in 5.00 mL of acetone resulting in a clear polymer solution after 30 minutes on an orbital shaker. Prior to the nanoprecipitation process all solutions were filtered over an Acrodisc LC25 mm Syringe filter 0.2 μm PVDF membrane to remove large dust particles. In Fig. 2.1 the basic nanoprecipitation process setup was sketched. A volume of 1.00 mL of the polymer/acetone solution was added to 10.00 mL of aqueous surfactant (PVA or Pluronic F127) solution with an Eppendorf pipette. The addition with the pipette was carried within one second, after which the suspension was manually homogenized by swirling the vial around for five seconds. We will compare our experiments to the proposed theoretical model for diffusion limited coalescence in the slow mixing regime and with data from literature. For the fast mixing regime we will test our theoretically predicted trends against data from literature.

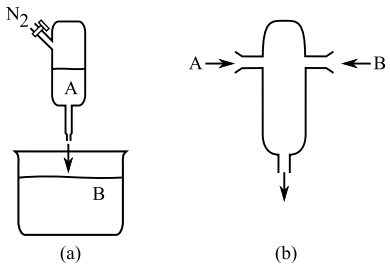

Figure 2.5: Scheme of a pressure driven injection device used in Ref. [38] (a) and an impinging jets mixer used in [15] (b). Fluid A is the organic phase comprising solvent, the carrier polymer and the drug, fluid B is an aqueous solution containing (polymeric) surfactant.

There are various other ways to perform nanoprecipitation. Two of them are depicted in Fig. 2.5. One will result in slow mixing times [38]. Experiments using an impinging jets mixer allow tuning the mixing time scale as to investigate both the fast and slow mixing

time regimes [15]. The results reported in literature will be used to verify our theoretically predicted trends:

- in the slow mixing regime, $\tau_{\mathrm{mix}}/\tau_{\mathrm{cls}} > 1$, a cube root scaling of the final polymer particle size with polymer concentration is predicted: $R_p^{\mathrm{end}} \sim R_{p0}(\tau_{\mathrm{mix}}/\tau_{\mathrm{cls}})^{1/3} \sim \tau_{\mathrm{mix}}^{1/3}[k_{\mathrm{B}}Tc_{mp}/(\eta\rho)]^{1/3}$ and thus: $R_p^{\mathrm{end}} \sim c_{mp}^{1/3}$,
- in the limit of fast mixing, $\tau_{\mathrm{mix}}/\tau_{\mathrm{cls}} \ll 1$, the final radius is of the order of R_{p0} and does not depend on τ_{cls}. Hence, the final particle size is expected to be independent of the polymer concentration, but dependent on the molar mass.

2.4 Results and discussion

2.4.1 Cryo-TEM images of NPs

To illustrate what kinds of particle sizes form after nanoprecipitation using real space analysis we show two (cryo-)TEM pictures. Fig. 2.6 (a) and 2.6 (b) depict the cryo-TEM pictures of a pure rapamycin particle and a rapamycin/PLGA (1/1 mass ratio) particle, respectively. The DLS results of the particles are in good agreement with size from the cryo-TEM analysis, see Fig. 2.6 (a) and 2.6 (b) and their legends. In Fig. 2.6 (b) a small gold particle can be seen in the right upper corner, which was added to serve as a reference point to perform tomography, revealing a spherical shape.

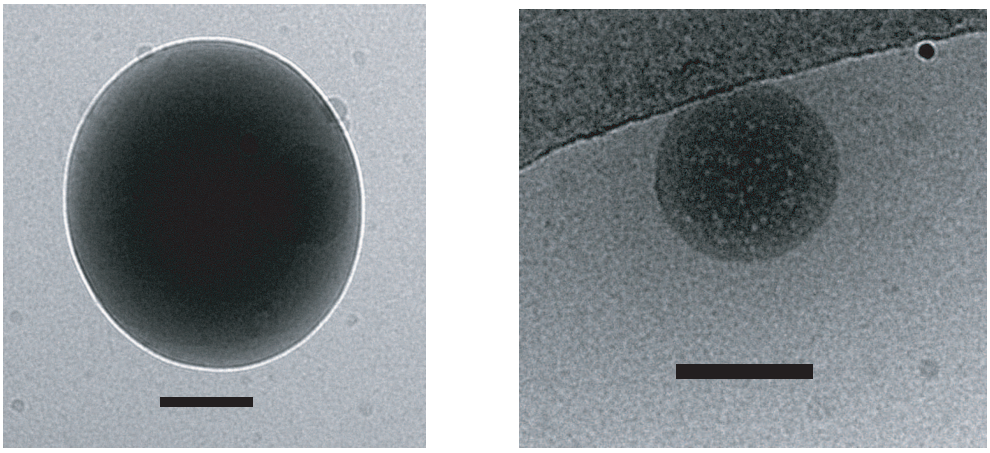

(a) **(b)**

Figure 2.6: Cryo-TEM picture of a nanoparticle prepared by nanoprecipitation). (a): Cryo-TEM picture of a nanoparticle prepared by nanoprecipitation filled with the drug rapamycin. The scale bar is 100 nm. The dispersion was prepared by adding 1.00 mL acetone containing 60 mg rapamycin to 10.00 mL with 1.00 wt% aqueous solution of 9-11 kDa PVA. (Corresponding DLS results: D_h = 344 nm and PdI = 0.10.). (b): Cryo-TEM picture of a rapamycin/PLGA nanoprecipitated particle. Scale bar is 100 nm. A volume of 1.00 mL with 15 mg rapamycin and 15 mg PLGA acetone was added to an aqueous solution of 10.00 mL with 1.00 wt% 9-11 kDa PVA. (Results from DLS: D_h = 148 nm and PdI=0.06.).

2.4.2 Influence of polymer concentration on size

To validate Eq. (2.19) we compare its scaling prediction $R_p^{\text{end}} \sim c_{mp}^{1/3}$ to our experiments as well as to data available in the literature. In the nanoprecipitation experiments we performed, PCL (CAPA 6250; 25 kDa) has been used as a carrier polymer and Pluronic F127 as a surfactant. 1.00 mL PCL/acetone solution (0.6, 1.0, 6.0 and 10.0 mg PCL (25 kDa)/mL acetone) was quenched in 10.00 mL, 1.00 wt%, Pluronic F127 aqueous solution with an Eppendorf pipette, a device similar to the one depicted in Fig. 2.5. The hydrodynamic particle diameter D_h has been measured by DLS.

As can be seen from Fig. 2.7, our results compare favorably to the data available in the literature [6] for the same system. As the experiments are performed in the $\tau_{\text{mix}} > \tau_{\text{cls}}$ regime, the scaling obeys the 1/3 power law as expected. The data presented only cover the $\tau_{\text{mix}} > \tau_{\text{cls}}$ regime and neither reach a particle size saturation limit at the very fast mixing, $\tau_{\text{mix}} < \tau_{\text{cls}}$, nor a crossover at $\tau_{\text{mix}} \approx \tau_{\text{cls}}$. The spread on the data of Molpeceres *et al* can be explained by experimental and analytical standard deviation since the spread is equal to the error bars in our experiments, see Fig. 2.7. Our experiments were repeated on different dates using freshly prepared solutions. The scaling $R_p^{\text{end}} \sim c_{mp}^{1/3}$ has been found and confirmed earlier by Cabane and co-workers [11, 13], for various systems such as cholesteryl acetate molecules dispersed in water in the presence of the block copolymer polystyrene-polyoxyethylene as surfactant or hexadecane molecules precipated in water with exthoxylated fatty acids as surfactants.

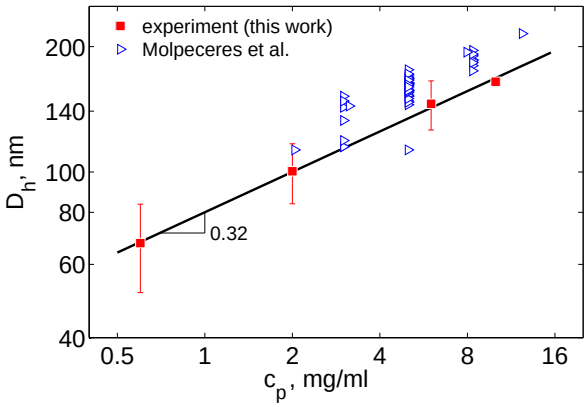

Figure 2.7: Polymer concentration dependence of the generated particle size expressed as the measured hydrodynamic diameter (D_h) with DLS. These particles form after adding 1.00 mL of different PCL concentrations (molar mass: 25 kDa) in acetone (mg/mL) to 10.00 mL water containing 1 wt% Pluronic F127 (squares). Each data point results from the average of three measurements. We compare these results to the theoretical scaling relation of Eq. (2.20) and data from Molpeceres [38] (open triangles).

One may wonder how polymer polydispersity affects the final particle size (distribution). This was considered by Whitesides and Ross [21] in a numerical study. They found that the final particle size is quite independent of the starting distribution. Hence it seems that the final particle size is not senstive to the initial polydispersity.

2.4.3 NP size dependence on polymer molar mass

In case of relatively slow mixing, typically encountered in our experiments, there should be no dependence between final particle size and the molar mass of the polymer as follows from Eq. (2.19). In order to verify this the influence of using PCL polymers with different molar masses (2, 4, 8, 25, 37, 50 and 80 kDa) on particle size was studied. The PCL polymers were dissolved at equal concentrations in acetone (5 mg PCL/mL acetone). A volume of 1.00 mL of the different polymer/acetone solutions were added to 10.00 mL aqueous solution containing 1.00 wt% Pluronic 127 F following the nanoprecipitation procedure. All experiments were done in triplicate after which a DLS analysis was performed.

In Fig. 2.8 we plotted the measured particle size as a function of the molar mass of the hydrophobic polymer. It is clear that changing the molar mass hardly affects the final particle size under the same experimental conditions. The particle size ranges between 130 nm and 150 nm, which can be explained by a slightly different viscosity of the polymer/acetone solutions. The lower molar masses hardly influence the viscosity of the polymer/acetone solution while the higher molar masses (80 kDa) of PCL have a more distinct effect on the viscosity of the polymer/acetone solution. The difference between the values for the viscosity of these solutions hardly alters the mixing times and therefore only modifies the final particle size to a small degree. Further the data for molar masses (below 10 kDa) could reflect slightly smaller sizes because the solubility starts to increase a bit for lower molar mass.

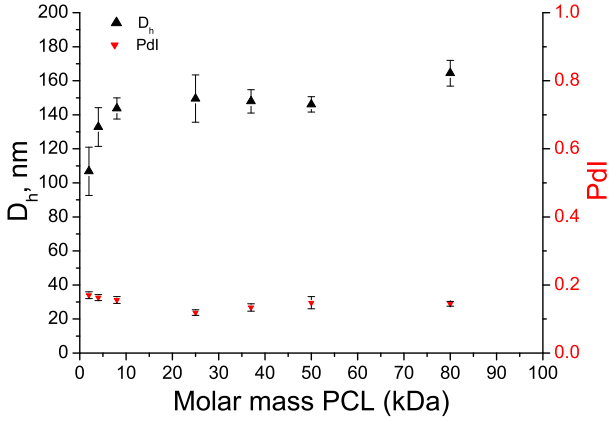

Figure 2.8: Hydrodynamic diameter (D_h) and PdI results (triplicates) as a function of the molar mass of PCL at fixed concentration. Samples were made by adding 1.00 mL acetone with 5 mg/mL PCL of different molar masses to 10.00 mL water containing 1 wt% Pluronic F127.

2.4.4 Influence of mixing time on particle size

The end particle size is governed by two relevant time scales; the mixing and the coalescence time. To assess the influence of the mixing time while maintaining the same experimental conditions only the phase containing the surfactant was changed. In a first experiment the surfactant was dissolved in the water phase (0.10 wt% Pluronic 127 F in water). A volume of 1.00 mL acetone/polymer-solution (5 mg PCL (25 kDa)/mL acetone) was added to 10.00 mL

1.00 wt% Pluronic 127F solution, according to the nanoprecipitation procedure. In a second experiment the surfactant was co-dissolved with the polymer in the acetone phase (1.00 wt% Pluronic 127F + 5 mg PCL (25 kDa)/ mL acetone. Then 1.00 mL surfactant/polymer/acetone solution was added to 10.00 mL Milli Q water according to the nanoprecipitation procedure. Both experiments were performed in triplicate followed by a DLS analysis. The difference of surfactant concentration in the acetone phase (1.0 wt%) and the surfactant in the water phase (0.10 wt%) was chosen such that the final surfactant concentration was the same for both experiments.

The presence of the surfactant in the aqueous phase or in the solvent (acetone) phase together with the hydrophobic polymer should have a distinct influence on the final particle size. This is explained by the mixing time which is decreased in the latter case. Since the hydrophobic polymer and surfactant are dissolved in the same phase the mixing time decreases resulting in a smaller final particle size. It is the diffusion time of the surfactant molecules to the coalescing droplets which is mainly decreased, resulting in a smaller final particle size, as can be seen in Fig. 2.9.

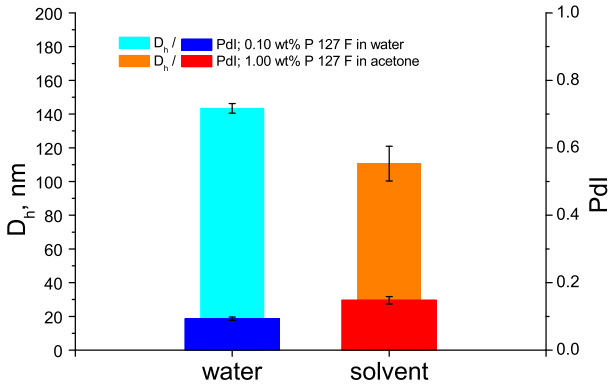

Figure 2.9: Effect of surfactant present in the organic phase or the aqueous phase. Averaged values for size and polydispersity D_h and PdI from triplicates. Results were obtained by adding 1.00 mL acetone with 5 mg PCL (25 kDa)to an aqueous solution with a volume of 10.00 mL. The surfactant, Pluronic F127, is either in the water phase (indicated by 'water') or in the acetone phase ('solvent'). The overall Pluronic F127 concentration in the final mixture is 0.1 wt%.

In case of relatively slow mixing, typically encountered in our experiments, there should be no dependence between final particle size and the molar mass of the polymer. To assess the dependency of the mixing time on the molar mass and the viscosity of the used surfactant solutions different molar masses of PVA (13-23, 31-50 and 85-124 kDa; similar degree of hydrolyzation of 87-89%) dissolved in water at different concentrations (0.10, 0.25, 0.50, 1.00 and 2.50 wt% of surfactant in water). The viscosity of these solutions was measured in order to grasp the influence of both the molar mass of the surfactant and the viscosity of the solutions in relation to the final particle size. In all experiments 5 mg PCL (25 kDa)/mL acetone was added to 10.00 mL of the different PVA/water solutions. Also here each experiment was done in triplicate after which DLS analysis was performed.

Besides a comparison of the size between these two extreme cases above we confront our theoretical predictions to the results obtained by Johnson and Prud'homme [15] who

have carefully varied τ_{mix}. They studied a somewhat different system comprising a methanol solution of an amphiphilic diblock copolymer (polybutylacrylate-b-polyacrylic acid, each block 7:5 kg/mol) quenched in water. By using a highly efficient impinging jet mixer Johnson and Prud'homme [15] succeeded in covering a very broad range of mixing times and observed various regimes, Fig. 2.10. Their original measured data for the hydrodynamic diameters of the particles formed as a function of the mixing time are shown in Fig. 2.10. The coalescence in a dispersion containing diblock copolymers must obey kinetics very similar to the one described by Eq. (2.1) and, thus, yield scaling Eq. (2.19) for the NP size. This implies that a master curve must be obtained in Fig. 2.10 if one shifts the data along the abscissa by the polymer mass fraction w_p. Moreover, a typical diameter scaling $(\tau_{\mathrm{mix}} w_{\mathrm{p}})^{1/3}$ is expected to be observed at long mixing times.

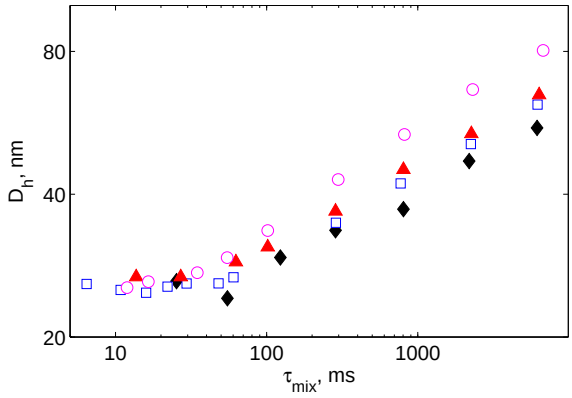

Figure 2.10: The original data from Johnson and Prud'homme [15].

One important difference between the concentration dependence of the size predicted by our theory and the work of Johnson and Prud'homme [15] is the fact that our Eq. (2.19) does not take into account the size of the surfactant layer on top of a NP. Indeed, such an approximation certainly holds in case of a polymeric surfactant. In case of diblock copolymers, however, the size of the hydrophilic corona surrounding the hydrophobic core cannot be neglected. To compute a hydrophobic core diameter from a hydrodynamic diameter of a copolymer micelle, we use the theoretical result of Daoud and Cotton [39] that the latter scales as a power 1/5 of the micelle mass. As the core of a micelle consists almost solely of the hydrophobic polymer segments, the core size scales as a power 1/3 of the mass, yielding $R_{\mathrm{core}} \propto D_{\mathrm{h}}^{5/3}$.

The data obtained by Johnson and Prud'homme [15], see Fig. 2.10, are redrawn in $D_h^{5/3}$ versus $\tau_{\mathrm{mix}} c_{\mathrm{p}}$ coordinates in Fig. 2.11. Indeed the data follow a master curve obeying Eq. (2.19): it is characterized by a typical $(\tau_{\mathrm{mix}}/\tau_{\mathrm{cls}})^{1/3}$ scaling at long mixing times and shows a plateau in the fast mixing regime, exactly as the theory predicts. Note, that the NP size in Fig. 2.11 is completely determined by the kinetics and is not related to the equilibrium diblock copolymer micelle size. Indeed the latter would depend solely on the molar mass, composition, and solvent quality, whereas the NP size is a strong function of concentration. Although the NP system is not in thermodynamic equilibrium, it is long-lived. As an x-

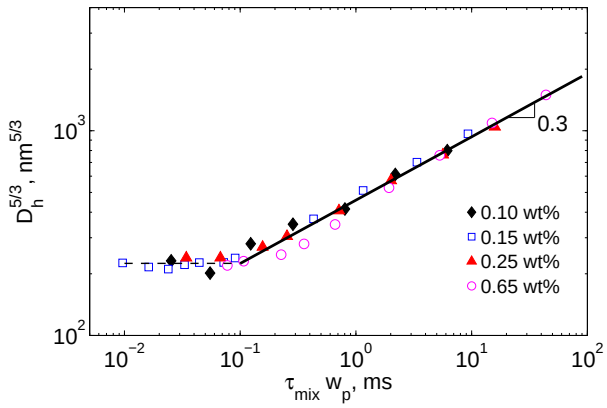

Figure 2.11: Master curve of the size of the core of the diblock copolymer NPs vs the rescaled mixing time, following the scaling predicted by Eq. (2.19), original data from Johnson and Prud'homme [15]. Note that we use the quantity w_p as polymer concentration on the abscissa. This is the weight fraction (dimensionless) which is directly linked to the mass concentration c_{mp} via the density. The quantity $w_p \tau_{mix}$ is proportional to $c_{p0} \tau_{mix}$ in Eq 2.20.

ray study on a somewhat different diblock copolymer system [40] shows, micellization of copolymers is a process consisting of two stages. The first rapid stage is totally controlled by kinetics and leads to the NP formation described in the present work. The second, a several orders of magnitude slower process, drives the NP system to the thermodynamic equilibrium. Study of this slow process is outside of the scope of the present work.

2.4.5 Surfactant molar mass influence

To assess the dependency of the mixing time on the molar mass and the viscosity of the used surfactant solutions the effect of different molar masses of PVA (13-23, 31-50 and 85-124 kDa with similar degree of hydrolyzation of 87-89%) was studied. These PVA samples were dissolved in water at different concentrations (0.10, 0.25, 0.50, 1.00 and 2.50 wt% of surfactant in water). The viscosity of these solutions was measured in order to assess the influence of both the molar mass of the surfactant and the viscosity of the solutions in relation to the final particle size. In all experiments 5 mg PCL (25 kDa)/mL acetone was added to 10.00 mL of the different PVA/water solutions. Also here each experiment was done in triplicate, followed by dynamic light scattering measurements of these samples.

In Fig. 2.12 the size obtained after nanoprecipitation as measured using DLS is plotted as a function of the solution viscosity when using PVA varying in molar mass. It is shown that the size is linearly dependent on the viscosity of the surfactant solution and slightly increases with the molar mass of the used surfactant. Based on our model, the influence of the surfactant molar mass can be explained qualitatively. Let us first focus on how particle size depends on viscosity. As the experiments are performed in excess of surfactant, one expects the final particle size scaling $R_p^{\text{end}} \sim R_{p0}(\tau_{\text{mix}}/\tau_{\text{cls}})^{1/3} \sim \tau_{\text{mix}}^{1/3}[k_{\text{B}}Tc_{mp}/(\eta\rho)]^{1/3}$. Note that the viscosity of the medium here refers to a surfactant-free environment where the coalescence of

polymer droplets takes place before surfactant penetrates into it at $t > \tau_{\text{mix}}$. Hence, η in the last form hardly depends on surfactant properties. The mixing time τ_{mix}, on the other hand, is expected to be determined by the viscosity of the surfactant solution in the vessel B in Fig. 2.5 (a): the higher the viscosity the slower the mixing.

Hence, based on the theoretical picture, one expects the final particle size to increase with increasing surfactant solution viscosity. As the viscosity has been varied by changing surfactant concentration and/or molar mass, one should anticipate surfactant solutions of different concentrations and molar masses but equal viscosities to yield roughly the same final particle size. As the experimental results in Fig. 2.12 show, indeed, the particle size is not very sensitive to the molar mass of the polymeric surfactant provided viscosity is kept constant. There is however a slight systematic increase in size with increasing molar mass. This might be due to a prolonged adsorption time needed for a larger polymeric surfactant to adsorb which is not accounted for in our theoretical description.

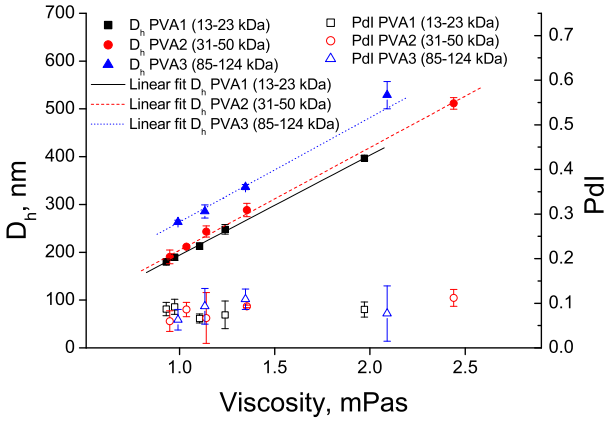

Figure 2.12: Linear dependence of the final particle size (D_h) and PdI on the surfactant molar mass and surfactant solution viscosity.

It therefore seems the influence of the molar mass of the surfactant and the viscosity of the surfactant solution is twofold. Firstly, a higher viscosity will result in a longer mixing time which increases the final particle size upon mixing. Secondly, using a higher molar mass of the surfactant will probably increase the adsorption time scale of the surfactant molecules to some degree. This might lead to the observed slight increase of the final particle size.

Finally, we remark that we assumed that the equilibrium between free surfactant and surfactants in the micelles is faster than the typical coalescence time scale. From Eq. 2.3 it follows that for a typical initial polymer concentration of 5 mg/mL for PCL with molar mass of 25 kDa the time scale for coalescence is of the order of 1 s. The typical time scale for block copolymers exchanging in a micelle is about 1 ms (see refs [41, 42]). This supports our assumption. Hence we may safely assume there is no effect of the value for the critical micelle concentration.

2.5 Conclusions

We have studied nanoprecipitation of polymers in a poor solvent in the presence of (polymeric) surfactants. The polymer is first dissolved in a good (organic) solvent, followed by a solvent switch towards a poor solvent environment in the presence of surfactant. The combined experimental and theoretical results on nanoprecipitation demonstrate that diffusion limited coalescence is a mechanism that enables an adequate description of the NP formation process. Two relevant time scales, the mixing and coalescence times, can be identified and their ratio is shown to be of a critical importance for the NP final diameter. It is shown that the final particle size is determined mainly by the surfactant concentration in the fast mixing regime. In the case of slow mixing the final particle size is also dependent on the initial concentration of the collapsing and coalescing polymers, and the mixing time. In the slow mixing regime the particle volume scales linearly with mixing time and polymer concentration.

The theoretical model illustrates that the NP size is predicted to scale in a universal manner; it is predominantly sensitive to the mixing time and the polymer concentration if the surfactant concentration is sufficiently high. The molar mass of the carrier polymer is shown to have little influence. Available experimental data corroborate the predictions of our model and provide a solid framework for tailoring NPs with *a priori* determined size, thus avoiding a laborious experimental trial and error approach.

Acknowledgments

We thank Professor R. Prud'homme for useful discussions and P.H.H. Bomans for performing the cryo-TEM analyses.

Bibliography

[1] T. Niwa, H. Takeuchi, T. Hino, N. Kunou, Y. Kawashima, J. Control. Release, **25**, 89-98 (1993).

[2] According to the IUPAC definition a nanoparticle is a particle of any shape with dimensions in the 1-100 nm range. The method of Niwa *et al*. allows to make particles in that size range. We note however that it is also possible to make larger particles using this precipitation method.

[3] K.S. Soppimath, T.M. Aminabhavi, A.R. Kulkarni and W.E. Rudzinski, J. Control. Release, **70**, 1 - 20 (2001).

[4] J. Panyam and V. Labhasetwar, Adv. Drug Deliv. Rev., **55**, 329 - 347 (2003).

[5] S. Hornig, T. Heinze C.R. Becer and U.S. Schubert, J. Mater. Chem., **19**, 3838-3840 (2009).

[6] S. Galindo-Rodriguez, E. Alleèmann, H. Fessi and E. Doelker, Pharm. Res., **21**, 1428-1439 (2004).

[7] T. Kietzke, D. Neher, K. Landfester, R. Montenegro, R. Gütner and U. Scherf, Nature Mater., **2**, 408-412 (2003).

[8] D. Peer, J.M. Karp, S. Hong, O.C. Farokhzad, R. Margalit and R. Langer, Nature Nanotechnol., **2**, 751-760 (2007).

[9] K. Koo, M.S. Huh, I.-C. Sun, S.H. Yuk, K. Choi, K. Kim and I.C. Kwon, Acc. Chem. Res., **44**, 1018-1028 (2011).

[10] N. Kamaly, Z. Xiao, P.M. Valencia, A.F. Radovc-Moreno and O.C. Farokhzad, Chem. Soc. Rev., **41**, 2971-3010 (2012).

[11] H. Lannibois, A. Hasmy, R. Botet, O.A. Chariol and B. Cabane, J. Phys. II France, **7**, 318-342 (1997).

[12] L.-T. Lee and B. Cabane, Macromolecules, **30**, 6559-6566 (1997).

[13] J. Aubry, F. Ganachaud, J.-P. Cohen Addad and B. Cabane, Langmuir, **25**, 1970-1979 (2009).

[14] K. Roger, R. Botet and B. Cabane, Langmuir, **29**, 5689-5700 (2013).

[15] B.K. Johnson and R.K. Prud'homme, Phys. Rev. Lett., **91**, 118302 (2003).

[16] T. Chen, S.M. D'Addio, M.T. Kennedy, A. Swietlow, I.G. Kevrekidis, A.Z. Panagiotopoulos and R.K. Prud'homme, Nano Lett., **9**, 2218-2222 (2003).

[17] Y. Liu, K. Kathan, W. Saad and R.K. Prud'homme, Phys. Rev. Lett., **98**, 036102 (2007).

[18] M. Akbulut, P. Ginart, M.E. Gindy, C. Therihault, K.H. Chin, W. Soboyejo and R.K. Prud'homme, Adv. Funct. Matter, **19**, 718-725 (2009).

[19] D. Horn and J. Rieger, Angew. Chem. Int. Ed., **40**, 4339-4361 (2001).

[20] C. Vauthier and K. Bouchemal, Pharm. Res., **26**, 1025-1058 (2009).

[21] T.H. Whitesides and D.S. Ross, J. Colloid Interface Sci., **169**, 48-59 (1995).

[22] S.J. Marrink, D.P. Tieleman and A.E. Mark, J. Phys. Chem. B, **14**, 12165-12173 (2000).

[23] T. Chen, A.-P. Hynninen, R.K. Prud'homme, I.G. Kevrekidis, and A.Z. Panagiotopoulos, J. Phys. Chem. B, **112**, 16357-16366 (2008).

[24] J.G.J.L Lebouille, T. Kockelkoren, L.F.W. Vleugels, R. Tuinier, **US 0223206 A1** (2011).

[25] J.G.J.L. Lebouille, R. Tuinier, L.F.W. Vleugels, M.A. Cohen Stuart and F.A.M. Leermakers, Soft Matter, **9**, 7515-7525 (2013).

[26] J.G.J.L. Lebouille, L.F.W. Vleugels, A. Dias, F.A.M. Leermakers, M.A. Cohen Stuart and R. Tuinier, Eur. Phys. J. E, **36**, 107 (2013).

[27] L.G.B. Bremer, T. Van Vliet and P. Walstra, J. Chem. Soc., Farad, Trans. 2, **85**, 3359-3372 (1989).
[28] L.G.B. Bremer, B.H. Bijsterbosch, R. Schrijvers, T. Van Vliet and P. Walstra, Colloids Surfaces, **51**, 159-170 (1990).
[29] L.G.B. Bremer, B.H. Bijsterbosch, P. Walstra and T. van Vliet, Adv. Colloid Interface Sci., **46**, 117-128 (1993).
[30] D. Ben-Avraham, Phys. Rev. Lett., **81**, 4756 (1998).
[31] R. Stepanyan, J.G.J.L. Lebouille, J.J.M. Slot, R. Tuinier and M.A. Cohen Stuart, Phys. Rev. Lett., **109**, 138301 (2012).
[32] J. Keizer, Chem. Rev., **87**, 167-180 (1987).
[33] M. von Smoluchowski, Kolloid Z., **18**, 48-54 (1916).
[34] M. von Smoluchowski, Kolloid Z., **21**, 98-104 (1917).
[35] W.B. Russel, D.A. Saville and R. Schowalter, *Colloidal Dispersions* (Cambridge University Press, Cambridge, 1989).
[36] M. Doi and S. Edwards, *The Theory of Polymer Dynamics* (Clarendon Press, Oxford, 1986).
[37] G.J. Fleer, M.A. Cohen Stuart, J.M.H.M. Scheutjens, T. Cosgrove, and B. Vincent, *Polymers at Interfaces* (Chapman and Hall, London, first edition, 1993).
[38] J. Molpeceres, M. Guzman, M.R. Aberturas, M. Chacon and Y. Kawashima, J. Control. Release, **85**, 206-213 (1996).
[39] M. Daoud and J.P. Cotton, J. Phys. Paris, **43**, 531-538 (1982).
[40] R. Lund, L. Willner, M. Monkenbusch, P. Panine, T. Narayanan, J. Colmenero and D. Richter, Phys. Rev. Lett., **102**, 188301 (2009).
[41] R. Lund, L. Willner, J. Stellbrink, A. Radulescu and D. Richter, Phys. B, **350**, 909-919 (2004).
[42] R. Lund, L. Willner and D. Richter, Macromolecules, **39**, 4566-4575 (2006).

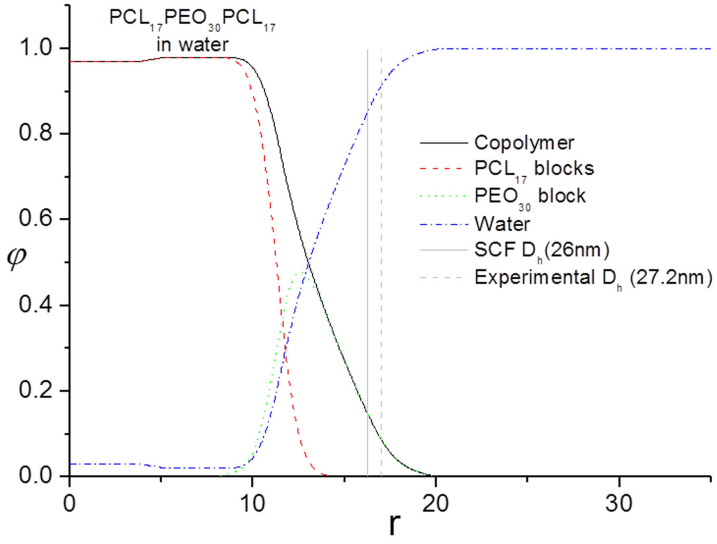
PCL17PEO30PCL17
in water
1.0
0.8
0.6
0.4
0.2
0.0
φ
0
10
20
30
r
Copolymer
PCL17 blocks
PEO30 block
Water
SCF Dh(26nm)
Experimental Dh (27.2nm)

SF-SCF predictions for spherical biocompatible triblock copolymer micelles

3

This chapter was published as:
J.G.J.L. Lebouille, R. Tuinier, L.F.W. Vleugels, M.A. Cohen Stuart and F.A.M. Leermakers , SF-SCF predictions for quenched spherical biocompatible triblock copolymer micelles, Soft Matter, **9**, 7515-7525 (2013).

Abstract

We have used the Scheutjens-Fleer self-consistent field (SF-SCF) method to predict the self-assembly of triblock copolymers with a solvophilic middle block and sufficiently long solvophobic outer blocks. We model copolymers consisting of polyethylene oxide (PEO) as solvophilic block and poly(lactic-co-glycolic) acid (PLGA) or poly(ε-caprolactone) (PCL) as solvophobic block. These copolymers form structurally quenched spherical micelles provided the solvophilic block is long enough.

Predictions are calibrated on experimental data for micelles composed of PCL-PEO-PCL and PLGA-PEO-PLGA triblock copolymers prepared via the nanoprecipitation method.

We establish effective interaction parameters that enable us to predict various micelle properties such as the hydrodynamic size, the aggregation number and the loading capacity of the micelles for hydrophobic species that are consistent with experimental finding.

keywords: Micelle, Scheutjens-Fleer Self-Consistent Field theory (SF-SCF), block copolymers, encapsulation.

3.1 Introduction

Surfactants, amphiphiles and copolymers in selective solvents are widely used to create micelles. For several applications the size, size distribution, loading capacity and stability (upon dilution) are requirements of great importance. It is feasible to invoke the statistical thermodynamical machinery on invariably coarse grained models to find detailed information on self-assembly phenomena. However, the insights from this have a qualitative rather than a quantitative character because of a lack of suitable parameter sets for such systems. This is why in practice the selection of appropriate copolymers capable of forming micelles with pre-set requirements is still based on trial and error or on experience rather than on theory. Confronting theory with experiments is the only way to improve this situation.

In this paper our focus is on triblock copolymers in a selective solvent (water). Several triblock copolymers have been studied both from a theoretical- [1–6] as well as from a practical [7–10] perspective, see Chapter 4. Many of these polymers, such as the poloxamers, were selected to have a finite (reasonably high) solubility in water, implying that if the systems are diluted below their critical micelle concentration (CMC), the micelles break up into freely dissolved unimers. When these micelles are used to encapsulate compounds then, upon dilution below the CMC, their cargo is released. We study biocompatible triblock copolymers that have a very limited water solubility. The micelles may still be used as drug carriers as one can employ alternative release strategies [11]. More specifically, we use copolymers made from PLGA [12] or PCL [13] as the hydrophobic fragment and PEO as the hydrophilic species. The PLGA and PCL blocks are biodegradable by hydrolysis of the esters and or are subject to enzymatic degradation [14–17] and the PEO block is mainly excretable via the renal pathway [18, 19].

The block lengths of the PLGA-PEO-PLGA and PCL-PEO-PCL polymers are chosen such that they exhibit ultra-low water solubilities. Experimentally one can reproducibly fabricate micellar objects by the precipitation method and the corresponding micelles may be referred to as frozen or 'dead' because after their formation they do not dissolve by dilution. Our interest is in the modeling of these structurally quenched systems by using an equilibrium self-consistent field (SCF) theory. This is not a trivial exercise because the micellar system clearly violates the important prerequisite of equilibration. We may justify our approach *postiori*, because for a particular set of interaction parameters it is found that there exists a good correlation between the predicted micelle structure and experimental observations.

Association colloids composed of molecules in strongly selective solvents have a densely packed core and a solvated corona. Based on this, particularly in the surfactant literature, the surfactant packing parameter $P = v/(a_0 \times l_c)$ is used to assess the capability of some amphiphile to form a certain association colloid. Here v is the volume of the hydrophobic block(s) (tails), l_c is the length of the tail(s) and a_0 is the surface area occupied by the polar fragments (head) at the CMC. For $P < 1/3$ spherical micelles are preferred, whereas for $1/3 < P < 1/2$ cylindrical micelles form. In the range $1/2 < P < 1$ vesicles, for $P \approx 1$ planar bilayers and for $P > 1$ reversed spherical micelles are expected [20, 21]. For surfactants that have relatively short tails with little conformational degrees of freedom, the main problem in using the packing parameter concept is to estimate a_0. This quantity can be derived from experiments. For polymeric self-assembly there are more hurdles to take. In addition to the issue to know the area per 'head' group, it is important to account for the conformational degrees of freedom of the copolymers.

In the field of polymer self-assembly it is known that the thermodynamic stability of micelles depend on the size of the core compared to that of the corona [22, 23]. More specifically, a particular geometry is stable when the corona is large compared to the core. Considering, for example, micelles of which the corona is relatively small, the system is expected to reduce the curvature. In the cylindrical geometry the ratio between surface area and volume is less and the corona chains are forced to stretch outward in the radial direction so that the size of the corona increases compared to the core. With a similar argument one can envision the choice of a system for the lamellar phase. In order to use this insight as a predictive tool, one must get involved in the field of polymer brushes and in particular the physics of curved polymer brushes. The analytical methods to estimate the core and corona sizes is mostly limited to scaling relations which must be somehow calibrated.

By using the SF-SCF theory and evoking a molecularly realistic model of the polymers, we can resolve these problems to a large extend. This gives us the capability to predict structural properties of the micelles for given composition of the copolymers.

In the following we will first give a brief introduction on the SF-SCF theory for micellisation. Subsequently our results are discussed and compared to experimental data presented in more detail in the companion publication [7], see Chapter 4. In our conclusions we elaborate on the use of an equilibrium theory to describe micelles formed by the precipitation method.

3.2 SF-SCF Theory

3.2.1 Thermodynamic considerations

Micellar solutions are macroscopically homogeneous. First and second law of thermodynamics for homogeneous solutions with $i = 1,2,\cdots,c$ different molecular components, the total numbers of molecules of the i^{th} component n_i, consisting of c components with a chemical potential of all components μ_i, give for the change of the internal energy $\mathrm{d}U$ for a homogeneous phase:

$$\mathrm{d}U = T\mathrm{d}S - p\mathrm{d}V + \sum_i^c \mu_i \mathrm{d}n_i \quad , \tag{3.1}$$

where the sum is over all molecular components, S is the entropy and V the system volume. For systems at a given temperature T and pressure p it is often better to turn to the Gibbs energy $G \equiv U - TS + pV$ and the change in the Gibbs energy reads:

$$\mathrm{d}G = -S\mathrm{d}T + V\mathrm{d}p + \sum_i^c \mu_i \mathrm{d}n_i \quad . \tag{3.2}$$

Classical thermodynamics cannot account for micellisation as specific correlations between molecules are fully acceptable from a thermodynamic perspective and the equations in the presence or in the absence of some finite size aggregates are completely the same. Equations only start to be different as soon as macroscopic phase changes occur.

Motivated by the knowledge that on some microscopic level the system is inhomogeneous, it may be of interest to consider the small system approach advocated by Hill [24]. Hill suggested that when there is a hidden parameter, here the number of micelles $\mathscr{N}$, there is an intensive quantity ε, which Hill referred to as the sub-division potential, coupled to the

number of micelles and the change of the Gibbs energy reads:

$$\mathrm{d}G = -S\mathrm{d}T + V\mathrm{d}p + \sum_{i}^{c} \mu_i \mathrm{d}n_i + \varepsilon \mathrm{d}\mathscr{N} \quad . \tag{3.3}$$

From Eq. 3.3 it follows that the sub-division potential is the work (Gibbs energy) needed to increase the number of micelles for given number of molecules, pressure and temperature. In equilibrium the Gibbs energy should be minimized. This must also apply to the dependence of the Gibbs energy on the number micelles:

$$\left(\frac{\partial G}{\partial \mathscr{N}}\right)_{T,p,\{n_i\}} = \varepsilon = 0 \tag{3.4}$$

and the second derivative of the Gibbs energy with number of micelles should be positive. In words, Eq. 3.4 expresses that in equilibrium there is no Gibbs energy associated to the formation of micelles and under these conditions Eq. 3.3 returns to Eq. 3.2 obviously. Hence the small system approach is consistent with (macroscopic) thermodynamics. The interesting point of the small system approach is that Scheutjens-Fleer Self-Consistent Field (SF-SCF) theory considers the system on the small system level and the small system thermodynamics approach becomes meaningful. In these calculations we focus on one micelle in the center of the spherical coordinate system of which we can change the aggregation number (by considering the number of copolymers in the small system). We may use Eq. 3.4 to select the relevant number of polymers per micelle.

Returning to Eq. 3.3 we notice that $G = \sum_i \mu_i n_i + \varepsilon \mathscr{N}$. The Gibbs energy per micelle is thus: $G/\mathscr{N} = \sum_i \mu_i n_i/\mathscr{N} + \varepsilon$ from which it follows that ε is interpreted as the excess Gibbs energy per micelle. This quantity is also referred to as the grand potential Ω per micelle. Hence, equilibrium in the SF-SCF protocol for micellisation is defined by the grand potential of the micelle being zero. Below we will return to this issue obviously.

3.2.2 SF-SCF machinery

We use the classical SF-SCF model for self-assembly, which in the context of surfactant micellisation has been presented in the literature several times [1, 25–27]. Here we will only outline the most important features so that the results of the modeling can be discussed properly. We will pay attention to (i) the discretization scheme, (ii) the molecular model, (iii) the optimization of the free energy, (iv) the propagator scheme and (v) the grand potential in the following subsections.

3.2.2.1 The discretization

The SF-SCF model is lattice based. This means we have to define exactly how the lattice sites are organized. Here and below we focus on the spherical lattice. We consider lattice sites with linear length b and volume b^3. The lattice sites are arranged in lattice layers with spherical topology. Starting with a central point at $r = 0$, we have layers of lattice sites at coordinate $r = 1, 2, \cdots, M$, which are a distance rb away from the center. The number of lattice sites at coordinate r is given by $L(r) = \frac{4}{3}\pi\left(r^3 - (r-1)^3\right) \approx 4\pi r^2$, where the approximation on the rhs of this equation (which is accurate only for large values of r) shows that the number of sites is related to the area of the shell at distance rb from the center. In this coordinate system

we need to compute so-called site averages defined by a three-layer average of some spatially varying quantity $\Phi(r)$, for which we use the angular bracket notation defined by:

$$\langle\Phi(r)\rangle \equiv \lambda_{r,r-1}\Phi(r-1) + \lambda_{r,r}\Phi(r) + \lambda_{r,r+1}\Phi(r+1) \quad . \tag{3.5}$$

In this equation the *a priori* step probabilities account for the geometry

$$\lambda_{r,r-1} = \lambda\,\frac{4\pi(r-1)^2}{L(r)} \quad , \tag{3.6}$$

$$\lambda_{r,r+1} = \lambda\,\frac{4\pi r^2}{L(r)} \quad , \tag{3.7}$$

$$\lambda_{r,r} = 1 - \lambda_{r,r-1} - \lambda_{r,r+1} \quad . \tag{3.8}$$

For a cubic lattice, the limiting values, that is for large values of r, of the step probabilities are $\lambda_{r,r-1} = \lambda_{r,r+1} = \frac{1}{6}$ and $\lambda_{r,r} = \frac{4}{6}$. For small values of r there is curvature information in the transition probabilities.

The SF-SCF theory makes use of the mean-field approximation. In practice this means that we are going to average various properties over all sites $L(r)$ at a particular coordinate r.

3.2.2.2 The molecular model

Scheutjens and Fleer promoted the idea that the polymeric species should be expressed in segments that fit on the lattice. In other words, a coarse-grained description of the polymer chains is implemented. In this approach the polymers are considered as a string of segments with linear length b. Let us for convenience number the different molecules with the index i and focus on linear chains of which the segments have ranking numbers $s = 1,2,\cdots,N$. where N is the total number of segments in the chain. The chain topology is an input for the calculations. This means that we have to specify exactly what the segment type is of each segment. Segment types are generically referred with the index X. For example, we may consider the symmetric triblock copolymers $A_{N_A}B_{N_B}A_{N_A}$, which has segments of type $X = A$ for the ranking numbers $s = 1,2,\cdots,N_A$ and $s = N_A + N_B + 1,\cdots,2N_A + N_B$, and $X = B$ for the remaining ones $s = N_A + 1,\cdots,N_A + N_B$. Besides polymeric species there may also be monomeric compounds in the system. These are treated similar to the chains, yet they have just one segment $s = 1$. Below we will assume that the solvent has a segment type S and is monomeric.

For convenience we introduce the so-called chain architecture operators

$$\delta^A_{s,i} = \begin{cases} 1 & \text{when segment } s \text{ of molecule } i \text{ is of type } A \\ 0 & \text{otherwise} \end{cases} \quad . \tag{3.9}$$

These values of these operators are fully defined by the input data.

The target of the SF-SCF equations is to find the equilibrium distribution of all segments and segment types in the coordinate system. The dimensionless concentration of segments of type X at coordinate r is given by the volume fraction $\varphi_X(r)$, which is given by the ratio between the number of segments of type X at this coordinate and the number of sites available:

$$\varphi_X(r) = \frac{N_X(r)}{L(r)} \quad . \tag{3.10}$$

The SF-SCF theory is based on a mean-field free energy expression. This expression features besides the segment volume fractions also segment potentials $u_X(r)$. Physically, the segment potentials should be interpreted as the work needed to bring segment X from the bulk to the coordinate r. From this definition it follows that in the bulk the segment potentials are zero.

3.2.2.3 The free energy and the optimization

In the calculation, the volume occupied by the M lattice layers and the number of molecules are specified. Hence, the Gibbs energy is the primary thermodynamic potential in the system. Schematically the Gibbs energy G can be presented as

$$\begin{aligned} G(\{\varphi\},\{u\},\alpha) = \\ -\ln Q(\{u\}) - \sum_r L(r) \sum_X u_X(r)\varphi_X(r) + F^{\text{int}}(\{\varphi\}) \\ -\sum_r L(r)\alpha(r)\left(1-\sum_X \varphi_X(r)\right) \quad . \end{aligned} \tag{3.11}$$

Here and below we normalize all energies by the thermal energy kT. The first term on the rhs of this equation features the mean-field partition function Q, which can be computed once the segment potentials are known. In the mean-field approximation it is composed of single-chain partition functions:

$$Q = \Pi_X \frac{(q_X(\{u\}))^{n_X}}{(n_X)!} \quad . \tag{3.12}$$

Where q_X is the single-chain partition function of the molecule type X, which in turn can be computed once the segment potentials are available. To compute this quantity it is necessary to specify the chain model. Below we will go in more detail. In Eq. 3.12 the variable n_X is the number of molecules of type X in the system.

The third term on the rhs of Eq. 3.12 expresses the free energy of interaction in the system. Again, we will go in more detail below. Here it suffices to mention that it can be evaluated once the volume fractions are known.

The second term on the rhs transforms the free energy which is specified in the potential domain (as expressed by the first term) to the classical free energy in the (n,V,T) ensemble.

The fourth term implements the incompressibility constraint for each coordinate. In other words, the value of the Lagrange field $\alpha(r)$ is coupled to the requirement that on each coordinate the volume fractions add up to unity. In passing we note that in the incompressible system there is no volume work and the Gibbs energy is the same as the Helmholtz energy.

Eq. 3.12 has dependences on the segment volume fractions, the segment potentials and the Lagrange field. The free energy as expressed in Eq. 3.12 not automatically has physical significance: it needs to be minimized with respect to the volume fractions and maximized with respect to the segment potentials and the Lagrange field. In equations we are looking for the so-called SF-SCF point for which:

$$\frac{\delta G}{\delta \varphi_X(r)} = 0 \quad , \tag{3.13}$$

$$\frac{\delta G}{\delta \alpha(r)} = 0 \quad , \tag{3.14}$$

$$\frac{\delta G}{\delta u_X(r)} = 0 \quad . \tag{3.15}$$

Eq. 3.13 leads to an expression for the segment potentials in term of the volume fractions. Here we take a Flory-Huggins [27] type Ansatz, wherein only nearest-neighbor interactions are accounted for. It implements the Bragg-Williams approximation [28] and use Flory-Huggins interaction parameters χ to specify the strength of the interactions which has non-trivial values for the unlike contacts only

$$u_X(r) = \alpha(r) + \sum_Y \chi_{XY} \left(\langle \varphi_Y(r) \rangle - \varphi_Y^b \right) \quad , \tag{3.16}$$

where the summation runs again over all segment types and φ_Y^b is the volume fraction of segments of type Y in the bulk.

Eq. 3.14 enforces that system obeys the compressibility constraint, that is:

$$\sum_X \varphi_X(r) = 1 \quad . \tag{3.17}$$

Last, but not least Eq. 3.15 leads to the rule to compute the volume fractions from the potentials. Formally the result is

$$\varphi_X(r) = -\frac{1}{L(r)} \frac{\partial \ln Q}{\partial u_X(r)} \quad . \tag{3.18}$$

The computation of the functional derivative $\partial \ln Q / \partial u_X(r)$ is, in general, rather hard. For a freely-jointed chain, however, there exist an extraordinary efficient propagator formalism which exactly computes the volume fraction as specified by Eq. 3.18. This formalism is outlined in the next paragraph.

3.2.2.4 The propagator formalism

Motivated by the close analogy between the diffusion of a Brownian particle and the flight of a random walk, there exist a diffusion-like equation to evaluate the partition function of Gaussian chains. Edwards [29] realized that the difference between the diffusion process and the polymer chain is that the polymer cannot visit previously occupied sites. This is known as the excluded-volume problem. He came up with a modified diffusion equation, which corrects, in first order, for the volume interactions which in spherical coordinates reads:

$$\frac{\partial G}{\partial s} = \frac{1}{6} \left(\frac{1}{r^2} \frac{\partial}{\partial r} r^2 \frac{\partial G}{\partial r} \right) - uG \quad , \tag{3.19}$$

which must be supplemented with initial and boundary conditions. The quantity $G = G(r;s)$ which obeys to this differential equation is related to the partition function and can be used to compute the volume fraction distribution for a given chain molecule. We map this differential equation onto the lattice. Here we cannot go in full details and discuss the resulting formalism instead. By implementing it, the chain model changes from the Gaussian chain to the freely jointed one. The fundamental difference being that formally the chain ends can be separated beyond the contour length in the Gaussian chain, whereas it is not possible in the freely

jointed model (finite extensibility).

Let's introduce the free segment distribution function for a segment type X as $G_X(r) = \exp[-u_X(r)]$, which is the Boltzmann weight for a segment X at location r. We generalize this quantity to the chain type i and ranking number s dependent quantity by using the chain architecture operators:

$$G_i(r,s) = \sum_X G_X(r)\delta_{i,s}^X \quad . \tag{3.20}$$

We may start for molecule i the propagators by setting the statistical weight for the first segment to the free segment distribution function: $G_i(r;1) = G_i(r,1)$. End point distribution functions for segments s along the chain now depend on similar quantities for segment $s-1$ according to the propagator:

$$G_i(r;s) = G_i(r,s)\,\langle G_i(r;s-1)\rangle \quad , \tag{3.21}$$

where the angular brackets are defined in Eq. 3.5. The end-point distribution of the terminal segment is related to the single-chain partition function:

$$q_i = \sum_r L(r)G_i(r;N) \quad . \tag{3.22}$$

In the general case one has to compute also the complementary end-point distribution functions before the volume fractions can be evaluated. As in our case the triblock copolymers are symmetric we can make use of a shortcut and compute the volume fractions by:

$$\varphi_i(r,s) = \frac{n_i}{q_i}\frac{G_i(r;s)G_i(r;N-s+1)}{G_i(r,s)} \quad , \tag{3.23}$$

where a chain fragment with s segments is combined with one with $N-s+1$ segments. The normalization with the free segment distribution is needed to correct for the fact that both walks already have the statistical weight for the connecting segment.

In passing we note that the normalization in Eq. 3.23 can be used to evaluate the volume fractions in the bulk. It can be shown that $\frac{n_i}{q_i} = \varphi_i^b/N_i$. The volume fractions in the bulk for the various segment types X follow trivially from the bulk volume fractions per molecule.

The volume fraction profile of the solvent reads:

$$\varphi_S(r) = \varphi_S^b G_S(r) \quad , \tag{3.24}$$

wherein the volume fraction of solvent in the bulk is given by $\varphi_S^b = 1 - \sum_X' \varphi_X^b$; the prime on the summation sign indicates that in the sum $X = S$ is not included. The latter equation enforces that the bulk is incompressible.

3.2.2.5 The SF-SCF solution and the grand potential

The previous paragraph outlined how the volume fractions can be computed from the potentials and Eq. 3.16 implemented the evaluation of the potentials from the volume fractions. Numerically we search for the so-called self-consistent field solution for which the potentials and the volume fractions are mutually consistent (we implemented a precision of at least 7 significant digits), while at the same time the incompressibility constraint is obeyed. When this solution is found, which typically takes only a few seconds CPU time on a modern PC, we can evaluate the free energy of Eq. 3.12. Starting from the free energy we can extract various other thermodynamic potentials. Relevant for self-assembly we should compute the

grand potential. It is possible to evaluate the grand potential Ω from the summation over the grand potential density: $\Omega = \sum_r L(r)\omega(r)$ and in turn the grand potential density $\omega(r)$ is given by

$$\omega(r) = -\sum_i \frac{\varphi_i(r) - \varphi_i^b}{N_i} - \alpha(r) - \frac{1}{2}\sum_{X,Y} \chi_{XY}\left(\varphi_X(r)\langle\varphi_Y(r)\rangle - \varphi_X^b\varphi_Y^b\right) \quad , \tag{3.25}$$

which may be interpreted as a local tangential pressure in the micelle.

In the section on the thermodynamics of micelle formation we already mention that the sub-division potential is related to the grand potential Ω. The formal difference between these two quantities is that in the grand potential as found in the SF-SCF model, the translational entropy of the micelle as a whole is not accounted for, whereas in the sub-division potential the translational entropy is part of it. We will consider polymer micelles for which the degrees of freedom in the translation of the micelle as a whole can be ignored with respect to other contributions, and therefore it is reasonable to equate the grand potential to the sub-division potential. Hence, our interest will be in micelles that have a vanishing grand potential only. As this point is rather subtle, we will pay more close attention to the thermodynamic stability of micelles at the start of the results section.

3.2.3 The Kuhn lengths

The calculations are targeted to model copolymers with PEO, PCL and PLGA blocks, see Fig. 3.1. For polymeric compounds it is required to describe the chains as Kuhn chains, so that each segment can assume any position in space with respect to the previous segment except for back folding. Since the PEO parts of the copolymers stick into the aqueous solution, and the flexibility of the PLGA and PCL parts do not have a very different chain stiffness chains, we use the Kuhn length of PEO chains, being $b = 0.8$ nm [30], as lattice unit in the SF-SCF computations. Each unit in terms of r thus equals 0.8 nm. For instance for a PEO chain with a molar mass of 6.0 kDa consists of $N = M/M_{mon} = 6000/44 \approx 136$ segments, M_{mon} being 44 g/mol for PEO. Each ethylene oxide monomer has a length of 0.36 nm. Hence a Kuhn segment consists of $0.8/0.32 \approx 2.22$ real segments. This means the number of Kuhn segments equals $136/2.22 \approx 60$ segments [30]. In a similar fashion we can estimate the effective number of Kuhn segments for PCL and PLGA blocks and we come to the numbers listed in Table 3.1.

Table 3.1: Number of Kuhn segments (N_K) of blocks used in the copolymers studied.

Blocks in copolymers	N_K
PEO 6.0 kDa	60
PEO 3.0 kDa	30
PLGA 7.5 kDa	60
PLGA 3.75 kDa	30
PCL 1.9 kDa	17

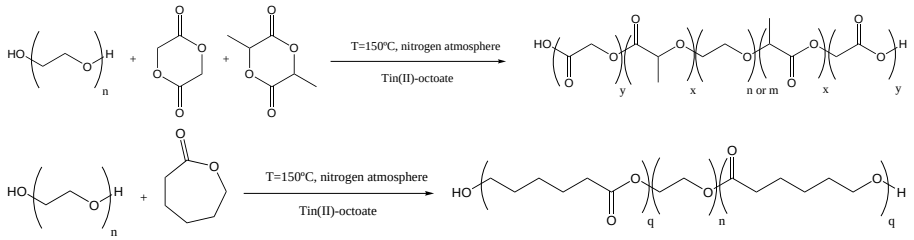

Figure 3.1: Schematic of the ring-opening polymerization of the triblock copolymers. In our case $x = y$, and $x + y$ is the number of D,L-Lactide and Glycolide repeating units randomly distributed in the hydrophobic end blocks. In the case of $m = 136$ ethylene oxide repeating units $x + y$ is 115, referred to as TBB1, and for $n = 68$ ethylene oxide repeating units $x + y$ is 58, referred to as TBB2 for the PLGA based triblock copolymers. For the PCL based triblock copolymer, referred to as TBC1, there are $n = 68$ ethylene oxide repeating units with $q = 17$ caprolactone repeating units.

3.2.4 The Flory-Huggins parameters

A key moment is to estimate the Flory-Huggins parameters between all components in the mixtures. It must be noted that the values of the interaction parameters should represent the average solvent quality upon solvent exchange upto the point that the micelles become kinetically frozen. It is known that PEO monomers are well-soluble in water at room temperature and often a χ-parameter of 0.4 is used for describing PEO chains in water [31]. PCL and PLGA are not soluble in water. The χ-parameters of their monomers must be bigger than 0.5. It is also known that the monomers in PCL are more hydrophobic than those in PLGA. Some preliminary calculations resulted in a set of χ-parameter summarized in Table 3.2. We note that we did not try to fine-tune the χ-values and mention that the reasonable comparison with experiments justifies the values used.

Table 3.2: χ-Parameters for the monomer-solvent interaction used in SF-SCF computations (EG: ethylene glycol, LGA: Lactic-co-glycolic acid and CL: caprolactone. The block lengths and the corresponding Kuhn lengths are collected in Table 3.1.

Monomer-solvent interaction	χ
EG - water	0.4
LGA - water	1.6
CL - water	3.0
LGA - EG	1.0
CL - EG	1.0

3.3 Results

Grand potential and equilibrium micelle

The SF-SCF model focuses on the most likely micelle for a system with specified copolymer chain, interaction parameters and concentration in a selective solvent. In the calculations there exists one single micelle in the center of the coordinate system bounded by M spherical lattice layers. For a given number of copolymers in the system, it is possible to compute the aggregation number g, defined by the excess number of copolymers in the micelle, i.e., $g = \frac{1}{N_i}\sum_r L(r)(\varphi_i(r) - \varphi_i^b)$. Above it was argued that thermodynamically stable micelles obey to $\varepsilon = 0$. In the SF-SCF model we compute the grand potential $\Omega(g)$ of a micelle that is at the center of the coordinate system and thus the micelle without translational degrees of freedom. For not too concentrated micellar solutions we may write

$$\varepsilon = \ln \varphi_m + \Omega \quad . \tag{3.26}$$

The quantity Ω is the grand potential of the micelle of which the translational degrees of freedom are frozen as indicated above. Adding $-TS/k_BT = -S/k_BT \approx \ln \varphi_m$ takes into account the mixing entropy. This yields the standard state subdivision potential ε [24] which equals zero under equilibrium conditions. Note again that all terms are normalized by kT. Using Eq. 3.26 we may compute the volume fraction of micelles from the grand potential, i.e. $\varphi_m(g) = \exp[-\Omega(g)]$. Clearly, $\Omega \geq 0$ or else the micelle volume fraction exceeds unity and clearly micelles with $\Omega >> 1$ can only exist at extremely low micelle concentrations.

From the above it is evident that it is necessary to analyze the grand potential Ω of the micelle as a function of g [1, 32]. In Fig. 3.2 we present, as an example, SF-SCF results for the grand potential for a spherical micelle composed with g $PLGA_{60}PEO_{60}PLGA_{60}$ copolymers. These copolymers contain three blocks of 60 segments each and is described using the χ-parameters of Table 3.2. For a micelle consisting of just a few copolymers Ω increases with g, analogously to the nucleation of small droplets in an oversaturated solution. These micelles are thermodynamically unstable due to the large surface-to-volume ratio. Indeed as long as $\partial\Omega/\partial g > 0$, the micelle is unstable (free energy has a local maximum), implying that micelles with this aggregation number will have a vanishing low probability. From Fig. 3.2 it is seen that for $g > 100$ the grand potential becomes a decreasing function of g. This is the signature of micelles that become thermodynamically stable (free energy has a local minimum).

The first micelles, that is when $\partial\Omega/\partial g = 0$, that are stable have an aggregation number $g = g^* \approx 100$ and the concentration in solution for this system may be identified as the CMC. For micelles with $g > g^*$ the grand potential decreases with aggregation number, that is $\partial\Omega/\partial g < 0$. The chains in the corona of the micelles are packed closer and closer to each other and this generates a pressure in the corona that opposes the growth of the micelles.

In the example of Fig. 3.2 the micelle concentration at the CMC is exceedingly low. From a practical point of view we should therefore focus on micelles that have a higher aggregation number. In surfactant problems it has been advised to focus on micelles with a reasonable amount of translational entropy, e.g., $\Omega(g) \approx 10\ k_BT$, implying a volume fraction of micelles that are still dilute, but measurable by light scattering.

Using this Ansatz, we extract from Fig. 3.2 that most-likely micelles consisting of $PLGA_{60}PEO_{60}PLGA_{60}$ copolymers are composed of on average 237 copolymers. Of course one should expect that in practice there are fluctuations in micelle composition. In other

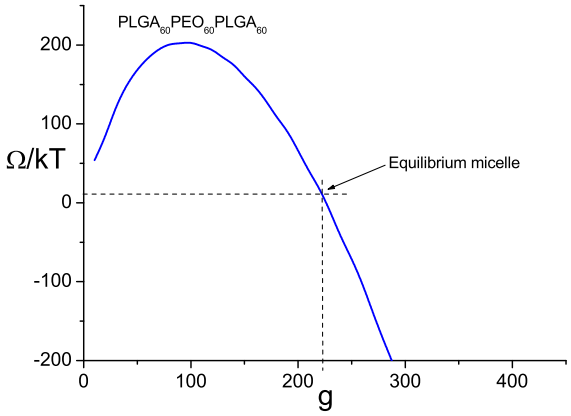

Figure 3.2: Grand potential of formation of a micelle consisting of $PLGA_{60}PEO_{60}PLGA_{60}$ of triblock copolymers as a function of the number of copolymers per micelle (g).

words that micelles with a smaller or larger aggregation number must be expected. Within the SF-SCF model it is also possible to estimate the width of the micelle size distribution.

From statistical thermodynamics it follows that $\partial g/\partial \mu = \langle g^2 \rangle - \langle g \rangle^2 = \delta g$, often referred to as the dispersion of fluctuations (in our case fluctuations in the micelle size), wherein μ is dimensionless. It can be shown that the Sf-SCF equations obey the Gibbs-Duhem relation

$$\partial \Omega / \partial \mu = -g \quad .$$

Multiplication of both sides with $\partial \mu / \partial g$ results in

$$\frac{\partial \Omega}{\partial g} = -\frac{g}{\delta g} \quad . \tag{3.27}$$

We give the resulting micelle size distribution in Fig. 3.3, assuming a Gaussian size distribution. The polydispersity, as predicted by the SF-SCF model, is very narrow; the standard deviation is just 4%. It should be realized that SF-SCF is based on a mean-field approach in which shape fluctuations are not accounted for and therefore we expect that the size distribution is somewhat underestimated. As compared to the experimental counterpart we further expect that the theory underestimates the width of the size distribution because in the experimental samples the polymers are both polydisperse in the overall molecular weight as well as with respect to the block sizes. A more detailed SF-SCF analysis can be implemented to account for a distribution of chain lengths. Here we can not do this because the detailed information about the distributions is not yet available.

In Fig. 3.4 we demonstrate what happens when the PEO block length is increased, while keeping the chain lengths of the PLGA blocks fixed. It follows that the equilibrium number of copolymers per micelle is decreasing with increasing chain length of the PEO block. This effect can easily be rationalized considering the packing arguments. The outside of the copolymer micelle must be covered with solvophilic polymer blocks being PEO. Obviously, a certain amount of PEO on the outside of the micelles is required in order to provide sufficient stability. As the PEO block length increases at given g there is more PEO on the outside of the micelle. Hence g can be lowered to maintain the same stability of a micelle.

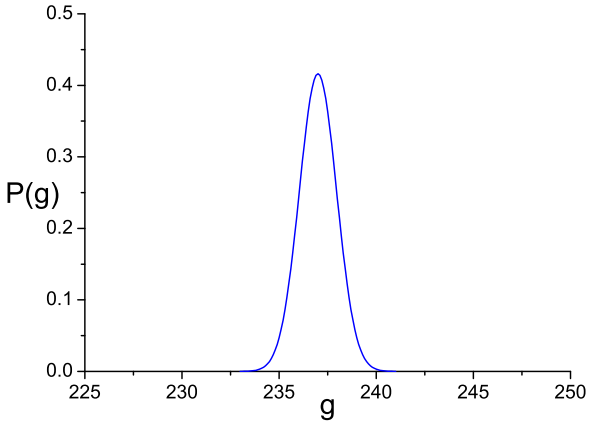

Figure 3.3: Probability distribution of the number of copolymers (g) per micelle for a micelle of $PLGA_{60}PEO_{60}PLGA_{60}$ triblock copolymers.

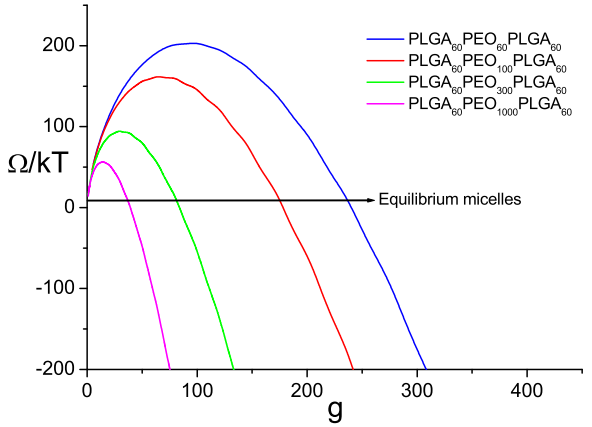

Figure 3.4: Grand potential of formation of a micelle consisting of $PLGA_{60}PEO_{N_X}PLGA_{60}$ triblock copolymers with varying PEO chain lengths N_X for $N_X = 60$ and larger.

In Fig. 3.5 we show stability curves for the case of decreasing the PEO chain length. The most like micelle size, that is g-value, increases with decreasing PEO chain length, as can be expected from the results in Fig. 3.4. When the length of the PEO moiety is decreased there exists a limit below which spherical micelles can no longer find their tensionless state. This is illustrated in Fig. 3.5. When the length of PEO is decreased towards a value of 30 segments, the grand potential does not drop to values near $\Omega = 0$, but start to increase with g above some $g > g^{**}$. This implies that the theory predicts that there is an upper limit in the micelle concentration. Spherical micelles with $g > g^{**}$ are unstable and micelles with a cylindrical or lamellar topology are expected instead. In other words, the overall composition of the copolymers is simply too solvophobic to self-assemble in stable spherical micelles. Obviously, there is a limit to the composition of the block copolymers that can self-assemble into spherical micelles. We have rationalized this limit in a patent application draft [33].

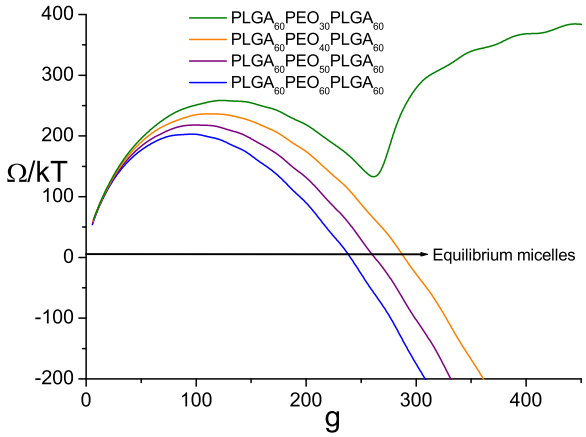

Figure 3.5: Grand potential of formation of a micelle consisting of $PLGA_{60}PEO_{N_X}PLGA_{60}$ triblock copolymers with varying PEO chain lengths N_X for $N_X = 60$ and smaller.

3.3.1 Radial density profiles and micelle size

Once the most-likely number of copolymers g in the micelle is known, the radial segment density profiles of all components composing the spherical micelle can be analyzed. In Fig. 3.6 we show the radial density profiles of copolymer segments, solvent, and separate PEO and PLGA blocks for a $PLGA_{60}PEO_{60}PLGA_{60}$ triblock copolymer micelle that corresponds to using 7.5-6.0-7.5 kDa, see Table 3.3. This micelle consists of 237 copolymers, see Table 3.4. The density profile as a function of the radial distance r, commences at $r = 0$, the center of the core towards large r values, far from the micelle. It is noted that r is given in lattice units. Each lattice unit thus corresponds to 0.8 nm; the Kuhn length for PEO.

Table 3.3: Comparison of experimental and theoretical SF-SCF hydrodynamic diameters D_h of copolymeric micelles prepared using the nanoprecipitation method using copolymers of compositions as indicated. D_{ht} = Theoretical hydrodynamic diameter, according to SF-SCF. D_{hp} = Practical hydrodynamic diameter measured by DLS [7], see Chapter 4. $|\Delta I|$ is the percentual deviation between what is practically measured and theoretically calculated. For copolymer ID see Table 3.4.

Copolymer ID	D_{hp} (nm)	D_{ht} (SF-SCF) (nm)	$\|\Delta I\|$
TBB1	45.2	45	0.44
TBB2	31.3	28	10.54
TBC1	27.2	26	4.41

In the center of the micelle, or core, there is a nearly constant volume fraction of copolymers of (in this case) about $\varphi \approx 0.87$ and about 13 vol% of water molecules, also confirmed in various other publications [34–37]. The amount of water is substantial for mixing entropy reasons: full exclusion of water is unlikely as this costs a lot of mixing entropy. The χ-value between PLGA monomers and water molecules is taken as 1.6, which causes demixing, but is not that extreme. Indeed the core will dry up with increasing χ-value. The slight increase

Table 3.4: SF-SCF determined averaged number of copolymers per micelle g.

Copolymer	Molar masses (1 kDa = 1000 g/mol)	Kuhn segments	g	Copolymer ID
PLGA-PEO-PLGA	3.75-3.0-3.75 kDa	30-30-30	132	TBB2
PLGA-PEO-PLGA	7.5-6.0-7.5 kDa	60-60-60	237	TBB1
PCL-PEO-PCL	1.9-3.0-1.9 kDa	17-30-17	155	TBC1

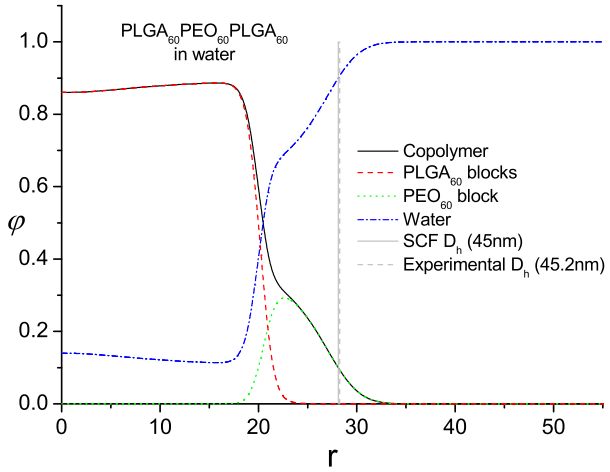

Figure 3.6: Equilibrium radial density profiles of water, total copolymer, PLGA blocks and PEO block as a function of the center from a micelle r. The micelle consists of $PLGA_{60}PEO_{60}PLGA_{60}$ triblock copolymers.

of water towards the core is caused by the presence of more PLGA end segments in the core. Near such end groups it is somewhat less unfavourable to have water molecules. Moreover the chains have to stretch to reach the micelle center. By having slightly more solvent in the core, the stretching of the chains can be reduced somewhat.

Around $r = 20$ the water concentration (dash dot line) increases significantly and the copolymer concentration drops correspondingly. The distribution of the PLGA (dash line) and PEO blocks are also plotted (dot line). The hydrophobic PLGA monomers are in the core, while the PEO segments are completely expelled from the core and are all located in the micellar corona. The PEO density goes through a maximum of about 25 vol% of segments providing steric stabilization. A rough estimation of the size can already be made based on these density profiles. Near $r = 30$ the density profile of copolymer segments drops to such low values that these can not be seen in these coordinates. This means an effective radius of about 30 times 0.8 nm= 24 nm or a diameter of 48 nm.

Since we measure the averaged hydrodynamic diameter D_h using dynamic light scattering we also computed the hydrodynamic diameter of the micelles using Brinkman-Debye theory [38, 39], for which the copolymer density profile is needed as input. The resulting values for D_h are plotted in Fig. 3 of the companion publication [7], see Chapter 4, so $D_h = 45$ nm for

the copolymer density profile in Fig. 3.6. This value corresponds very well to the predicted hydrodynamic diameter given in Table 3.3. In view of polydispersity effects and uncertainties in estimating the properties of the micelles for the SF-SCF computations we may only claim that the micellar size can be well predicted. It seems therefore that the micelles can be described by an theory that focuses on equilibrium structures.

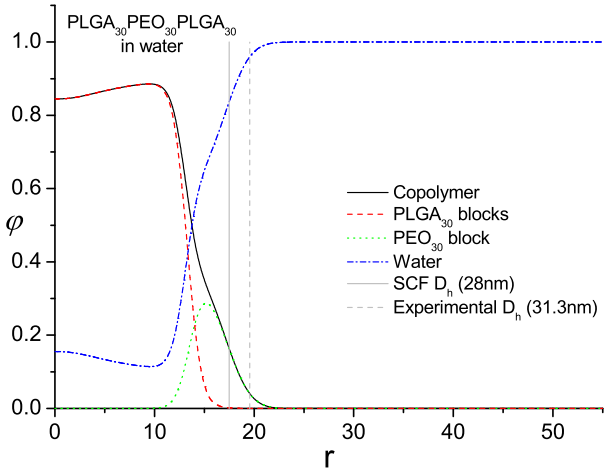

Figure 3.7: Equilibrium radial density profiles of water, total copolymer, PLGA blocks and PEO block as a function of the center from a micelle r. The micelle consists of $PLGA_{30}PEO_{30}PLGA_{30}$ triblock copolymers.

In Fig. 3.7 we show the radial density profiles of a $PLGA_{30}PEO_{30}PLGA_{30}$ triblock copolymer micelle composed of 3.75-3.0-3.75 kDa PLGA-PEO-PLGA triblocks (Table 3.3). This micelle consists of 132 copolymers (Table 3.4).

In comparison to the profile in Fig. 3.6 for the micelle with larger copolymers we observe the density profile inside the core of the micelle varies more strongly. Also the size of the micelles is smaller as can be expected; the hydrophobic chains are only 30 segments long, so the cores are smaller, and the stabilizing PEO chains on the outside are smaller as well. As a rough estimation one might speculate that g is half of the value for micelles composed of $PLGA_{60}PEO_{60}PLGA_{60}$ micelles ($g = 237$). Indeed the g value of 132 is only a bit larger than an estimated 119. As a consequence the size should in a naive picture scale as $d_1 \approx d_2(1/2)^{1/3}$, implying a diameter of about 36 nm for $d_2 = 45$ nm. Still, the SF-SCF size of 28 nm (Table 3.3) is even smaller. Hence more copolymer as expected is needed to stabilize a smaller particle as the molar mass decreases.

Next, we discuss the effect of encapsulation of hydrophobic compounds in the triblock copolymer micelles. Here we choose PLGA (homopolymer) chains with a molar mass of 20 kDa , corresponding to 180 segments, as the guest molecules. These will be fairly insoluble in the aqueous bulk and will prefer to be encapsulated in the core of the micelle because of the PLGA environment. The composition of the micelle with 7.6% encapsulated free PLGA in a micelle composed of identical copolymers as in Fig. 3.6 is plotted in Fig. 3.8. The number of copolymers per micelle now increased from 237 to 337 and the diameter increases from 45 to 51 nm. As expected we see that, whereas the PLGA monomer concentration in the core is

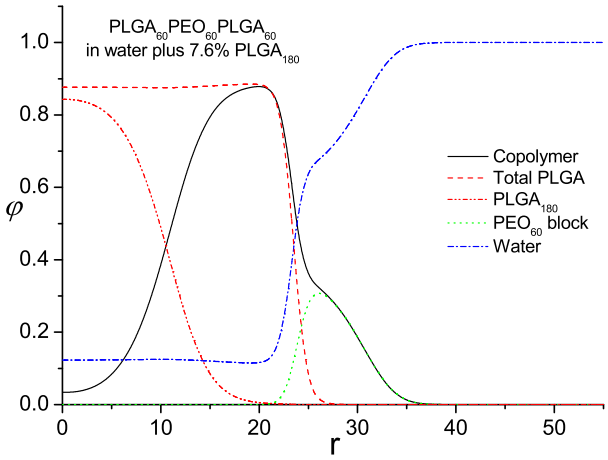

Figure 3.8: Equilibrium radial density profiles of water, total copolymer, PLGA blocks and PEO block as a function of the center from a micelle r. The micelle consists of $PLGA_{60}PEO_{60}PLGA_{60}$ triblock copolymers with added free $PLGA_{180}$ copolymers.

constant, the free PLGA is more concentrated close to the centre of the micelle and the PLGA monomers connected to the triblocks concentrate in the outer core region. Not shown is the finding that the influence of molar mass of the free PLGA is nearly imperceptible. SF-SCF obviously enables to study encapsulation effects and efficiencies. Once all Flory-Huggins χ-parameters are known between any drug molecule, the polymer segments and the solvent, SF-SCF allows studying encapsulation equilibriums. This computation inspired us to make the study leading to the results that will be presented in the companion publication [7], see Chapter 4.

We have also studied triblocks with the hydrophobic polymer PCL, replacing PLGA. In Fig. 3.9 we have plotted SF-SCF results for a micelle composed of $PCL_{17}PEO_{30}PCL_{17}$ triblock copolymers using 1.9-3.0-1.9 kDa PCL-PEO-PCL triblocks (see again Table 3.3 for the χ-parameters used). For this micelle we find it consists of 155 copolymers per micelle (Table 3.4). Since the χ-parameter is estimated to be substantially larger (3.0) the core now hardly contains water and can merely be viewed upon as a PCL melt environment. In the corona the PEO again goes through a maximum volume fraction that now reaches a maximum value of nearly 50 vol% of PEO segments. It seems the PEO segments here screen the hydrophobic core more strongly. They interact as a 'mediator' between water and the very hydrophobic core and in this case the peak is more sharp due to a more hydrophobic core environment. This might also have consequences for drug release; once the drugs leave the hydrophobic core the drugs need to pass the PEO barrier before they are released from the micelle.

In summary, we have shown that the SF-SCF theory may be used as a tool to unravel the structure-function relationship between copolymer composition and micellar size and morphology, also for situations that the resulting micelles are structurally quenched. Hence, using SF-SCF predictions allow for more efficient experimentation. As discussed more thoroughly in the companion publication [7], see Chapter 4, by utilizing this approach we were able to prepare nanosized particles consisting of PLGA-PEO-PLGA (7.5-6-7.5 kDa and 3.75-3-3.75

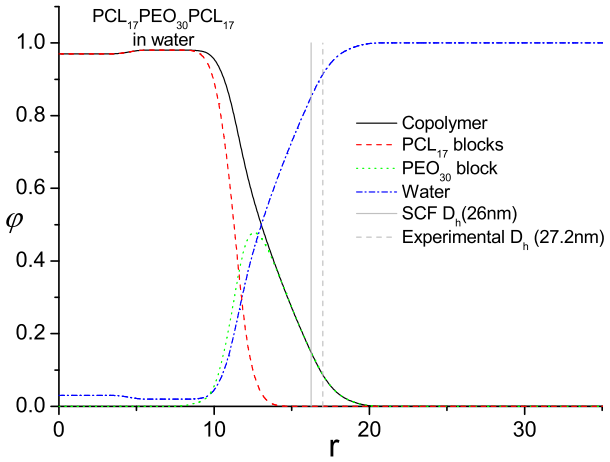

Figure 3.9: Equilibrium radial density profiles of water, total copolymer, PEO blocks and PCL block as a function of the center from a micelle r. The micelle consists of $PCL_{17}PEO_{30}PCL_{17}$ triblock copolymers.

kDa) or PCL-PEO-PCL (1.9-3-1.9 kDa) block copolymers in which (several) hydrophobic compounds can be encapsulated, see Chapter 4. One of the reasons to do this is that Ostwald ripening was minimized. Stabilization of micelles by block copolymers prevents particle aggregation, but the stabilizing polymer layer is open enough to allow solute mass transfer. In order to prevent/minimize solute transfer it is desired to tune the particle core composition to prevent this mass transfer. Additionally, the solubility of the encapsulated compound can be decreased by antisolvent addition to the bulk resulting in a significant slow down of Ostwald ripening. The extremely low solubility of the used triblock copolymers limits copolymer exchange between micelle and bulk again minimizing solute mass transfer and slowing down Ostwald ripening. There is no need to use surfactant in this process, conventional nanoprecipitation processes need an excess of surfactant, mostly very water soluble with relative high CMC's. Since we incorporated the surfactant function in the polymer backbone no exchange of adsorbed and free surfactant is needed for stable suspensions. This also avoids washing the nanoparticle suspension to remove excess of free surfactant used in the process and limits Ostwald ripening. We were able to synthesize different kinds of triblock copolymers allowing simultaneous tuning of the size and loading. When performing the nanoprecipitation process there is hardly an influence of temperature and triblock copolymer molar mass polydispersity. However, using these micelles in electrolytes, e.g. in vivo, care must be taken to avoid destabilization of the micelles due to electrostatic interactions. Non reported data shows that it is feasible to perform the nanoprecipitation process, using the mentioned triblock copolymers, in different electrolytes at different pH's and that the suspension stays stable in time.

3.4 Conclusions

We have shown that SF-SCF predictions provide an accurate prediction of structural properties of micelles processed via nanoprecipitation and composed of PCL-PEO-PCL and PLGA-PEO-PLGA copolymers. The hydrodynamic size that follows from these computations matches surprisingly well with the measured particle sizes from dynamic light scattering. From the computations it follows that the size of the nanoparticles is determined by the number-averaged molar mass of the block copolymers; polydispersity hardly affects the size of the micelles. We may speculate about reasons why an equilibrium theory can be used for an intrinsically off-equilibrium micelle formation process. One must realize that in the micelle formation procedure the solvent quality goes from a good solvent to a selective solvent. We may suggest that this solvent exchange is sufficiently slow so that chains can respond for some time to a local equilibrium, which we can mimic using some effective (intermediate) parameters. When the solvent quality subsequently becomes more extreme, the cores solidifies and the aggregation number is quenched. The latter may occur relatively suddenly in the process, so that the chains effectively cannot respond to these more selective solvent conditions. The prediction of the aggregation number corresponding to the quench point is apparently possible using a set of effective interaction parameters. For given aggregation number, the theory can then predict accurate radial distribution functions and corresponding hydrodynamic sizes. Modifications of the nanoprecipitation method, for instance by changing the initial solvent quality and/or the exchange time for the solvent going from good to selective, is expected to have an influence on the best values for the interaction parameters that should be used in subsequent SF-SCF modeling. However, once calibrated for given process conditions, one can proceed also for these new conditions to predict by the SF-SCF theory a value for the aggregation number, the hydrodynamic size and loading capacities.

Bibliography

[1] P.N. Hurter, J.M.H.M. Scheutjens and T.A. Hatton, Macromolecules, **26**, 5592-5601 (1993).

[2] Y. Lauw, F.A.M. Leermakers and M.A. Cohen Stuart, J. Phys. Chem. B, **110**, 465-477 (2006).

[3] P. Alexandridis, J.F. Holzwarth and T.A. Hatton, Macromolecules, **27**, 2414-2425 (1994).

[4] M. Monzem, T. Kawakatsu, M. Doi and R. Hasegawa, Computional and Theoretical Polymer Science, **10**, 275-280 (2000).

[5] R. Wang, P. Tang, F. Qiu and Y. Yang, J. Phys. Chem. B, **109**, 17120-17127 (2005).

[6] E.B. Zhulina and O.V. Borisov, Macromolecules, **45**, 4429-4440 (2012).

[7] J.G.J.L. Lebouille, L.F.W. Vleugels, A. Dias, F.A.M. Leermakers, M.A. Cohen Stuart and R. Tuinier, Eur. Phys. J. E, **36**, 107 (2013).

[8] J-G. Ryu, Y-I. Jeong, Y-H. Kim, I-S. Kim, D-H. Kim and S-H Kim, Bull. Korean Chem. Soc., **22**, 467-475 (2001).

[9] S. Chen, R. Pieper, D.C. Webster and J. Singh, Int J. Pharm., **288**, 207-218 (2005).

[10] H. Ge, Y. Hu, X. Jiang, D. Cheng, Y. Yuan, H. Bi and C. Yang, J. Pharm. Sci., **91**, 1463-1473 (2002).

[11] N. Kamaly, Z. Xiao, P.M. Valencia, A.F. Radovc-Moreno and O.C. Farokhzad, Chem Soc Rev., **41**, 2971-3010 (2012).

[12] J.M. Anderson and M.S. Sshive, Adv. Drug Deliver. Rev., **28**, 5-24 (1997).

[13] V.R. Sinha, K. Bansal, R. Kaushik, R. Kumria and A. Trehan, Int. J. Pharm., **278**, 1-23 (2004).

[14] R. Peters, J.G.J.L. Lebouille, B. Plum, P. Schoenmakers and S. van de Wal, Pol. Degrad. Stabil., **96**, 1589-1601 (2011).

[15] A. Sodergard and M. Stolt, Prog. Polym. Sci., **27**, 1123-1163 (2002).

[16] T. Nie, Y. Zhao, Z. Xie and C. Wu Macromolecules, **36**, 8825-8829 (2003).

[17] Y. Hu, L. Zhang, Y. Cao, H. Ge, X. Jiang and C. Yang, Biomacromolecules, **5**, 1756-1762 (2004).

[18] R. Webster, E. Didier, P. Harris, N. Siegel, J. Stadler, L. Tilbury and D. Smith, Drug Metab. Dispos., **35**, 9-16 (2007).

[19] K. Knop, R. Hoogenboom, D. Fisher and U.S. Schubert, Angew. Chem. Int. Edit., **49**, 6288-6308 (2010).

[20] J.N. Israelachvilli, D.J. Mitchell and B.W. Ninham, J. Chem. Soc. Faraday Trans. 2, **72**, 1525-1568 (1976).

[21] J.N. Israelachvilli, *Intermolecular and surface forces*, (Academic press, London, First edition, 1985).

[22] O.V. Borisov and E.B. Zhulina, Macromolecules, **35**, 4472-4480 (2002).

[23] E.B. Zhulina and O.V. Borisov, Macromolecules, **35**, 35, 9191-9203 (2002).

[24] T.L. Hill, *Thermodynamics of Small Systems* (Part 1 and Part 2, Dover Publications, NY, 1991 and 1992).

[25] J.M.H.M. Scheutjens and G.J. Fleer, J. Phys. Chem., **83**, 1619-1635 (1979).

[26] J.M.H.M. Scheutjens and G.J. Fleer, J. Phys. Chem., **84**, 178-190 (1980).

[27] G.J. Fleer, M.A. Cohen Stuart, J.M.H.M. Scheutjens, T. Cosgrove, and B. Vincent, *Polymers at Interfaces* (Chapman and Hall, London, first edition, 1993).

[28] T.L. Hill, *An Introduction to Statistical Thermodynamics* (Addison-Wesley, New York, 1962).
[29] S.F. Edwards, Proc. Phys. Soc., **85**, 613 (1965).
[30] B. Vincent, Colloids and Surfaces, **50**, 241-249 (1990).
[31] J. Brandrup, E.H. Immergut, E.A. Grulke, A. Abe and D.R. Bloch, *Polymer Handbook* (John Wiley and Sons,4th Edition, 2005).
[32] F.A.M. Leermakers, J.C. Eriksson and H. Lyklema, *Fundamentals of interface and colloid science* (Chapter 4: Association colloids and their equilibrium modelling, First edition, Elsevier Ltd., London, 2005).
[33] J.G.J.L Lebouille, T. Kockelkoren, L.F.W. Vleugels and R. Tuinier, **US 0223206 A1** (2011).
[34] I. Goldmints, G.E. Yu, C. Booth, K.A. Smith and T.A. Hatton, Langmuir, **15**, 1651-1656 (1999).
[35] S.M. King, R.K. Heenan, V.M. Cloke and C. Washington, Macromolecules, **30**, 6215-6222 (1997).
[36] P. Linse, Macromolecules, **26**, 4437-4449 (1993).
[37] J.S. Pedersen and M.C. Gerstenberg, Colloids Surf., A, **213**, 175-187 (2003).
[38] M.A. Cohen Stuart, F.H.W.H. Waaijen, T. Cosgrove, B. Vincent and T.L. Crowley, Macromolecules, **17**, 1825-1830 (1984).
[39] J.M.H.M Scheutjens, G.J. Fleer and M.A. Cohen Stuart, Colloids and interfaces, **21**, 285-306 (1986).

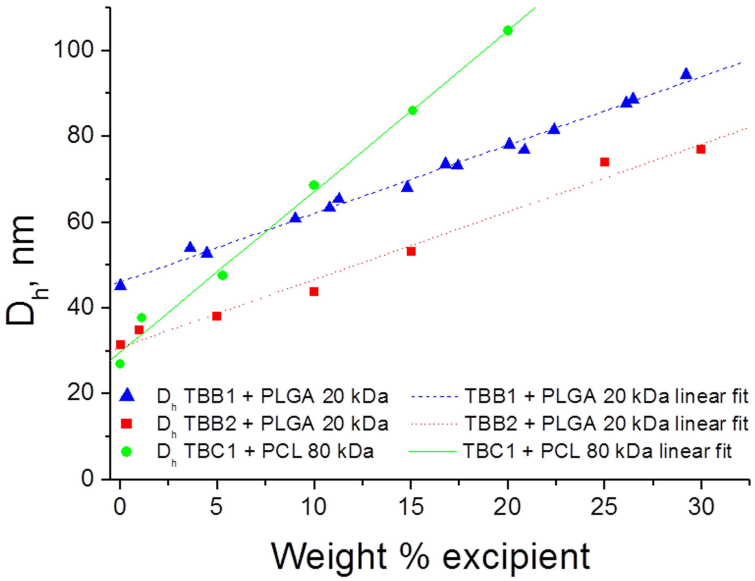
D_h, nm
100
80
60
40
20
0
0
5
10
15
20
25
30
Weight % excipient
D_h TBB1 + PLGA 20 kDa
D_h TBB2 + PLGA 20 kDa
D_h TBC1 + PCL 80 kDa
TBB1 + PLGA 20 kDa linear fit
TBB2 + PLGA 20 kDa linear fit
TBC1 + PCL 80 kDa linear fit

Controlled block copolymer micelle formation

4

This chapter was published as:
J.G.J.L. Lebouille, L.F.W. Vleugels, A.A. Dias, F.A.M. Leermakers, M.A. Cohen Stuart and R. Tuinier, Controlled block copolymer micelle formation for encapsulation of hydrophobic ingredients, Eur. Phys. J. E, **36**, 107 (2013).

Abstract

We report on the formation of polymeric micelles in water using triblock copolymers with a polyethylene oxide middle block and various hydrophobic outer blocks prepared with the precipitation method.
We form micelles in a reproducible manner with a narrow size distribution. This suggests that during the formation of the micelles the system had time to form micelles under close-to thermodynamic control. This may explain why it is possible to use an equilibrium self-consistent field theory to predict the hydrodynamic size and the loading capacity of the micelles in accordance with experimental finding.
Yet, the micelles are structurally quenched as concluded from the observation of size stability in time. We demonstrate our approach enables to prepare rather hydrophobic block copolymer micelles with tunable size and loading.

keywords: Micelle, (nano)precipitation, particle size prediction, encapsulation, block copolymers.

4.1 Introduction

Encapsulating active compounds in a controlled fashion is of paramount importance for applications in food [1–3] and pharmaceutical technology [4–6]. One can use nanosized micellar structures formed by amphiphilic molecules in a selective solvent. Here we focus on water as the (selective) solvent and consider block copolymers with two apolar and one polar block, the so-called ABA block copolymers where A is an apolar block and B a polar block. The hydrophobic entities are collected in a compact core, whereas the water soluble compound remains hydrated and forms a corona. Flavors, vitamins and drugs are often rather hydrophobic ingredients for which polymeric micelles are promising carriers, with potential for controlled encapsulation of compounds at high loadings. Additionally, using polymeric micelles offers routes to control release, stability and bio-distribution of active agents in the body. The bio-distribution mainly depends on the micelle size and corona structure [7–10]. It is known that small sized micelles, e.g., below 30 nm, distribute freely in the human body due to a lack of tissue retention/obstruction. Larger sized objects, i.e., exceeding 400 nm, may cause problems in the vascular system, especially in the capillaries which can easily be obstructed by such particles. Indeed, sizes below 100 nm result in relatively long circulation times and these objects can accumulate in inflammatory or tumor tissues by the enhanced permeability and retention (EPR) effect [11–15]. This phenomena can be exploited to give passively targeted drug delivery systems. There is ample evidence that the average size and its size distribution mainly determine the biological fate, and therefore also the efficiency of a treatment, when nanoparticles/micelles are used for drug delivery purposes. The corona composition is also of importance for the distribution and tissue uptake of the particle. It has been shown that PEGylated entities, sometimes called stealth or 'disguise' particles, have even longer blood circulation times [16]. Furthermore, presence of the cationic surfactant dimethylammonium bromide on the surface of a particle was shown to improve uptake by arterial tissue [17, 18].

There is a broad range of amphiphiles, for instance poloxamers and PEO-PCL or PEO-PLGA (di- and tri-) block copolymers, that can be used to prepare micelles with encapsulated hydrophobic compounds [19–29]. Relatively polar copolymers and surfactants that readily dissolve in water form rather dynamic micelles with unimeric exchange rates up to the microsecond time scale [30, 31]. Encapsulated compounds in such micelles will also be released rapidly because usage as drug delivery systems is always accompanied with significant dilution. A fast unimer exchange implies a high CMC and therefore a fast release, almost instantaneously upon administration.

We may distinguish thermodynamically stable systems, which have an equilibrium size and typically a narrow size distribution that do not depend on the route of how the micelles are formed, from kinetically frozen aggregates. For the latter the route of formation becomes important. Kinetically frozen aggregates may show Ostwald ripening, a phenomenon that over extended periods of time large particles grow at the expense of smaller ones [32], similarly as emulsion droplets. The growth of large particles at the expense of smaller ones is facilitated by the solubility of the constituent molecules in the solvent. Copolymers with a sufficiently long hydrophobic block form micelles at very low critical micelle concentrations. The micelles have a compact hydrophobic core and a hydrated corona. Although the chainparts in the corona continuously change conformations due to thermal motion, the chainparts that form the core are much less dynamic. Indeed, very often the core is in the glassy state.

The combination of a low (unimeric) polymer concentration in the bulk (low CMC) and the slow dynamics in the core (glassy core), results in marginal Ostwald ripening. Micelles with limited Ostwald ripening have a long shelf life.

A complication is that such 'frozen' micelles cannot be prepared by simply dissolving the copolymer in water, since water is a non-solvent for the relatively long hydrophobic blocks of the copolymers. We apply he 'solvent shifting' or nanoprecipitation procedure [33–36] to prepare micelles in aqueous solutions composed of otherwise water-insoluble polymers. In this procedure, the (co)polymers are first dissolved in an organic (good) solvent for both blocks. The solvent should also have a reasonable miscibility with water. This solution is subsequently added, rapidly, to an excess of water. During the mixing procedure the block copolymers gradual goes from a good solvent to selective solvent conditions, because the organic phase is dispersed in the water phase. As a result, the core-forming blocks aggregate (as they are insoluble) and form the micellar cores. The solvophilic blocks remain solvated during the solvent exchange process and accumulate outside the core to form a corona. It is expected that in the core the organic phase will preferentially accumulate. This keeps the micelles mobile for some time. Depending on the conditions, however, the organic phase may be lost for the micelles and then the polymeric micelles go into a 'frozen' or 'dead' state, meaning that they no longer can exchange copolymers between each other. One may intuitively expect that the solvent exchange is very fast and the micelles become very quickly trapped in a frozen state. However, this is not always the case and one can, alternatively, imagine that the micelles have sufficient time to equilibrate their size and possibly to some extend their size distribution. In such a scenario, it is feasible that the micelle size and micelle size distribution are dictated by some equilibration process that continued in one way or another until (relatively suddenly) the constituent molecules lose their mobility. In this line of reasoning it is fair to try to attempt a modeling effort to seek guidance to rationalize the relation between molecular structure and micellar topology.

To this end we performed numerical Scheutjens-Fleer self-consistent field (SF-SCF) computations. The method and results are explained in [37], see Chapter 3. SF-SCF is known to be very accurate for densely packed polymer systems including micellar structures [38–41]. However, the theory pre-assumes that the molecules have reached their thermodynamic equilibrium. Although we are sure that the final micelles are kinetically frozen, we envision that it is possible that we can find effective parameters that are relevant for the micelles that are being formed transiently and to some extend were under thermodynamic control. The molecules form flower-like micelles in the dispersions studied which is supported by unpublished cryo-TEM analyses and DLS measurements at higher triblock copolymer concentrations. This implied that the corona is built up by looping chains, which arguably have some advantage for targeting. The idea for this is that, when a minority amount of the triblocks is replaced by copolymers for which one hydrophobic block is replaced by a (water-soluble) targeting moiety, one has flower-like micelles intermixed with polymers that have their targeting moiety dangling well outside the corona of the remaining triblock copolymers. This makes the targets to be better, biologically, accessible.

In the following we will first give information on the polymeric species. In the results section we will focus on the characterisation of the micelles and elaborate on the use of SF-SCF modeling. In our conclusions we argue that the micelles formed by the precipitation method assume a structure that resembles equilibrium characteristics that were present somewhere in the production process.

4.2 Experimental aspects

4.2.1 Copolymers and amphiphiles

The used polymeric surfactants are all amphiphilic copolymers with a general composition of A-B-A, where A is the hydrophobic group poly(lactic-co-glycolic)acid, poly(ε-caprolactone) (further referred to as: PLGA and PCL) and B the hydrophilic group polyethylene oxide, polyvinyl pyrolidone, polyvinyl alcohol (PEO, PVP, PVA). The (co-)polymer blocks of which these triblock copolymers are made of comply with the following prioritized requirements: non-toxic, biocompatible, biodegradable and excretable.

The hydrophilic part of the copolymer is PEO, exhibiting good water solubility and meets the above requirements. Although its non degradability PEO is non-toxic and can easily be removed from the body by the normal excretion pathways as long as the molecular weight is below 20 kDa [42]. The hydrophobic part consists of known biodegradable polymers used in commercially available drug delivery applications: PLGA and PCL.

4.2.2 Stability; dynamic, static or dead/frozen micelles

In order to prepare ”frozen” micelles in water several requirements need to be met. Importantly, water should be a selective solvent for the surfactant/copolymer, that is, a non-solvent for one block and a good solvent for the other. It is known that the $\log CMC \propto N_t$, where N_t is the number of apolar segments in the copolymer/surfactant. Provided the non-solvent block is long enough ($N_t >> 1$), this results in a extremely low CMC-values, inhibiting Ostwald ripening. Finally, the conditions of the core forming block should be such that the mobility of the chains is retarded, that is, preferably there should not be a plasticizer in the system. Typically, these requirements preclude using the normal way of making micelles by dissolving the surfactant/copolymers, because of the exceedingly low critical solution temperature (LCST), in the surfactant science often referred to as the Krafft temperature [43, 44].

To overcome this we opted for the nanoprecipitation method: One first co-dissolves the active ingredient, the stabilizer and the excipient, that is, the surfactant/copolymer together with a compound that protects or tunes the release of the active ingredient, in a suitable water-miscible common solvent and then precipitates it into a nanoparticulate form in water, which is a selective solvent. The common solvent is used to bring the copolymers into a homogeneous molecular solution, from which the self-assembly into micelles proceeds when added to a selective solvent: one block avoids the selective solvent and forms the core and the other blocks remain solvated and form the corona. Typically, the macromolecular nature of the species involved prevents the molecular dispersion of the copolymers. In other words, the bulk concentration of the copolymers (unimers) is extremely low resulting in static or frozen micelles, minimizing the possible elution of active ingredients and or excipients out of the particle.

The micellar shape strongly depends on the copolymer composition. Typically the spherical shape is stable as long as the dimension of the (highly solvated) corona H exceeds that of the (almost solvent free) core R_c. The core forming blocks collapse and then occupies a volume proportional to its length. Thus the size of the core is proportional to $R_c \propto N_t^{1/3}$. The corona block, on the other hand, remains solvated and is grafted by the ends onto the cores. Due to the lateral interactions the corona blocks become stretched outward and form

a molecular brush. The height of the brush H (equal to the corona size) is proportional to the degree of polymerization N_t, that is $H \propto N_t^1$. Hence, the stability of the spherical micelle may occur already for relatively short corona blocks ($N_c < N_t$). Of course, in principle it remains possible that the dimension of the core and that of the corona are comparable. Then the cylindrical or lamellar structures become the geometry of choice. In the current project, however, the corona block is long (dimensionally big) enough to expect spherical micelles to form.

The molecular weight of the micelle, that is the number of copolymers in one micelle, is also controlled by the copolymer composition. Basically, the longer the corona block the smaller the aggregation number, whereas an increase in the molecular weight of the core forming blocks increases the aggregation number. The molecular weight of the micelle is also a strong function of the driving force for micellisation. In some mixtures of a common solvent and a selective solvent the driving force is expected to increase with the increase of the ratio 'selective solvent' / 'common solvent'. Indeed, during the precipitation procedure we expect the driving force to be an increasing function of the time after the addition of the selective solvent. In the SF-SCF modeling [37] we have simplified this process by taking a simple selective solvent, which presents a moderate driving force for micellisation. This leads to predictions in trends in micelle size and molecular weight which can directly be tested experimentally.

The micelles that can be generated by the precipitation method have ideal sizes for drug delivery formulations. These formulations are very stable in time and the elution profiles can be governed by the excipients, species only present in the core of the micelle together with the active ingredient, and the used copolymer, present on the interface between micelle core and corona. Most release profiles are governed by diffusion and or desorption, an excipient can alter the desorption of an active ingredient from micellar core to corona and thus having an effect on release. In other cases an excipient can also act as a preservative for the active ingredient. Butylhydroxytoluene [45, 46] (BHT) or β-carotene [47] is often used as a preservative (antioxidant), to avoid oxidative decline of the active ingredient due to oxygen, hydrolyses, salt, pH or other chemical species chemically altering the original active ingredient.

4.2.3 Self-consistent field theory and molecular model

The theoretical toolbox for the study of self-assembly of copolymers is not very large. Important for the success is that the molecular structure of the copolymers is relatively accurately accounted for both from a structural as well as well as from an interactions point of view. Molecular simulations can be used, but effectively need a significant coarse graining step in order to keep the simulation time within reasonable bounds. As an output, simulations give very detailed picture, that is, the micelle structure presents itself in full glory. Importantly, the thermodynamic information of the system is typically lacking and therefore it is hard to estimate the relevance of a particular micellar structure for a practical system of interest.

In this work we opt for an approximate mean-field approach. More specifically we choose for the Scheutjens-Fleer self-consistent field (SF-SCF) method. The important argument in favor of this approach is that the method starts with a (mean field) free energy formula and therefore the results are readily analyzed in the thermodynamic context. This means that one can estimate more easily the relevance of a particular result for the experimental system.

The optimization of the mean-field free energy gives structural information of the micelles, which is still rather detailed. The fact that the micelles are composed of copolymers that are densely packed appears important. For this situation each molecule interacts with many neighbors and therefore the mean-field approximation is relatively accurate. On top of this the calculation time is extremely short (in comparison to simulations). Last, but not least, molecularly realistic models can be implemented with relatively few effective interaction parameters. Although, in principle the interaction parameters can be measured, in practice they are largely unknown. The same holds true, obviously, for the current systems under investigation.

Polymers are considered to be composed of (so-called) Kuhn-segments, see Table 4.1. A Kuhn-segment occupies one grid unit (r) in our calculations which corresponds with $0.8nm$. This allows for the use of a freely-jointed chain model. Within this chain model, there exists an efficient procedure to compute the partition function and thus full thermodynamic information can be obtained. In this approach the architecture of the chain parts in the copolymers is accurately accounted for. The interactions are accounted for using the Bragg-Williams approximation, which ignores local density correlations analogous to the Flory-Huggins theory for polymer solutions. The Flory-Huggins interaction parameters that specify the solvent quality of the segments, as well as the interactions between the segments are easily estimated see Table 4.2.

Table 4.1: Number of Kuhn segments (N_K) of compounds studied.

Blocks in copolymers	N_K
PEO 6.0 kDa	60
PEO 3.0 kDa	30
PLGA 7.5 kDa	60
PLGA 3.75 kDa	30
PCL 1.9 kDa	17
β-carotene	5
Rapamycin	9

As the accurate value of the interaction parameters depends on how many details of the polymeric chains is accounted for, it is not trivial to tabulate these. Hence, one should calibrate the parameter for each system under investigation. This means that there should be relevant experimental observables to do so. In practice therefore, one typically selects a particular case (here a particular copolymer system), adjusts the interaction parameters somehow until there is a reasonable match between, e.g., the micelle size predicted by theory and found experimentally. Subsequently, the set of parameters is fixed and the model is used to predict the structural features of the micelles for other systems. In Fig. 4.1 equilibrium density profiles of active ingredient loaded PLGA based triblock copolymer micelles are shown comparing the SF-SCF calculated and DLS measured hydrodynamic diameters. In Fig. 4.1 (a) the loaded active ingredient is β-carotene, see Fig. 4.6 for the stability data of the β-carotene loaded micelles. In Fig. 4.1 (b) the loaded active ingredient is rapamycin, see Table 4.16 for the stability data of the rapamycin loaded micelles. We refer to ref. [37] for more details.

Table 4.2: χ-Parameters for the monomer-solvent interaction used in SF-SCF computations (EG: ethylene glycol, LGA: Lactic-co-glycolic, CL: caprolactone, BC: β-carotene and Rapa: rapamycin. The block lengths and the corresponding Kuhn lengths are collected in Table 4.1.

Monomer-solvent interaction	χ
EG - water	0.4
LGA - water	1.6
CL - water	3.0
LGA - EG	1.0
CL - EG	1.0
BC - water	4.0
BC - EG	1.0
BC - LGA	0.4
Rapa - water	6.0
Rapa - EG	1.0
Rapa - LGA	0.4 or 2.0

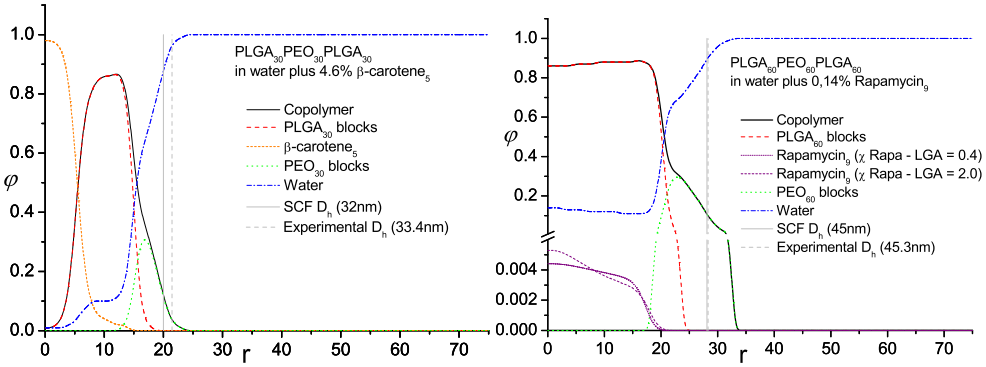

(a) **(b)**

Figure 4.1: Equilibrium radial density profile of water, total copolymer, PLGA blocks and PEO block as a function of the center from a micelle r. (a): β-carotene added to a $PLGA_{30}PEO_{30}PLGA_{30}$ triblock copolymer micelle. (b): Rapamycin added to a $PLGA_{60}PEO_{60}PLGA_{60}$ triblock copolymer micelle. In this way we compare via SF-SCF and DLS measurement the influence on the hydrodynamic diameter and the difference between the theoretical calculation and the experiment. The SF-SCF hydrodynamic diameter in Fig. 4.1 (a) is calculated as follows: $(20*0.8)(nm)*2 = 32(nm)$ and for Fig. 4.1 (b): $(28*0.8)(nm)*2 = 45(nm)$.

4.3 Materials and methods

4.3.1 Materials

All triblock copolymers were synthesized by ring-opening polymerization of D,L-lactide, glycolide or caprolactone using PEO-(3.0 kDa and 6.0 kDa)-diol as an initiator and stannous octoate as a catalyst at 150°C under vacuum. D,L-Lactide and glycolide were purchased from Purac (Goringchem, the Netherlands), polycaprolactone and β-carotene from Sigma (St. Louis, USA). PLGA 20 kDa was purchased from Ingelheim Boehringer (Ingelheim am Rhein, Germany). Polycaprolactone 80 kDa was purchased from Solvay (Oudenaarde, Belgium) PEO (3.0 kDa and 6.0 kDa) and Sn_2Oct were purchased from Aldrich (St. Louis, USA). Acetone was purchased from BASF (Bayern, Germany). Rapamycin was purchased from Oscar Tropitzsch (Germany).

4.3.2 Methods

4.3.2.1 Ring-opening polymerization method for the triblock copolymers [48, 49]

PLGA-PEO-PLGA triblock copolymers
The PEO was weighed into a two-necked round bottle flask after drying for 24 hours in a vacuum oven at 90°C and subsequently placed in an oil bath at 150°C. A vacuum was employed for at least 60 minutes before continuing the synthesis. The addition of lactide and glycolide (molar ratio of lactide:glycolide = 50:50) was carried out by removing the vacuum and at the same time flushing with nitrogen gas. When a homogeneous melt was obtained under stirring, the catalyst, stannous octoate (Sn_2Oct), was added in the same way as the addition of the monomers. The reaction conditions were maintained for 20 hours whereafter the vacuum was replaced by nitrogen gas and the ring-opening polymerization was completed, see Fig. 4.2 for reaction scheme and Table 4.3 for synthesis weights. The copolymers obtained in this way are listed in Table 4.5.

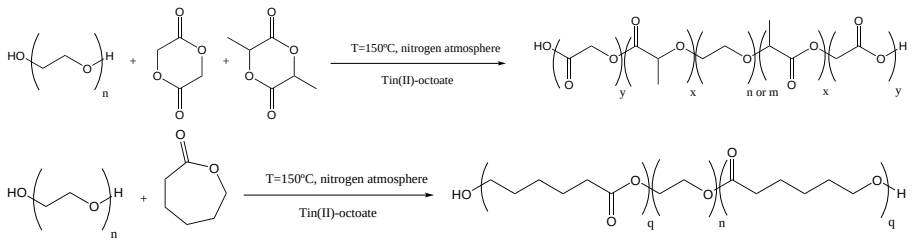

Figure 4.2: Schematic of the ring-opening polymerization of the triblock copolymers. In our case $x = y$, and $x + y$ is the number of D,L-Lactide and Glycolide repeating units randomly distributed in the hydrophobic end blocks. In the case of $m = 136$ ethylene oxide repeating units $x + y$ is 115, referred to as TBB1, and for $n = 68$ ethylene oxide repeating units $x + y$ is 58, referred to as TBB2 for the PLGA based triblock copolymers. For the PCL based triblock copolymer, referred to as TBC1, there are $n = 68$ ethylene oxide repeating units with $q = 17$ caprolactone repeating units.

Table 4.3: PLGA-based triblock copolymer synthesis weights.

Triblock copolymer ID	Initiator; hydrophilic PEO block (grams)	Hydrophobic blocks		Catalyst Sn_2Oct (mg)
		D,L-Lactide (grams)	Glycolide (grams)	
TBB1	PEO-6000-diol; 2.8467	3.9131	3.2471	4.4
TBB2	PEO-3000-diol; 2.8573	3.9098	3.3233	4.4

PCL-PEO-PCL triblock copolymers
The PEO along with ε-caprolactone was charged in a 100 mL round bottomed flask. The reaction mixture was heated to 100°C and stirred till a homogenous mixture was formed. A catalyst stock solution of tin(II)octoate was prepared in hexane. 1 mL of the catalyst stock solution was added to the reaction mixture at 100°C. The reaction mixture was further heated to 150°C for an additional 18 hours (overnight) to allow the reaction to proceed. The following morning the reaction mixture was cooled to room temperature, an off white waxy solid material was obtained, Table 4.4 shows the synthesis weights. The copolymers obtained in this way are listed in Table 4.5.

Table 4.4: PCL-based triblock copolymer synthesis weights.

Triblock copolymer ID	Initiator; hydrophilic PEO block (grams)	Hydrophobic blocks ε-caprolactone (grams)	Catalyst-solution 58.10 mg Sn_2Oct/ 5mL Hexane (mL)
TBC1	PEO-3000-diol; 8.8554	11.1555	1.000

Table 4.5: Triblock copolymers ID and composition.

Triblock ID	Triblock (A-B-A) copolymer composition		
	PLGA-block (A)	PEO-block (B)	PLGA-block (A)
TBB1	7.5 kDa	6.0 kDa	7.5 kDa
TBB2	3.75 kDa	3.0 kDa	3.75 kDa
	PCL-block (A)	PEO-block (B)	PCL-block (A)
TBC1	1.9 kDa	3.0 kDa	1.9 kDa

4.3.2.2 Purification of the synthesized triblock copolymers

The triblock copolymer was dissolved in acetone at a weight percentage of 10-20%, filtered over an Acrodisc premium 25 mm Syringe filter, GxF/0.45μm PVDF membrane, to remove particulate impurities and dust particles, which can interfere with the nanoprecipitation process, collected into an 500 mL PTFE beaker and evaporating of the solvent over night (10-12 hours) at maximum 40°C and minimum 300 mbar.

4.3.2.3 Nanoprecipitation / nanoparticle preparation method

Typically, 300 mg of copolymer was weighed and dissolved in 5.000 mL of acetone resulting in a clear copolymer solution after 30 minutes on an orbital shaker. Prior to the nanoprecipitation process all solutions (milliQ water, copolymer-, copolymer / excipient (homopolymer)- and copolymer / active ingredient- solutions) were filtered over an Acrodisc LC25 mm Syringe filter 0.2 μm PVDF membrane. See Fig. 4.3 for basic nanoprecipitation process setup. In order to obtain excipient loaded micelles 300 mg copolymer was weighed and subsequently dissolved in solvent, the excipient was weighed and dissolved in the copolymer solution. The excipients were chosen from two different homopolymers. The weight percentage of the excipient in ratio to the copolymer was calculated as follows: weight% = [(excipient mass)/(excipient mass + copolymer mass) $\times$ 100]. A volume of 0.400 mL of the copolymer or copolymer/excipient solution was added to 10.00 mL of aqueous solution with an Eppendorf pipette, the addition with the pipette was carried out within one second, whereafter the suspension was manually homogenized within five seconds.

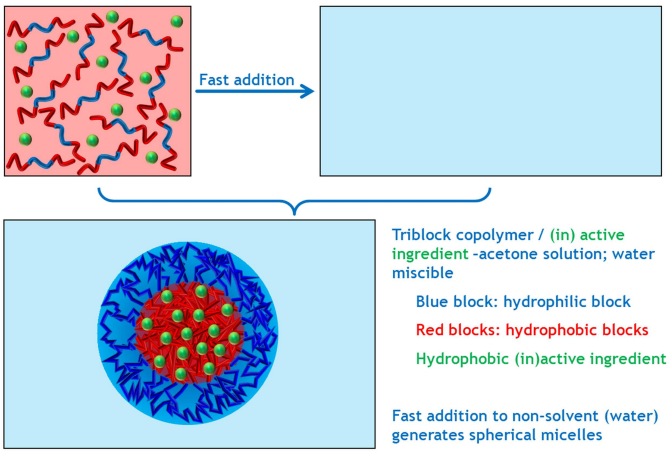

Figure 4.3: Schematic of basic nanoprecipitation process setup.

Nanoprecipitation reproducibility

To check the reproducibility of the nanoprecipitation process three different formulations were made, weighed and dissolved, at three different days per triblock copolymer type. After nanoprecipitation the sample was measured within 15 minutes. TBB2 and TBC1 triblock copolymers were used to check the reproducibility of 'empty' micelles. The TBC1 triblock copolymer was also mixed with an active ingredient, rapamycin, to check the reproducibility on the active ingredient loaded nanoprecipitation process. Table 4.6 shows the concentrations used of the TBB2 and TBC1 copolymer in the nanoprecipitation setup. 0.400 mL of the copolymer solution was precipitated in 10.00 mL MilliQ water. Table 4.7 shows the weights of the used copolymer triblock together with the active ingredient rapamycin (RAPA) weights in the nanoprecipitation setup. 0.400 mL of the copolymer/active ingredient solution was precipitated in 10.00 mL MilliQ water.

Table 4.6: Different weights for the reproducibility test on the nanoprecipitation process for 'empty' triblock copolymer, TBB2 ($PLGA_{30}PEO_{30}PLGA_{30}$; 3.75-3.0-3.75 kDa) and TBC1 ($PCL_{17}PEO_{30}PCL_{17}$; 1.9-3.0-1.9 kDa), based micelles.

Triblock ID	Triblock mass (mg) / mL acetone	Sample ID	Group ID
TBB2	59.89	TBB2R1	TBB2R
TBB2	60.07	TBB2R2	
TBB2	60.13	TBB2R3	
TBC1	60.07	TBC1R1	TBC1R
TBC1	60.28	TBC1R2	
TBC1	60.19	TBC1R3	

Table 4.7: Different weights for the reproducibility test on the nanoprecipitation process for active ingredient, rapamycin, loaded micelles for TBC1 ($PCL_{17}PEO_{30}PCL_{17}$; 1.9-3.0-1.9 kDa) triblock copolymer based micelles.

Triblock ID	Triblock mass (mg) / mL acetone	Mass active ingredient (RAPA; mg)	Sample ID	Group ID
TBC1	30.14	1.59	TBC1RE1	TBC1RE
TBC1	30.05	1.63	TBC1RE2	
TBC1	30.11	1.54	TBC1RE3	

Single excipient, homopolymer, loaded micelles

The interest in copolymer micelles is in part due to their relatively large loading capacity, even for relatively high molecular weight compounds, the following experiments were carried out. All three triblock copolymers were tested together with a homopolymer as an excipient to determine the loading capacity / capability and the relation between excipient weight percentage and size. TBB1 copolymer was made in a stock solution of 62.68 mg TBB1 triblock copolymer per mL acetone (1.2536 gram / 20.00 mL acetone). Different masses (see Table 4.8) of PLGA 20 kDa were weighed into a vial. Afterwards 1.000mL of the TBB1 triblock copolymer solution was added to all weighed excipients. TBB2 copolymer was made in a stock solution of 63.45 mg TBB2 triblock copolymer per mL acetone (0.6345 gram / 10.00 mL acetone). Different masses (see Table 4.9) of PLGA 20 kDa were weighed into a vial. 1.000 mL TBB2 triblock copolymer solution was added to the excipient vials. TBC1 copolymer was made in a stock solution of 63.21 mg TBC1 triblock copolymer per mL acetone (0.6321 gram / 10.00 mL acetone). Different masses (see Table 4.10) of PCL 80 kDa were weighed into a vial and dissolved as the other copolymer excipient solutions. After complete dissolution on an orbital shaker, resulting in a clear copolymer / excipient solution, the solution ready to be precipitated in MilliQ water (0.400 mL of the copolymer / excipient solution was precipitated in 10.00 mL MilliQ water).

Table 4.8: TBB1 ($PLGA_{60}PEO_{60}PLGA_{60}$; 7.5-6.0-7.5 kDa) triblock copolymer excipient (PLGA 20 kDa) loaded micelles (62.69 mg TBB1 triblock copolymer per mL acetone) series.

Mass excipient (PLGA 20 kDa) (mg)	wt% excipient (%)	Sample ID
0.000	0.00	TBB1E1
2.334	3.39	TBB1E2
2.912	4.44	TBB1E3
6.222	9.03	TBB1E4
7.581	10.79	TBB1E5
7.969	11.28	TBB1E6
10.888	14.80	TBB1E7
13.554	17.78	TBB1E8
13.213	17.41	TBB1E9
15.758	20.09	TBB1E10
16.521	20.86	TBB1E11
18.072	22.38	TBB1E12
22.126	26.09	TBB1E13
22.541	26.45	TBB1E14
25.864	29.21	TBB1E15

Table 4.9: TBB2 ($PLGA_{30}PEO_{30}PLGA_{30}$; 3.75-3.0-3.75 kDa) triblock copolymer excipient (PLGA 20 kDa) loaded micelles (63.45 mg TBB2 triblock copolymer per mL acetone) series.

Mass excipient (PLGA 20 kDa) (mg)	wt% excipient (%)	Sample ID TBB2E
0.000	0.00	TBB2E1
0.641	1.00	TBB2E2
3.339	5.00	TBB2E3
7.050	10.00	TBB2E4
11.197	15.00	TBB2E5
21.150	25.00	TBB2E6
27.193	30.00	TBB2E7

Table 4.10: TBC1 ($PCL_{17}PEO_{30}PCL_{17}$; 1.9-3.0-1.9 kDa) triblock copolymer excipient (PCL 80 kDa) loaded micelles (63.21 mg TBC1 triblock copolymer per mL acetone) series.

Mass excipient (PCL 80 kDa) (mg)	wt% excipient (%)	Sample ID TBC1E
0.000	0.00	TBC1E1
0.703	1.10	TBC1E2
3.538	5.30	TBC1E3
7.023	10.00	TBC1E4
11.242	15.10	TBC1E5
15.803	20.00	TBC1E6

Nanoprecipitation of single component loaded micelles

TBB1 copolymer and TBB2 copolymer were dissolved in acetone, see Table 4.11 for the triblock copolymer solutions. The excipient, PLGA 20 kDa and the active ingredients rapamycin and β-carotene, were dissolved in acetone solution, see Table 4.12 for the single component solutions. 0.300 mL of the triblock copolymer solution was mixed with 0.100 mL of the single component solution, resulting in 0.400 ml of copolymer / single component-solution, see Table 4.13. 0.400 mL of the copolymer / single component solution was nanoprecipitated into 10.00 mL of MilliQ water and measured by DLS in time to monitor stability.

Table 4.11: Triblock copolymer solutions.

Copolymer ID	Copolymer mass (mg)	mL acetone	Copolymer solution ID
TBB1	164.1	2.400	TBB1CS1
TBB2	1894.47	31.575	TBB2CS1

Table 4.12: Single component solutions.

Component ID	Component mass (mg)	mL acetone	Component solution ID
PLGA 20 kDa	6.8375	1.000	ES1
Rapamycin	0.800	0.800	ES2
β-carotene	8.75	1.000	ES3

Table 4.13: Copolymer/single component solution; 0.400mL precipitated in 10.00mL Milli Q water.

Copolymer solution		Single component solution		
1-4 Copolymer solution ID	mL copolymer solution	Component solution ID	mL single component solution	Micelle suspension ID
TBB1CS1	0.300	ES1	0.100	TBB1EX
TBB1CS1	0.300	ES2	0.100	TBB1R
TBB2CS1	0.300	ES3	0.100	TBB2BC

4.3.2.4 Particle size analysis

Particle size analyses were performed using three different techniques. First a cryo-TEM study was performed showing only the presence of perfectly spherical particles. Secondly, a static multi angle light scattering analysis was performed. The static light scattering experiment was done to validate; the more straight forward Dynamic Light Scattering (DLS) measurement we performed. Both static multi angle and dynamic light scattering revealed similar sizes. Cryo-TEM and static multi angle light scattering were both performed on non-loaded, empty, and loaded micelles. Cryo-TEM and static multi angle light scattering results are not included. We have limited ourselves to report DLS results which could be performed on all samples.

The size of the micelles was determined by Dynamic Light Scattering (DLS) (Zetasizer Nano ZS, Malvern Instruments Ltd., Malvern, UK) at 25°C at a scattering angle of 173°. Ideally the number of photon counts is high enough to get a good signal to noise ratio and yet small enough to prevent multiple scattering effects. The reported polydispersity index (PdI) is as given by the Malvern Zetasizer Nano ZS, as for the reported hydrodynamic diameter (D_h) (z-averaged hydrodynamic diameter). Polydispersity for this light scattering analysis is used to describe the width of the particle size distribution, derived from the polydispersity index. The polydispersity index is a parameter calculated from the Cumulants analysis of the DLS measured intensity autocorrelation function. In the cumulants analysis, a single particle size is assumed and a single exponential fit is applied to the autocorrelation function. All samples were measured as processed, undiluted. Size distributions measured with DLS were unimodal.

4.4 Results

4.4.1 DLS results on reproducibility on empty and active ingredient loaded micelles

To enable a nanoprecipitation reproducibility test, TBB2 and TBC1, see Table 4.5, triblock copolymers were made in three separate copolymer solutions in acetone and precipitated in MilliQ to see what the reproducibility of the process is. Table 4.14 shows the results of the reproducibility test of empty and active ingredient loaded micelles. We note that the PdI for all samples in this table are below 0.1. TBB2R series is to check the reproducibility of

making empty TBB2 copolymer micelles, TBC1R shows the results on the reproducibility of TBC1 copolymer micelles and TBC1RE shows the reproducibility of rapamycin loaded TBC1 copolymer micelles, see Tables 4.6 and 4.7 sample group ID.

Table 4.14: Reproducibility results on separate performed nanoprecipitation processes on empty and active ingredient loaded micelles in terms of the (averaged) hydrodynamic diameter, $D_h^{(av)}$ and the standard deviation, σ_{Dh}.

		DLS results for the size (nm)		
Sample group ID	Sample ID	D_h	$D_h^{(av)}$	σ_{Dh}
TBB2R	TBB2R1	31.1	31.3	0.3
	TBB2R2	31.6		
	TBB2R3	31.3		
TBC1R	TBC1R1	26.8	26.9	0.2
	TBC1R2	27.1		
	TBC1R3	26.9		
TBC1RE	TBC1RE1	26.5	26.4	0.1
	TBC1RE2	26.4		
	TBC1RE1	26.4		

The reproducibility of all three sample groups is excellent, showing low standard deviations (σ_{Dh}) on hydrodynamic diameter and PdI. The hydrodynamic diameters of the separate sample groups are within 1 nm (range). The PdI of the separate sample groups shows narrow monomodal particle distributions. Another observation is the smaller averaged hydrodynamic diameter size of the TBC1RE sample group compared to the TBC1R sample group. Although the TBC1RE sample group is loaded with rapamycin and the TBC1R sample group only consists of empty micelles. Still the TBC1RE group has a smaller hydrodynamic diameter size which can only be explained by strong (hydrophobic) interactions between active ingredient, rapamycin, and the hydrophobic end blocks in the core leading to a higher packing density and lower water content in the core resulting in slightly smaller particles.

4.4.2 DLS results of single excipient, homopolymer, loaded micelles

Inspired by the SF-SCF results in Fig. 3.8 of Chapter 3 [37], we investigated whether a hydrophobic polymeric excipient with a chemical composition similar to the hydrophobic blocks of the copolymers used can be encapsulated. In this way we determined the loading capacity/capability and the relation between excipient weight percentage and (hydrodynamic diameter) size. It indeed appears to be possible to fill the micelles with inactive ingredients as follows from the increase of the size of the micelles and it turns out that the amount of excipient allows tuning the particle size of the resulting micelles. We have collected DLS results of the hydrodynamic diameter and PdI in Fig. 4.4 and 4.5.

These results indicate that we can produce tailor-made nanoparticles for drug delivery, at a given size with a given loading. See the appendix for a rationale for the linear dependence of D_h (hydrodynamic diameter) on the amount of excipient.

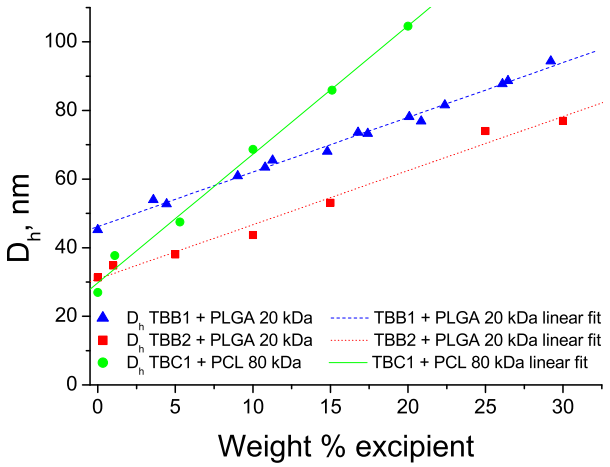

Figure 4.4: Hydrodynamic diameter as function of the loading wt% TBB1, TBB2 and TBC1 excipient loaded, PLGA 20 kDa for TBB1 and TBB2 and PCL 80 kDa for TBC1, micelles, as measured by DLS.

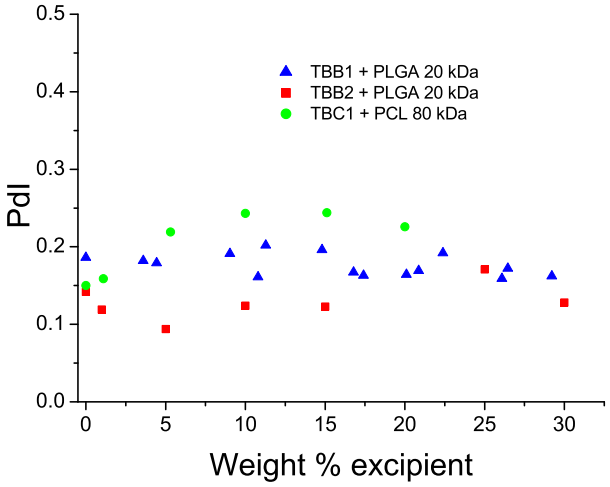

Figure 4.5: TBB1, TBB2 and TBC1 excipient loaded, PLGA 20 kDa for TBB1 and TBB2 and PCL 80 kDa for TBC1, micelles, DLS measurement results for the PdI.

For most medical applications micellar size is of paramount importance for the therapeutic efficacy of the treatment. Some anti-cancer therapies take advantage of the EPR-effect where size control between 50 and 80 nm is mandated. Using TBB1, see Table 4.5, copolymer triblocks with a 5% weight loading of excipient will render micelles with a hydrodynamic diameter of approximately 50 nm, if using TBB2, see Table 4.5, copolymer triblocks with the same weight percentage of excipient loading will render micelles with an approximate hydrodynamic diameter of 40 nm. If the drug loading / concentration is important the size can be tuned using higher or lower molecular weights of the triblock copolymers resulting in respectively smaller or bigger micelles with the same loading of active ingredient, mass of active ingredient per micelle.

Remarkable is the difference in slope comparing TBB triblock copolymer excipient loaded micelles with TBC1, see Table 4.5, triblock copolymer loaded micelles. In the Appendix there is a rationale about the linearity of the slope. From Equation 4.5, see Appendix, it follows that the slope is proportional to $\Gamma_\infty / c_{\text{copol}}$. Since in these experiments c_{copol} is fixed a higher slope indicates the corona density is higher for the PCL triblock copolymers. This actually agrees with the SF-SCF computations, see Fig. 3.6, 3.7 and 3.9 in Chapter 3 [37].

4.4.3 Size stability of single component, homopolymer and active ingredient (rapamycin and β-carotene) loaded micelle formulations in time

Using hydrolytically degradable polymers (PLGA and PCL) will have an impact on micellar suspension stability in time due to hydrolytic degradation of the (hydrophobic) blocks in the triblock copolymers in an aqueous environment. In order to assess the real micellar stability it is decided to focus on the stability before hydrolytic degradation can have an effect on micellar stability. Arbitrarily we chose 15 days as the time after which the hydrolytic degradation of the block copolymers will have the most prominent effect on the stability [50]. The lack of change in size, hydrodynamic diameter, and PdI within 15 days after preparation will reveal the stability of micellar suspensions in time. To avoid continuous DLS measurements, the samples were subjected to a daily visual inspection. In this way we could detect instabilities such as agglomerates, change in appearance and / or color. If such a change was detected the sample was measured by DLS. If no changes were observed the formulation was measured after preparation at day 1 and after 15 days. First homopolymer excipient loaded micelles were tested on stability and subsequently active ingredient loaded micelles were tested on stability, all stability testing was at room temperature.

4.4.3.1 Size stability of single component, homopolymer-loaded micelle formulations in time

TBB1, see Table 4.5, triblock copolymer excipient loaded, PLGA 20 kDa, micelles were tested on stability in time. Between the first day and the following 14 days no visual change of the micellar suspension was observed. From the reproducibility data in Table 4.14 it is clear that the results of day 1 and day 15 are (Table 4.15) very similar. This implies that the particles are stable for 15 days.

Table 4.15: TBB1 homopolymer, PLGA 20 kDa, loaded micelle stability; TBB1EX-series, DLS results.

Sample ID	Time (days)	D_h (nm)	PdI
TBB1EX	Day 1	48.7	0.19
	Day 15	49.1	0.10

4.4.3.2 Size Stability of single component, active ingredient (rapamycin and β-carotene), loaded micelle formulations in time

TBB1 (see Table 4.5) triblock copolymer micelles were loaded with rapamycin as an active ingredient to test the stability of active ingredient loaded micelles. Since the weight percentage of the active ingredient with respect to the triblock copolymer content is small (approximately 0.5% (wt%) in ratio to the used triblock copolymer) the size of the active ingredient loaded micelle does not change very much compared to the empty micelles. However, it was expected that the active ingredient would have some effect on the size, therefore it was decided to measure this sample without any visual indications also on the second day after processing to see if something happens with the initial processed size.

As can been seen in table 4.16 there was a slight decrease in size within the first two days. Subsequently, however there were no visual indications implying any instability. At day 15 the sample was measured and the hydrodynamic diameter turned out to be similar to the measurement on day 1. The PdI however, seems to decline in time, which is the same for homopolymer loaded micelles (table 4.15). The reason for the initial size change between day 1 and day 2 needs more investigation as the drop for the PdI. Overall, it seems that the particle size is fairly constant and the dispersion appears to have a long shelf-life.

Table 4.16: TBB1 active ingredient, rapamycin, loaded micelle stability; TBB1R-series, DLS results.

Sample ID	Time (days)	D_h (nm)	PdI
TBB1R	Day 1	45.3	0.20
	Day 2	43.8	0.20
	Day 15	45.3	0.11

TBB2, see Table 4.9, triblock copolymers were loaded with β-carotene as an active ingredient. For making micelles loaded with β-carotene it is known that they suffer from Ostwald ripening [32]. If these micellar suspensions can resist Ostwald ripening (constant size in time) we can conclude that active ingredient transport from inner-micelle to bulk is limited. Fig. 4.6 shows the results of the TBB2 triblock copolymer β-carotene loaded micelle stability test. On day 8 the suspensions color changed from orange to yellow, probably due to oxidation of the β-carotene. From the DLS measurements it appeared that the hydrodynamic diameter was increasing slightly while the PdI was still more or less stable at day 8. At day 14 there was a turn over from the color from yellow to white resulting in a stable hydrodynamic diameter but an increase in PdI. In order to see what was further happening we continued the measurement until visual aggregation of the suspension was observed on day 26 were after DLS measurements were no longer possible.

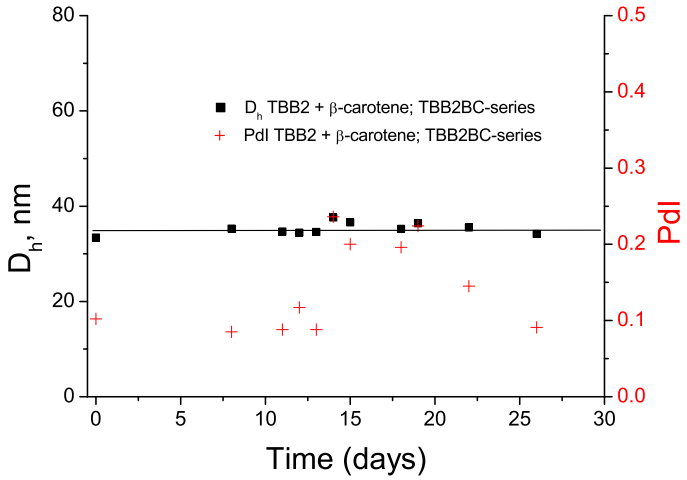

Figure 4.6: TBB2 triblock copolymer active ingredient (β-carotene) loaded micelles stability, TBB2BC-series, DLS results (line in the hydrodynamic diameter results to guide the eye).

4.5 Conclusions

We have shown that well-defined micelles can be prepared composed of PCL-PEO-PCL and PLGA-PEO-PLGA triblock copolymers using the nanoprecipitation approach. By adding hydrophobic compounds we can load the micelle in order to achieve a desired particle size and loading. Ostwald ripening was minimized with this approach. Stabilization of micelles by block copolymers prevents particle aggregation, but the stabilizing polymer layer is open enough to allow solute mass transfer. In order to prevent/minimize solute transfer it is desired to tune the particle core composition to prevent this mass transfer. Additionally, the solubility of the encapsulated compound can be decreased by antisolvent addition to the bulk resulting in a significant slow down of Ostwald ripening. The extremely low solubility of the used triblock copolymers limits copolymer exchange between micelle and bulk again minimizing solute mass transfer and slowing down Ostwald ripening. There is no need to use surfactant in this process, conventional nanoprecipitation processes need an excess of surfactant, mostly very water soluble with relative high CMC's. Since we incorporated the surfactant function in the polymer backbone no exchange of adsorbed and free surfactant is needed for stable suspensions. This also avoids washing the nanoparticle suspension to remove excess of free surfactant used in the process and limits Ostwald ripening. We were able to synthesize different kinds of triblock copolymers allowing simultaneous tuning of the size and loading. When performing the nanoprecipitation process there is hardly an influence of temperature and triblock copolymer molar mass polydispersity. However, using these micelles in electrolytes, e.g. in vivo, care must be taken to avoid destabilization of the micelles due to electrostatic interactions. Non reported data shows that it is feasible to perform the nanoprecipitation process, using the mentioned triblock copolymers, in different electrolytes at different pH's and that the suspension stays stable in time.

SF-SCF computational predictions that we recently performed provide an accurate prediction of the size of active ingredient loaded and unloaded micelles. SF-SCF computations

enable to predict equilibrium copolymer micelles. The hydrodynamic size that follows from these computations matches well with the measured particle sizes from dynamic light scattering. From the computations it follows that the size of the nanoparticles is determined by the number-averaged molar mass of the block copolymers; polydispersity hardly affects the size of the micelles. SF-SCF is a useful tool to unravel the structure-function relationship between copolymer composition and micellar size and morphology. Using theoretical SF-SCF predictions will lead to more efficient experimentation.

Appendix

The linear dependence of D_h on the amount of loaded component(s) can be rationalized as follows. The micelles are stabilized by the copolymers with the PEO parts forming a steric stabilization layer. Consider N_p copolymer particles, each having a diameter d and volume $v_p = (\pi/6)d^3$, in a total volume V. Such a dispersion has a volume fraction ϕ of particles:

$$\phi = \frac{N_p v_p}{V} \tag{4.1}$$

The total amount of surface in the volume V is:

$$A_T = N_p \pi d^2 \tag{4.2}$$

From equations 4.1 + 4.2 it follows:

$$A_T = \frac{6\phi V}{d} \tag{4.3}$$

Imagine all copolymers (acting as surfactants) are at the particle-solvent interface. Then the total (initial) copolymer concentration equals:

$$c_{\text{copol}} = \frac{\Gamma_\infty A_T}{V} \tag{4.4}$$

where Γ_∞ is the adsorbed amount of polymers (surfactant) at saturation. For example, for homopolymers this amount is ≈ 1 mg/m^2. Insertion of 4.3 into 4.4 yields:

$$D_h = \frac{6\Gamma_\infty \phi}{c_{\text{copol}}} \tag{4.5}$$

This means that for instance for $\Gamma_\infty = 1$ mg/m^2, $d = 30$ nm and $\phi = 0.1$ one expects an overall copolymer concentration of 20 g/L is covering the surfaces. From 4.5 it follows that it is fair to assume that D_h increases linearly with the wt% of loaded component(s) because it is proportional to the volume fraction of particles.

Acknowledgments

The authors wish to thank J. Put for supporting this study, M. Boerakker, H. Langermans, L. Bremer and B. Voogt for stimulating discussions, T. Kockelkoren, G. Draaisma and T. Handels for synthetic assistance during copolymer synthesis and N. Woike for technical assistance. A special thanks goes to R.K. Prud'homme for inspiring discussions.

Bibliography

[1] R. Ravichandran, Int. J. Green nanotech., **1:2**, 72-96 (2010).
[2] C.C. Chen and G Wagner, Trans. IChemE, Part A, **82**, 1432-1437 (2004).
[3] N.S. Sozer and L. Kokini, Trends Biotechnol., **27**, 82-89 (2009).
[4] K.S. Soppimath, T.M. Aminabhavi, A.R. Kulkarni and W.E. Rudzinski, J. Control. Release, **70**, 1-20 (2001).
[5] J. Panyam and V. Labhasetwar, Adv. Drug Deliver. Rev., **55** 329-347 (2003).
[6] N. Kamaly, Z. Xiao, P.M. Valencia, A.F. Radovc-Moreno and O.C. Farokhzad, Chem Soc Rev., **41**, 2971-3010 (2012).
[7] A. Vila, H. Gill, O. McCallion and M-J. Alonso, J. Control. Release, **98**, 231-244 (2004).
[8] M.G. Qaddoumi, H. Ueda, J. Yang, J. Davda, V. Labhasetwar and V.H.L. Lee, Pharm. Res., **21**, 641-648 (2004).
[9] H. Suh, B. Jeong, F. Liu and S.W. Kim, Pharm. Res., **15**, 1495-1498 (1998).
[10] Y. Matsumura and H. Maeda, Cancer Res., **6**, 6387-6392 (1986).
[11] L.H. Reddy, J. Pharm. Pharmacol., **57**, 1231-1242 (2005).
[12] H. Maeda, J. Wu, T. Sawa, Y. Matsumura and K. Hori, J. Control. Release, **65**, 271-284 (2000).
[13] H. Maeda and Y. Matsumura, Crit. Rev. Ther. Drug, **6**, 193-210 (1989).
[14] H. Maeda and J. Fang, Adv. Polym. Sci., **193**, 103-121 (2006).
[15] H. Maeda and J. Daruwalla, Eur. J. Pharm. Biopharm., **71**, 409-419 (2009).
[16] D.E. Owens and N.A. Peppas, Inter. J. Pharm., **307**, 93-102 (2006).
[17] L. Mei, H. Sun, X. Jin, D. Zhu, R. Sun, M. Zhang and C. Song, Pharm. Res., **24**, 955-962 (2007).
[18] C. Song, V. Labhasetwar, X. Cui, T. Underwood and R.J. Levy, J. Control. Release, **54**, 201-211 (1998).
[19] K. Letchford and H. Burt, Eur. J. Pharm. Biopharm., **65**, 259-269 (2007).
[20] V.P. Torchilin, J. Control. Release, **73**, 137-172 (2001).
[21] R. Tong and J. Cheng, Pol. Rev., **47**, 345-381 (2007).
[22] Y. Kakizawa and K. Kataoka, Adv. Drug Deliv. Rev., **54**, 203-222 (2002).
[23] M.L. Adams, A. Lavasanifar and G.S. Kwon, J. Pharm Pharm. Sci.,**92**, 1343-1355 (2003).
[24] M.L. Forrest, A. Zhao, C-Y. Won, A.W. Malick and G.S. Kwon , J. Control. Release, **116**, 139-149 (2006)
[25] Y. Zhao, H. Liang, S. Wang and C. Wu, J. Phys. Chem. B, **105**, 848-851 (2001).
[26] T. Nie, Y. Zhao, Z. Xie, and C. Wu, Macromolecules, **36**, 8825-8829 (2003).
[27] H.M. Burt, X. Zhang, P. Toleikis and L. Embree and W.L. Hunter, Colloids Surf., B, **16**, 161-171 (1999).
[28] Z. Song, R. Feng, M. Sun , C. Guo, Y. Gao, L. Li and G. Zhai, J. Colloid Interface Sci., **354**, 116123 (2011).
[29] B. Jeong , Y.H. Bae and S.W. Kim, Colloids Surf., B, **16**, 185193 (1999).
[30] R. Lund, L. Willner, J. Stellbrink, A. Radulescu and D. Richter, Phys. B, **350**, 909-919 (2004).
[31] R. Lund, L. Willner and D. Richter, Macromolecules, **39**, 4566-4575 (2006).
[32] Y. Liu, K. Kathan, W. Saad and R.K. Prud'homme, Phys. Rev. Lett., **98**, 036102 (2007).

[33] T. Niwa, H. Takeuchi, T. Hino, N. Kunou and Y. Kawashima, J. Control. Release, **25**, 89-98 (1993).
[34] H. Fessi, F. Puisieux, J.Ph. Devissaguet, N. Ammoury and S. Benita, Int. J. Pharm., **55**, R1-R4 (1989).
[35] H. Lannibois, A. Hasmy, R. Botet, O.A. Chariol and B. Cabane, J. Phys. II France, **7**, 318-342 (1997).
[36] D. Horn and J. Rieger, Angew. Chem. Int. Ed., **40**, 4339-4361 (2001).
[37] J.G.J.L. Lebouille, R. Tuinier, L.F.W. Vleugels, M.A. Cohen Stuart and F.A.M. Leermakers, Soft Matter **9**, 7515-7525 (2013).
[38] G.J. Fleer, M.A. Cohen Stuart, J.M.H.M. Scheutjens, T. Cosgrove, and B. Vincent, *Polymers at Interfaces* (Chapman and Hall, London, first edition, 1993).
[39] P.N. Hurter, J.M.H.M. Scheutjens and T.A. Hatton, Macromolecules, **26**, 5592-5601 (1993).
[40] Y. Lauw, F.A.M. Leermakers and M.A. Cohen Stuart, J. Phys. Chem. B, **110**, 465-477 (2006).
[41] E.B. Zhulina and O.V. Borisov, Macromolecules, **45**, 4429-4440 (2012).
[42] K. Knop, R. Hoogenboom, D. Fisher and U.S. Schubert, Angew. Chem. Int. Edit., **49**, 6288-6308 (2010).
[43] M. Kodama and S. Seki, Adv. Colloid Interface Sci., **35**, 1-30 (1991).
[44] N. Nishikido, J. Coll. Interf. Sci., **136**, 401-407 (1990).
[45] L.R. Fukumoto and G. Mazza, J. Agric. Food Chem., **48**, 3597-3604 (2000).
[46] A. Sokmen, M. Gulluce, H.A. Akpulat, D. Daferera, B. Tepe, M. Polissiou, M. Sokmen and F. Sahin, Food Control., **15**, 627-634 (2004).
[47] G.W. Burton and K.U. Ingold, Science, **224**, 569-573 (1984).
[48] S. Chen, R. Pieper, D. C. Webster and J. Singh, Int. J. Pharm., **288**, 207-218 (2005).
[49] G.M. Zentner, J. Control. Release, **1**, 203-215 (2001).
[50] R. Peters, J.G.J.L. Lebouille, B. Plum, P. Schoenmakers and S. van der Wal, Polym. Degrad. Stabil., **96**, 1589-1601 (2011).

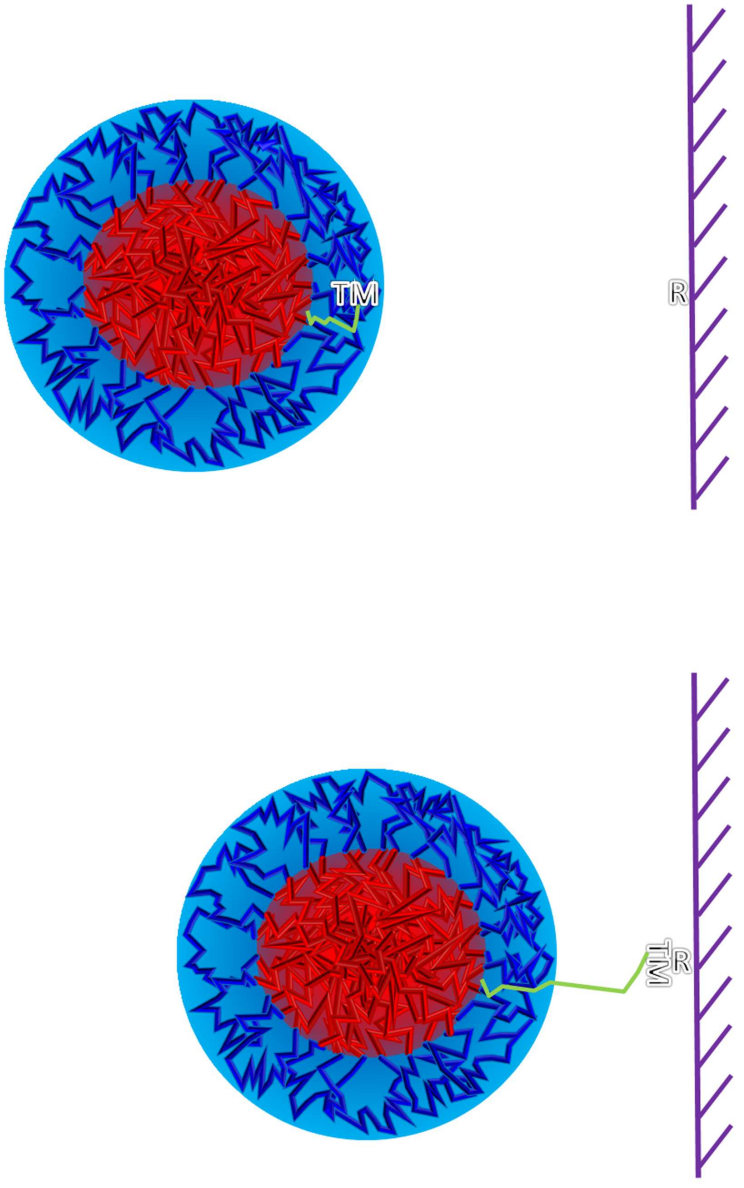
TM
R
TM
R

Design of block copolymer based micelles for active and passive targeting

5

This chapter will be submitted for publication:
J.G.J.L. Lebouille, R. Tuinier, M.A. Cohen Stuart and F.A.M. Leermakers,
Design of block copolymer based micelles for active and passive targeting.

Abstract

A self-consistent field study is presented on the design of active and passive targeting block copolymeric micelles. These micelles form in water by the self-assembly of triblock copolymers with a hydrophilic middle block and two hydrophobic outer blocks. A minority amount of diblock copolymers, typically just one, with the same chemistry, are taken to co-assemble into these micelles. At the end of the hydrophilic block of the diblock copolymers a targeting moiety (TM) is present. Assuming that the rotation of the micelle towards the target is sufficiently fast, we can elaborate a one-gradient cell model, wherein the micelle is in the center and the receptor (R) substrate exists on the outer plane of the spherical coordinate system.
The distribution function of the targeting moiety can be converted into a Landau free energy as a function of the distance of the targeting moiety from the adsorbing substrate. Typically, this Landau free energy has local minima and corresponding maxima. The lowest minimum, which is the ground state, shifts from within the micelle to the adsorbing state upon bringing the substrate closer to the micelle, implying a jump-like translocation of the targeting moiety. Equally deep minima represent the binodal of the phase transition, which is, due to the finite chain length, first-order like. The maximum in between the two relevant minima imply that there is an activation barrier for the targeting moiety to reach the receptor surface. The time to cross this barrier is expected to increase exponentially with the barrier height.
We localize the parameter space wherein the targeting moiety is (when the micelle is far from the target) preferably hidden in the stealthy hydrophilic corona of the micelle, which is desirable to avoid undesired immune responses, and still can jump out of the corona to reach the target quick enough, that is when the barrier height is sufficiently low. The latter requirement may be identified by a spinodal condition. We found that such hidden TMs can still jump-like establish a TM-R contact at distances up to twice the corona size. The translocation transition will work best when the affinity of the TM for the core is avoided and when hydrophilic TMs are selected.

keywords: Micelle, Scheutjens-Fleer Self-Consistent Field theory (SF-SCF), particle size prediction, active and passive targeting micelles, copolymers, targeting moiety receptor contact.

5.1 Introduction

Nanoparticles are nowadays used for pharmaceutical applications [1–4]. The drug delivery performance of such particles depends on control over particle size, drug loading and active targeting capability. One can use nanosized micellar structures formed by a combination of (different) amphiphilic molecules in a selective solvent. Nanoprecipitation enables the formation of self-assembled block copolymer spherical micelles, even for rather hydrophobic copolymers. Potent drugs are often rather hydrophobic ingredients for which polymeric micelles are promising carriers, with potential for controlled encapsulation of compounds at high loadings. Additionally, using polymeric micelles offers routes to control release, stability and bio-distribution of active agents in the body for both passive and active targeting [5–13]. Here we focus on water as the solvent and consider block copolymers with two apolar and one polar block, the so called ABA blockcopolymers which readily form spherical flower-like micelles. To assure active targeting we propose to combine the triblock copolymers with AB diblocks with targeting moieties at the end of the hydrophilic block B. Within the spherical micelles the hydrophobic entities are collected in a compact core, whereas the water-soluble blocks remain hydrated and form a corona. The diblocks are designed in such a way that their B blocks are preferably located outside the hydrophobic core of the micelle. As hydrophobic blocks A we envision poly-(lactic-co-glycolic) acid (PLGA) and as hydrophilic block B polyethylene oxide (PEO). Although PEO is non-degradable it is non-toxic and can easily be removed from the body by the normal excretion (renal) pathways as long as the molar mass is below 20 kDa [14]. The hydrophobic part consists of PLGA, an FDA approved and well known biodegradable polymer used in commercially available drug delivery applications [4, 15]. In principle PEO and/or PLGA can be replaced by other hydrophilic and hydrophobic (co)polymers.

The goal is to obtain more fundamental insight in the behaviour of copolymers with targeting moieties within composite micelles. Our method is to use the Scheutjens-Fleer self-consistent field (SF-SCF) theory [16–18], successfully used earlier (see Chapters 3 and 4) to theoretically study the triblock copolymer micelle structure and stability [19, 20]. It was found that by implementing a model wherein segments are represented as amorphous beads, i.e. $A_{60}B_{60}A_{60}$ ($PLGA_{60}PEO_{60}PLGA_{60}$; 7.5-6.0-7.5 kDa), there exists a set of interaction parameters that leads to structural properties of micelles that compare favourably with the ones found experimentally using the solvent precipitation method [21]. Once such micelles have formed, we envision that the core becomes unresponsive, i.e. glassy, and this allows us to focus here exclusively on what happens in the molecularly quenched, but conformationally adaptive corona. Basically we take the core to be a solid particle (composed of units of type A; PLGA) of which the size is set equal to that found for the micelle cores. We graft both ends of a hydrophilic chain B_{60} (PEO; 6.0 kDa) onto the core so that a spherical brush is formed of looped chains. The grafting density of this brush is set equal to the aggregation number found for the self-assembled micelles. Next we consider that onto the same core there is one chain grafted by one end only, the AB (PLGA-PEO) diblocks leaving one free dangling chain end. We take the chemistry of this chain identical to that of the triblocks, only the length of the B (PEO) block of this minority chain is a free variable. The key is that the free end is given some different properties, consistent with the idea that this end is functionalized by a targeting moiety (TM). The focus of this paper is to understand the behaviour of the minority chain and in particular understand the whereabouts of the functional free end. In more detail

our attention will be on the translocation transition of the minority chain end going jump-like from being inside the corona to outside the brush, a transition which is driven by the potential energy gain received when the TM is in contact with a receptor (R). In our simple cell model the receptor is expected to be present homogeneously along the surface that surrounds the central micelle.

Biodistribution of micelles in the human body is mainly dependant on their size, surface and corona structure. Micellar size control exploits passive targeting via the enhanced permeation and retention (EPR) effect [22–26]. For targeting purposes we focus on tumor cells and tissue as an example. Improving chemotherapy offers a major challenge in human health treatments. Of course other diseased tissues will demand different targeting moiety (TM) receptor (R) combinations. Especially for micellar accumulation in tumor tissues the size and surface structure is of crucial importance for passive targeting.

For active targeting one needs to incorporate moieties for specific targeting into or onto the micellar corona. Ideally targeting moieties are included that are specific for the targeted tissue. When the connection between targeting moiety and receptor is strong enough active targeting will be enabled. From the biological perspective there is a number of requirements. First of all the micelle needs to have the proper chemistry. It is known that polyethylene oxide micelles are stealthy (non interfering with the immune system) and have long blood circulation times [27]. Hence we take the interaction parameter for the B group with water accordingly. To avoid any undesired interaction with the immune system we believe that it is favourable to have the chain end well inside the micelle corona, that is under normal operation conditions, when the micelle is far from its target. We can implement this requirement in two ways. In the first option we take the length of the minority chain to be less then half the length of the loops that form the bulk of the corona, i.e. $N_B < 30$. To go outside the corona will imply extra stretching of the minority chain which is entropically unfavourable. The second option is to give the free chain end an affinity for the core of the micelle. Typically this already occurs when the targeting moiety is hydrophobic. Then there is a natural tendency that the TM is associated to the core. In the adsorbed state of the TM to the cote the TM is obviously inside the corona, even when the length of the minority chain exceeds that of the half-loop length. Experimentally, when the TM is hydrophobic, it may be locked inside the core and is subsequently unable to escape from it. Here we will ignore this scenario because we take the core to be composed of A-segments only (the core is a boundary condition in the current calculations). On top of the hydrophobic interaction we may introduce some extra surface affinity, e.g. due to some specific interactions. Of course this will complicate our analysis because there will be a free energy barrier associated with the detachment of the end-group from the core and the time limiting step for the translocation transition may well be associated with the desorption process, rather than being associated to the entropic stretching towards the adsorbing surface itself.

The design, manufacturing and characterization of ABA block copolymer micelles composed of rather hydrophobic copolymers was reported previously [19–21], see Chapters 3 and 4. It was demonstrated that tuning the size and loading can be achieved by using triblock copolymers with a particular chain length combined with active ingredients. The synthesis and incorporation of targeting moieties onto existing particles is difficult and tedious. In most cases the targeting function on a nanoparticle/micelle is established after its formation. Since most of these processes demand surface chemistry instead of physical interactions, a purification step is mandative to remove reactants [28–32]. To omit the post processing and

purification steps we propose a single micellar processing method. This allows incorporation of the targeting moieties, present on the diblocks, from the start of the micellar production process using the nanoprecipitation method.

The remainder of this Chapter is the following. We will first give elementary background information on the modeling method, focusing on the main approximations. We then give detailed information on the model used and discuss the relevant parameters. We will present the structure of the polymeric micelle that is used to further study the escape or translocation transition of the minority chain. We will subsequently discuss in somewhat more detail on how we are going to analyse the translocation transition of the TMs. More specifically we will elaborate on the Landau free energy as a function of the position of the free end. We use this free energy to judge when the jump-like phase transition occurs and what the origin is of the free energy barriers that are encountered. We will elaborate on a typical example. The main results are collected in diagrams of state wherein the binodal and spinodal curves are collected. These diagrams facilitate the search for the most optimal properties of the minority chain in a composite micelle. In our discussion and conclusions we sum up our theoretical modelling results with regard to the design of an active targeting capacity for composite micelles.

5.2 Theory

This section contains two major parts. In the first one the focus is on the SF-SCF theory. We explain the main approximations of the modelling in combination with the model that is used for the copolymer self-assembly. For more detailed information we refer to Chapters 3 and 4 [19, 20]. We then will present the micelle that is selected as a representative case in some detail and reproduce a result from Chapter 4 [20] for ease of reference. Subsequently we will elaborate on the model used for the remainder of the paper, for which the standpoint is implemented that the micelles are molecularly quenched, implying that the aggregation numbers and core structure are frozen in. Important is that the micelles remain responsive in the micelle corona for which the chains can conformationally rearrange. In the second section we elaborate on the use of the Landau free energy. We will do this by elaborating on a specific example, and explain in detail the physics that are accounted for. In this section we will pay attention to the binodal and the relevant spinodal. Finally, we discuss the relevant SF-SCF parameters which will be investigated on their influence on TM-R contact.

5.2.1 SF-SCF theory

Making use of the mean field approximation, and more specifically the Bragg-Williams approximation (more about this below) allows to formulate for a system a free energy in terms of two conjugate profiles, namely the measurable volume fraction (dimensionless concentrations) $\varphi(r)$ and complementary segment potential $u(r)$ distributions. In a way these potentials are external potentials because we use them to obtain statistical weights, the so-called Boltzmann weights as in a barometric height equation $G(r) = \exp(-u(r))$. (Here and below we will make all energy quantities dimensionless by normalising them with the thermal energy k_BT). The weights are not fixed, but the segment potentials appear to be a function of the volume fractions. The functionality follows uniquely from the free energy optimisation.

As a result the segment potential take the interaction of a given segment with its surroundings into account. These interactions are parameterized by Flory-Huggins interaction parameters χ_{X-Y} wherein both X and Y are segment (or solvent) types. A positive value means that the XY contacts are less favourable than the average of XX and YY contact. Hence a sufficiently large positive value implies segregation. Low values or negative values are needed for proper miscibility.

Interestingly, not only do the potentials depend on the volume fractions, the inverse is also true: the volume fractions are a function of the segment potentials. To implement this dependence, it is necessary to invoke a chain model. Typically we use freely jointed chain model, which guarantees that neighbouring segments of the chain are at a distance of a bond length. However, as no further through-bond correlations are imposed a chain can also fold back on previously occupied places. Let us next focus on a particular conformation c of the chain, completely specified by the coordinates of the individual segments. This conformation is found to have a particular potential energy u_c, which is computed by the sum over the segment potentials felt by the consecutive segments along the contour of conformation c. The statistical weight of this conformation is then again given by a Boltzmann weight, $G_c = \exp(-u_c)$. Such weight is found for all possible and allowed conformations. With these statistical weights we can construct the overall volume fraction distribution. Of course this requires a sum over the contributions of all possible and allowed conformations. As the total number of possible conformations is very large indeed, these sums suggests an insurmountably large job. Fortunately there exists an elegant propagator method that copes with it efficiently, in a computation time which is linearly proportional to the number of segments in the chain (not shown).

Summarizing, characteristic for the SCF method we have

$$\varphi[\{u\}] \leftrightarrow u[\{\varphi\}] \quad . \tag{5.1}$$

In words, the left hand side of this equation says that the volume fractions can be computed from the potentials and the right hand side says the opposite. In the case that the set of potentials and volume fractions is consistent, that is, that the potentials both follow from and determine the same volume fractions and vice versa, we refer to the solution being self-consistent. There is a pitfall, namely as specified thus for there are many SCF solutions to the equations. That is why one additional requirement is necessary to make the solution unique. This additional requirement specifies the use of an incompressibility relation. Here we opt the system to be incompressible and therefore we impose

$$\sum_X \varphi_X(r) = 1 \tag{5.2}$$

for each coordinate r.

In very few cases it is possible solve the self-consistent field solution analytically. It is of no surprise that the self-assembly of copolymers into spherical micelles is not one of these rare cases. As a result we have to implement the equations into a computer model and solve for the fixed point numerically. Invariably, one needs to discretize the equations somehow. Here we follow the method of Scheutjens and Fleer and make use of a lattice of sites leading to the SF-SCF method. The characteristic length of a lattice site is taken equal to the bond length, so that one polymer segment exactly fits into a lattice site. Solvent molecules are taken to have the same volume as a segment for simplicity.

For many problems one can recognize some sort of symmetry element. For example in spherical micelles we can easily imagine that the relevant gradients in polymer densities occur in the radial direction and that the density fluctuations in a shell of lattice sites with equal distance to the center are very small. This motivates us to reduce the three-dimensional system and implement this in a one-gradient spherical geometry. Then lattice layers are numbered starting from the center $r = 1, 2, \cdots, M$. Naturally, the number of lattice sites $L(r)$ in layer r scales as $L(r) \propto r^2$. By ignoring the density fluctuations in the layer (mean field approximation) we can implement the volume fraction $\varphi_X(r) = n_X(r)/L(r)$, wherein $n_X(r)$ is the number of segments of component X in layer r. At the upper boundary at $r = M$ typically reflecting boundary conditions apply. This is implemented by forcing all density gradients to be zero at this boundary, i.e., $\varphi_X(M+1) = \varphi_X(M)$. Usually the value of M is taken very large, far from the micelle, which is positioned at the center of the spherical coordinate system, where the density gradients have vanished (bulk). Then these reflecting boundary conditions are inconsequential for any physical property of the system. However, when the system size M is not very large, the reflecting boundaries will simulate the interactions between micelles, wherein the micelle center to micelle center distance d is given by $d = 2 \times M$.

Below we will consider a spherical 'micelle' in the vicinity of a surface. This typically cannot be captured in a spherical geometry. Instead we should use a two-gradient cylindrical coordinate system. We have not implemented this here and insist on keeping our spherical geometry. More specifically, we are going to assume that the rotational diffusion of the micelle is quick enough so that the probe will find the receptor even when some rotation of the micelle is needed. Then having a surface in all directions around the micelle (as is explicitly implemented) is a reasonable approximation. This idea is realized by imposing an impenetrable boundary at layer $r = M+1$, that is, at layer $r = M+1$ the volume fraction of a segment with type R is unity. Segments with type X feel this boundary when they sit in layer $z = M$ through the interaction parameter χ_{X-R}. Also the solvent W has an interaction with this surface, χ_{W-R} and typically segments may adsorb onto the surface only when a solvent molecule is displaced from it, hence micelleadsorption is expected only when $\Delta\chi_R \equiv \chi_{X-R} - \chi_{W-R} < 0$, otherwise the solvent is preferentially absorbed at the surface. It is well known that polymer chains experience conformational entropy losses when they are directly next to an impenetrable wall, the reason for this is that the orientation of bonds is hindered as these cannot enter into the solid phase. To compensate for this, it is necessary that $\Delta\chi_R < \chi_{\text{critical}}$, for the segment X (part of a chain) to adsorb, where in good approximation $\chi_{\text{critical}} = -1$ for typical segments in a polymer chain. The critical adsorption energy for end-segments is expected to be less negative as these segments have just one bond connected to them. The critical adsorption is also a function of the solvent quality. To understand this, one should realize that a segment next to the surface cannot interact with the solvent in all directions. Hence it can avoid one contact with the solvent and thus there is an increased tendency to be next to the (receptor) surface. Below the affinity of the probe for the (receptor) surface is implemented using the parameter χ_{TM-R}.

In the SF-SCF method the molecules are discretized, they are taken to be composed of segments numbered $s = 1, 2, \cdots, N$. We refer to N as the chain length, but possibly the degree of polymerization is a better term for it. We do not take any structural features on the segment level into account. However, we do allow for copolymer type of interactions, e.g. one segment is hydrophobic and the other is hydrophilic. We do this by specifying the Flory-Huggins interaction parameters for each segment type accordingly (see section 5.2.3).

5.2.1.1 The molecular model and self-assembly

The study of the self-assembly of copolymers into, e.g., thermodynamically equilibrated spherical micelles is a key application of the Scheutjens-Fleer self-consistent field (SF-SCF) theory. In Chapters 3 and 4 we considered the formation of spherical micelles composed of $A_{60}B_{60}A_{60}$ where A_{60} (7.5 kDa) is the hydrophobic block mimicking PLGA and B_{60} (6.0 kDa) the hydrophilic block representing PEO (also called PEG, polyethyleneglycol). Even though the micelles were formed by the solvent precipitation method, we adopted an equilibrium model wherein the copolymers are assumed to exist in some sort of effective solvent.

One may question how it is possible to use an equilibrium theory to capture an intrinsic state of the system that was reached by a complicated dynamic route. The model, however, was not arbitrarily chosen. To explain the rationale behind the model it is necessary to qualitatively describe what happens in the solvent precipitation method. In this method the copolymers are originally in a good solvent and then suddenly mixed in with a selective solvent. As the solvent quality for one block quickly drops, a number of copolymers come together and form what will become a spherical micelle. The density of the core increases because the solvent quality deteriorates when time goes on. In the initial stages the core size will grow, but typically the size will go through a maximum, because in later stages, when the addition of copolymers slows down, the core compresses due to the removal of the good solvent. During the assembly process the corona chains accumulate in the so-called ('looped') corona. As soon as the local concentration exceeds the overlap concentration they start to stretch in the radial direction and form a so-called brush. The corona size is expected to be strictly increasing in time. The pressure in the brush eventually provides a stopping force for the assembly. Typically in the initial stages of the self-assembly the size of the corona may not be large compared to that of the core. Then the micelle is still expected to grow, either by the addition of individual copolymers or through a process of micelle with micelle fusion. However, when the core becomes more dense, i.e. by loosing more and more good solvent, the radius may go down, that is when the addition of copolymers does not compensate for it. Meanwhile the corona becomes more dense and the chains stretch more and more. Consequently, we should arrive at the situation that the corona size exceeds that of the core. At this point the tendency that cores from different micelles can fuse can be neglected because in this situation the spherical micelles dominate over linear micelles. Also the tendency for new chains to add to the micelle will drop dramatically: the passage of freely dispersed chains through the brush becomes a rare event. Meanwhile the majority of copolymers should have found a place in one of the micelles already and the micelles become molecularly quenched. Hence, the point where the core size is approximately the same as that of the corona demarcates an important point in the evolution of the copolymer self-assembly. It is this state of the process that the parameter set in the SF-SCF model is designed to produce a result for the given copolymer chain and the effective solvent.

Let us now formulate a key property of the molecular model. The set of parameters should result in micelles wherefore the core and corona sizes are of the same order of magnitude. Even though the topological stability requires the size of the core to be less than that of the corona, as explained, the dynamic process by which the micelles form is more likely characterized by the situation that the micelle corona is somewhat smaller than that of the core. We have opted for a driving force for micellisation using a modest value $\chi_{LGA-H_2O} = 1.6$, whereas the solvent quality for PEO is marginal: $\chi_{EO-H_2O} = 0.4$. This value ensures that

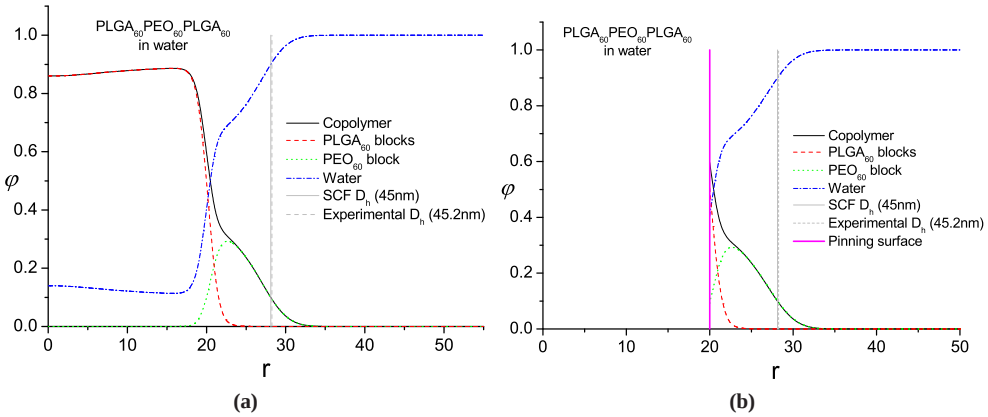

Figure 5.1: Equilibrium radial density profiles. (a): The equilibrium radial density profile of $PLGA_{60}PEO_{60}PLGA_{60}$ in a spherical coordinate system. The profiles for the apolar segments PLGA, the polar segments PEO and the solvent W (water) are given. Parameters $\chi_{LGA-H_2O} = 1.6$, $\chi_{LGA-EO} = 1.0$ and $\chi_{EO-H_2O} = 0.4$. The aggregation number $g = 237$. The grand potential $\Omega = 10\ k_BT$. (b): The equilibrium radial density profile of the brush made of $PLGA_1PEO_{60}PLGA_1$ where the A-units are pinned to be next to the particle surface, with radius $R = 20 \times 0.8 = 16$ nm. The particle is made of segments of type A. In line with the aggregation number of the micelle of panel a, the grafting density $\sigma = 0.047$. Here the radial coordinate is given in latice sites. For the radial coordinate we have used a lattice site dimension of $r = 0.8$ nm.

the corona is well-solvated and the pressure in the brush provides the stopping mechanism for the self-assembly of the micelles. The spatial segregation of A segments in the core and the B segments in the corona is improved by a repulsion between these segments. Here we have used $\chi_{LGA-EO} = 1.0$ for simplicity. The justification of this set that it largely obeys with our requirements. We stress that small modifications of the parameter set will do the same.

In Fig. 5.1 (a) the micelle structure, wherein the radial volume fraction profiles for the polar segments, the apolar segments and the solvent molecules is given, here we see that the core has approximately a homogeneous density of polymer. The small decrease of density towards the center of the core is attributed to an inhomogeneous stretching of the corona chains, being largest near the core-corona interface (where they then pack a bit more efficient). The solvent in the core is not extremely low, which is consistent with the relatively low value for the χ_{LGA-H_2O} that was adopted to mimic the assembly at the quench conditions. The corona has a much lower density, as it is well solvated. The profile is quasi parabolic, and the height (dimension) of this brush is expected to scale linearly with the length of the B block.

Inspection reveals that the core radius, which in this case is approximately 16 nm, is slightly larger than that of the corona. The latter may be estimated from the hydrodynamic diameter of the micelle which is found to be 45 nm. This is consistent with one of the targets that were used for the molecular model. The overall dimension of the micelle is in good agreement with the micelles found in the experimental condition. From the modelling point of view the micelles are stable and relevant. For example we have selected a micelle with a grand potential (work of micelle formation) $\Omega = 10\ k_BT$. This value is thought to be compensated by translational entropy of the micelle, and thus represents the situation that

the micelles are far apart (dilute regime). Thermodynamical stability requires that the slope $\partial\Omega/\partial g$ is negative, which was shown to be the case (see Chapter 4). The aggregation number, that is the number of tri-block copolymers in the micelle is predicted to be $g = 237$. Again the order of magnitude is consistent with experimental data. We recall that a brush of loops with chains of length $N_B = 60$ is usually seen as a brush composed of tails of length $N_B = 30$ with double grafting density. We have checked that this is a good approximation also in this case (result not shown).

In the following we will use the presented micelle and analyse the behaviour of a minority chain that is added to this micelle. The analysis is facilitated when the micelle is replaced by a simpler structure. Considering the sharp interface between the core and the corona, we argue that it is possible to replace the core by a solid particle and replace the corona by a set of polymers that are anchored by both ends to this solid particle. In Fig. 5.1 (b) we present the structure of a brush of loops connected to a spherical particle. The parameters are chosen to resemble the corona of the micelle presented in Fig. 5.1, that is, the number of grafted 'loops' is equal to the aggregation number g, and the solvent quality is again set to $\chi_{EO-H_2O} = 0.4$. The differences in radial structure of Fig. 5.1 (a) and (b) are minor which proofs that the model of Fig. 5.1 (b) is sufficiently accurate to mimick a triblock copolymer micelle for our purpose as used below. The most significant differences between the two radial profiles occur just next to the 'core'-corona interface. As explained above the entropic penalty for chains next to a sharp interface results in a small depletion of polymers and a small adsorption of solvent. In the micelle the core corona interface is less sharp and then the latter effects do not occur. One can easily correct for this entropy loss by adding an adsorption affinity of the corona chains for the core. Here we do not implement this.

5.2.1.2 A minority chain within the corona of the micelle

Following the line of arguments we take the corona structure presented in Fig. 5.1 (b) and admix in this structure one minority chain with a structure $A_1B_{N_B}TM_1$. One single chain is not expected to strongly influence the colloidal stability of the micelle, but we do not forward a proof of this. Instead our attention is drawn to the radial profile of this minority chain inside the corona made of $A_1B_{60}A_1$. More specifically our interest is in the profile of the end-segment referred to as TM. In Fig. 5.2 we present a number of radial volume fraction profiles of the TM segment in semi-logarithmic coordinates. One of the profiles, that is for $N_B = 30$, is dotted. This case represents a mimic of the majority chains that makes up the bulk of the corona. When the minority chain is shorter, the chain is more likely to fully remain inside the corona. Longer chains typically escape from the corona. The shape of the free end distribution is not much affected by the length and thus not much affected whether or not it is predominantly inside or outside the corona; the end points are distributed throughout the corona, but the most likely position is further from the core when the probe length is larger. The average position of the end point, e.g. measured by the first moment over the end-point distribution, grows approximately linear with length N_B and in this dependence there is no discontinuity around $N_B = 30$.

For the remainder of the discussion it is important to mention that upon the transition of the chain from the inside to the outside of the corona, the end-point distribution has just a single maximum and smoothly goes to zero for large r values and approaches a value of $1/(4\pi R^2)$ at the core surface. This result is true for an ideal TM, which is small (similar to

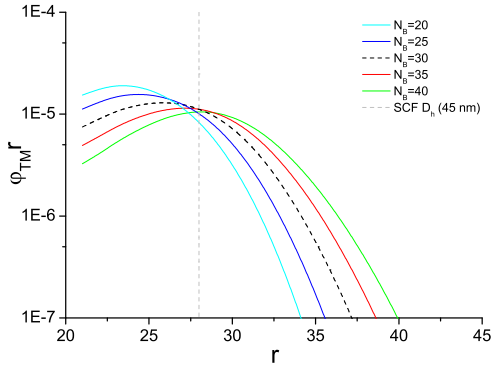

Figure 5.2: The equilibrium radial density profile of the end-point (TM) of the minority chain in the corona of the micelle-like particle given by Fig. 5.1 (b) in log-lin coordinates and lattice site units ($r = 0.8$ nm). The minority chain length is modified from $N_B = 20$ to 40 as indicated. The curve for the chain length 30 is dashed. The dashed grey line represents the hydrodynamic diameter (D_h).

an A-segment) and for the case that the water has the same solvent quality for the TM as the tether A. We are interested in parameters that deviate from this ideal situation and then there are discontinuities, meaning that there is a minor jump-like transition from the TM being inside to being outside the corona upon, e.g. an increase of the length of the minority chain.

Continuing with the ideal TM case, let us now consider the presence of a surface (receptor) at the upper boundary of the spherical coordinate system, that is at $r = M + 1$. Below we refer to the position of the receptor by the distance $\Delta r \equiv (M - R_h) \times 0.8$ nm, wherein $M - R_h$ is the distance of the receptor from the hydrodynamic radius of the micelle in lattice units and 0.8 is the length in nm of one lattice site. Obviously, as long as an adsorbing receptor surface is present for distances larger than the chain length ($M - R > N_B$), the probe chain cannot reach this receptor surface and the end-point distribution is unaffected. However, when the receptor is in close proximity, the end of the probe can reach the receptor. When the end has a significant affinity for the receptor, we expect that the end segment, that is the targeting moiety (TM), is able to reach and adsorb onto the receptors. By doing so, the probability for the TM to be near the surface will dramatically increase as compared to the value at the same coordinate in the absence of the substrate. A cartoon of this situation is given in Fig. 5.3 (b), which mimics the situation depicted in Fig. 5.3 (a). In this figure the end-point sits at the substrate. However, in reality it is at the receptor surface only with a given probability less than unity. Our interest is in the probability distribution of the end point (receptor), which in fact is proportional to the radial volume fraction profile. The end-point distribution may potentially have two maxima, namely one in/around the corona (we will call this the central maximum) and one next to the adsorbing surface (we call this the distal maximum) and two minima, namely between the core and the periphery of the corona (the proximal minimum), and one between the adsorbing surface and the periphery of the corona (the distal minimum).

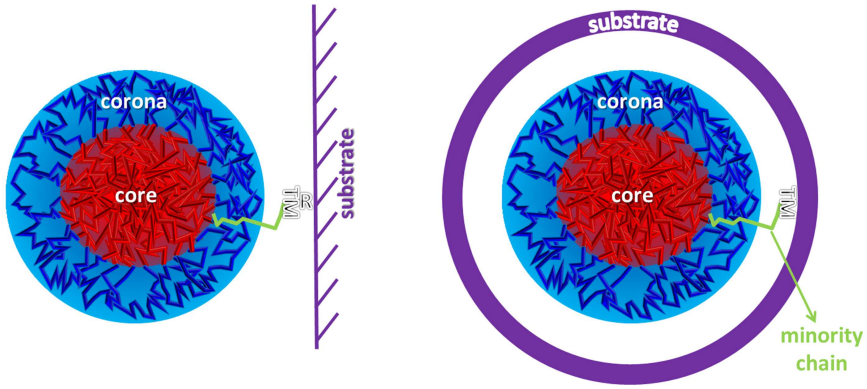

(a) **(b)**

Figure 5.3: Schematic two-dimensional representation of (a): A micelle with a minority chain adsorbing with a targeting moiety (TM) to a receptor (R) site on an external planar substrate (e.g. a cell wall with receptor). (b): A central micelle surrounded by a spherical 'substrate' as considered in the cell model; the TM of the minority chain adsorbed on this substrate, which is expected to be covered by receptors (not indicated). The core of the micelle is red, the corona blue (a few corona chains -loops- are indicated). The minority chain is green and has a TM (represented by TM).

5.2.2 Landau free energy and a short case study

The free energy of the system F in units of k_BT is found by $F = -\ln Q$, where Q is the canonical partition function. In a mean field theory, we can decompose this partition function into so-called single molecule sub-partition functions q_i,

$$Q = \pi_i \frac{q_i^{n_i}}{n_i!} \tag{5.3}$$

where n_i is the number of molecules of type i. Following the line of arguments, it is natural to take a closer look at the minority chain, while assuming that the other sub-partition functions are invariant upon changes in the conformational properties of the minority chain, e.g., when it binds onto a nearby receptor. Of course for this to be true we should insist on the case that the receptor surface remains outside the corona of the micelle in all cases.

The sub-partition function for the minority chain in principle should contain the statistical weights of all possible and allowed conformations. The evaluation of this partition function is simplified because the first segment is strictly positioned to be next to the core surface. In practice we use the propagator formalism to generate the partition function. In this formalism there are distribution functions $G(r,s|R+1,1)$ that specify the statistical weight of having segment s at coordinate r, under the constraint that the first segment $s = 1$ is at coordinate $r = R+1$, that is next to the core. In the propagator equation this distribution function is computed starting with $s = 1$, and ending with segment $s = N$ giving $G(r,N|R+1,1)$. Interestingly this end point distribution function can be used to directly compute the volume fraction profile of the free end, that is, $\varphi(r,N) \propto G(r,N|R+1,1)$. The proportionality constant is found to be

$1/q$, wherein the single chain partition function q is found by summing this quantity over all available coordinates r

$$q = \sum_r L(r)G(r,N|R+1,1) \quad . \tag{5.4}$$

Inspired by this relation we can identify $G(r',N|R+1,1)$ as a positional sub-partition function of the probe chain, which starts (per definition) with segment $s = 1$ at $r = R+1$ and ends with segment $s = N$ at coordinate $r = r'$. The free energy associated with this positional sub-partition function is called the Landau free energy $F(r)$ [33–35], which in units of k_BT is given by

$$F(r) = -\ln G(r,N|R+1,1) = \ln q - \ln \varphi(r,N) \quad . \tag{5.5}$$

The constant $\ln q$ can be absorbed into the Landau free energy. Here and below we will use $\tilde{F}(r) \equiv F(r) - lnq$. Below we will not write the tilde and trust that this will not lead to confusion, hence the Landau free energy can directly be computed from the radial volume fraction profile of the end point of the minority chain. In the current context the position of the free end r is often referred to as the order parameter. Following standard procedures one may normalize the order parameter by the chain length N_B and convert the end-point position into a distance to the substrate. However, we do not implement such transformations for practical reasons.

In practice a targeting moiety (TM) consists of a somewhat larger fragment than an ethylenoxide segment. We can mimic this by taking a minority chain with the following architecture: $A_1B_{N_B}TM_{N_{TM}}$, with $N_{TM} > 1$. We may subsequently generalize the Landau formalism by relating the Landau energy to the volume fraction distribution of all the TM-segments, that is, $F(r) = -\ln \varphi_{TM}(r)$.

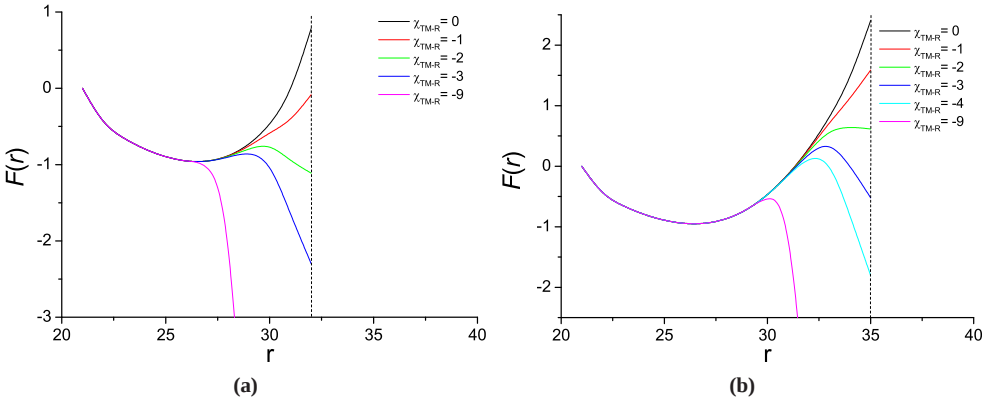

Figure 5.4: The dimensionless Landau free energy $F(r)$, where r is the distance to the center of the core for a probe chain $A_1B_{25}TM_5$ in lattice site units ($r = 0.8$ nm) for various values of the affinity of the TM for the receptor χ_{TM-R} as indicated, for the position of the receptor surface. (a): Position of the receptor surface $r = 32$ ($= r_R = 32 \times 0.8nm = 25.6$ nm). (b): Position of the receptor surface $r = 35$ ($= r_R = 35 \times 0.8nm = 28.0$ nm). The Landau free energy is normalized such that $F(16.8) = 0$. Note that in panel (a) the curves for $r < 27$ overlap. The same happens in panel (b) for $r < 30$. The vertical (dashed black) line represents the upper limit of the cell and where the receptor surface is present.

At this stage it is of interest to discuss an example of how we are going to use this Landau free energy. For this we will use the minority (probe) chain $A_1B_{25}TM_5$. The segments TM are taken similar to that of B, with the exception of the affinity of the TM for the receptor surface χ_{TM-R}. While all affinities $\chi_{X-R} = 0$, the (strong) affinity for the targeting moiety for the receptor is reflected in a negative value for this parameter. Landau free energy curves are presented in Fig. 5.4. Without loosing generality one can add a constant to the Landau function. Here we choose to shift each curve such that all Landau functions attain a zero value at the core side. For illustration purposes we set the receptor surface very close to the edge of the corona, namely at $r_R = 25.6$ nm in Fig. 5.4 (a) and slightly further outward, that is $r_R = 28.0$ nm in Fig. 5.4 (b).

As can be seen in Fig. 5.4, as long as $\chi_{TM-R} = 0$ the Landau function has one central minimum and two maxima. With respect to the core, we have a proximal maximum at $F^{\max} = 0$ and a distal maximum at the receptor surface. Of course this central minimum corresponds to the central maximum in the volume fraction profile (see Fig. 5.2). With increasing affinity for the receptor a new (distal) minimum develops, that is, near the receptor surface. The distal maximum is naturally moved to lower values of r. For a particular value of χ^*_{TM-R} the depths of the central and the distal minimum are the same. This occurs for $\chi^*_{TM-R} \approx -2$ in Fig. 5.4 (a) and $\chi^*_{TM-R} \approx -3$ for Fig. 5.4 (b). Using phase transition terminology we can identify the equal depth condition as the binodal. The distal maximum in between the central and distal minimum is identified by the activation barrier that needs to be overcome by the TM to reach the receptor. At the binodal the height of the barrier U does not depend on which minimum is used to measure the height. When $\chi_{TM-R} < \chi^*_{TM-R}$, the height as measured from the central minimum is lower than that measured from the distal minimum. Below, when we discuss the height of the barrier, we will always measure this height taking the central minimum as the reference. The physical origin of the barrier is clear. Before the TM can reach the receptor, it has to stretch even further than its naturally stretched conformation in the corona. This stretching costs entropy and hence the free energy increases. The lowest minimum in $F(r)$ corresponds to the ground state. Taking the affinity for the receptor as the control variable it is clear that at $\chi_{TM-R} = \chi^*_{TM-R}$, the ground state is degenerate. For lower affinities the lowest free energy is when the TM is inside the brush, whereas at larger affinities the ground state is when the the TM is at the receptor. For successful targeting the latter is required.

In all cases the height of the barrier U decreases when χ_{TM-R} becomes more negative. In this case the probability of finding the TM next to the receptor increases more and more and eventually the height $U = 0$. This condition is identified by the spinodal of the translocation transition. In Fig. 5.4 (a) this happens for $\chi^{**}_{TM-R} \approx -9$. In Fig. 5.4 (b) the receptor is placed just beyond the corona. In all cases the height U of the barrier is higher than in Fig. 5.4 (a), and the spinodal condition has shifted to much lower values of χ_{TM-R}. When this barrier is gone, all chain ends have moved to the receptor and the 'population of conformations' that otherwise would have remained as the unperturbed conformations in the corona, has vanished.

Fig. 5.4 (a) and (b) can be used to understand that χ^*_{TM-R} decreases with r_R, and that the height of the barrier at the binodal U^* increases with r_R. Also the spinodal χ^{**}_{TM-R} decreases strongly with r_R. Clearly, for the minority chain to be a good targeting moiety we need r_R to be larger than the hydrodynamic radius of the micelle, and the affinity for the target should be $\chi_{TM-R} < \chi^*_{TM-R}$. Meanwhile, the barrier U should be not too high. Of course it is not necessary that the barrier vanishes (spinodal condition) completely. We expect that

when $U \approx 3\ k_B T$ the barrier can easily be crossed and therefore we will monitor besides the binodal and the spinodal also the $U = 3$ situation. Obviously the latter is only relevant when the barrier at the binodal $U^* > 3\ k_B T$.

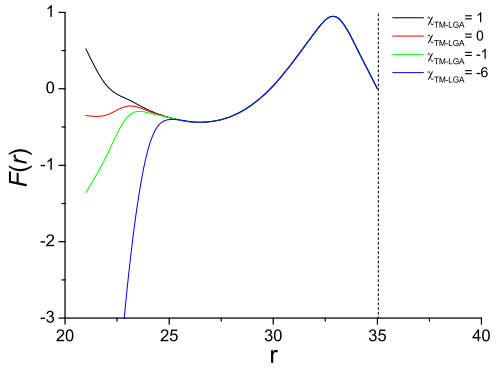

Figure 5.5: The dimensionless Landau free energy $F(r)$, where r is the distance to the center of the core for a probe chain $A_1B_{25}TM_5$ in lattice site units ($r = 0.8$ nm) for various values of the affinity of the TM for the core (composed of units A) χ_{TM-LGA} as indicated, for the position of the receptor surface (dashed black line), $r = 28.0$ ($= r_R = 35 \times 0.8nm = 28.0$ nm) nm and $\chi_{TM-R} = -3$. The Landau free energy is normalized such that $F(28.0) = 0$. Note that all curves overlap for $r > 25$.

Before advancing to the results section we need to consider one more complication, namely when the TM has an affinity for the core. In this case it is more natural to normalize the Landau free energy so that the value at the receptor surface is zero. In Fig. 5.5 we show results for the Landau function for which the receptor substrate is set to $r_R = 28.0$ nm, and the TM has, in addition to a mild affinity for the receptor, $\chi_{TM-R} = -3$ (close to the binodal of the translocation transition), some extra affinity of the TM for the core. A more negative value for χ_{TM-LGA} implies stronger adsorption of the TM onto the surface of the core. The curve for $\chi_{TM-LGA} = 1$ also given in Fig. 5.4 and is here reproduced for comparison reasons. When $\chi_{TM-LGA} < 1$ a proximal minimum develops in the Landau free energy and the natural proximal maximum is shifted to a position in between the proximal minimum and the central minimum. Now the situation is significantly more complex: there are three minima, the proximal, central and distal minimum (compared to the core) and two maxima (proximal and distal). Again we may identify the condition that the proximal and central minima are equally deep. This binodal corresponds to the detachment transition of the TM from the surface and occurs for $\chi^*_{TM-LGA} \approx 0$. We may also identify a spinodal for the detachment transition. In this case $\chi^{**}_{TM-LGA} \approx -6$ and the barrier between the proximal and central minimum vanishes. When $\chi_{TM-LGA} < \chi^{**}_{TM-LGA}$ the proximal maximum and the central miminum are gone and we are left with two minima, namely a proximal and a distal one with one maximum in between. When the three minima are equally deep, that is when $\chi_{TM-LGA} = \chi^*_{TM-LGA}$ and $\chi_{TM-R} = \chi^*_{TM-R}$, we have so-called triple point conditions as three 'phases' (types of conformations of the probe chain) can coexist.

From this result we can already extract our first design-rule for a successful targeting for a receptor. We should avoid a strong affinity of the TM for the substrate. Indeed, it is not expected that the receptor can successfully fish for the TM when it is strongly attached to the

core. Of course as long as the affinity of the TM for the receptor is much higher than that for the core, we should expect that at a sufficient close proximity of the receptor to the micelle, the TM-R contact is the ground state. However the energy barrier for this case will always be very high and the translocation transition will be a very slow one. That is why, in the following we will restrict ourselves to the case that the TM has a small repulsion to the core, which technically is equivalent with the situation that there is no affinity with the core. This does not mean that the TM cannot adsorb onto the core. As explained, also when the TM is not very soluble with water, there may be an induced adsorption energy and corresponding high concentration of the TM next to the core. As a result the Landau free energy will have a primary minimum and when this minimum is deeper than the central one, we will use this one to measure the height of the barrier U^* for obvious reasons.

Below our focus is on finding conditions so that the ground state is the distal minimum, while the central minimum is at a position lower than the hydrodynamic radius of the micelle. Then the minority chain will try to reach the receptor starting from a 'hidden' (for the immune system) position. However, the energy barrier U that needs to be overcome to reach the receptor may well be so large that the translocation of the TM towards the receptor is a rare event. The idea is then to monitor the $U = 3\ k_BT$ condition (as measured from the micelle core/corona). The numerical value is an *ad hoc* estimate below which the receptor is expected to be found fast enough and above which this is too slow. Results can be collected in so-called phase diagrams. Such diagram collects the binodal and spinodal points when one parameter (e.g. the length of the minority chain) is varied and the transition is triggered by some control parameter (e.g r_R). The binodal curve(s) in such phase diagram give the important information regarding the translocation and/or detachment transitions. The spinodals give information on where the respective barriers vanish. The $U = 3\ (k_BT)$ curve will be presented for discussion purposes only.

5.2.3 SF-SCF parameters

Similarly as above, we base our analysis on the model derived from the spherical micelle composed of $PLGA_{60}PEO_{60}PLGA_{60}$ chains (see Chapters 3 and 4 [19, 20]). Again, the core was replaced by a spherical particle composed of PLGA segments with radius $R = 16$ nm, decorated by 237 chains with length 60 grafted on both ends to the core. These chains are assumed to be composed of PEO and this was modelled by the solvent quality parameter $\chi_{EO-H_2O} = 0.4$. We used minority chains with lengths N_B = 5, 10, 15, 20, 25, 30, 35, 40, 60 and 120, composed of EO units that are end-grafted onto the solid particle, while they have a targeting moiety at their free ends. There are three types of interaction parameters connected to the TM: (i) the affinity of the TM for the core. As argued above we will avoid large affinities of the TM for the core and here take χ_{TM-LGA}= 1.0 (recall $\chi_{LGA-H_2O} = 1.6$), (ii) that for the receptor χ_{TM-R} = –3, –6, –12 and –18 (recall χ_{R-H_2O} = 0) and (iii) the solvent quality χ_{TM-H_2O} = 0.1, 0.4, 1.0 and 3.0. On top of this the length of the TM (the volume of the TM or the repeating TM units) was varied N_{TM}) = 1, 3, 5 and 10. Without mentioned otherwise just one minority chain was used.

5.3 Results and discussion

The relevance of several parameters for the translocation transition of the targeting moiety is conveniently presented in phase diagrams. We will present a representative set of these in the first part of this section. After that we will zoom in onto the optimized system for the use of polymer micelles as a targeting device for medical (drug delivery) applications.

5.3.1 The default phase diagram

Below we will adopt the convention to define the position of the receptor surface with respect to the hydrodynamic radius of the micelle, that is we introduce $\Delta r = r_R - (D_h)/2$. Hence, $\Delta r = 0$ means that the receptor is 'touching' the micelle corona layer. Negative values of the receptor distance $\Delta r < 0$ (overlap of corona and receptor surface) were disregarded, whereas positive values are of interest (the larger the better). We present phase diagrams (cf. Fig. 5.6 (a)) in the coordinates (i) N_B, that is the length of the hydrophilic block of the minority chain (y-axis), and (ii) Δr, which is the distance, in nm, of the receptor to the micelle surface on the x-axis. We adopt the following conventions. Solid curves represent the binodal condition and dashed curves represent the spinodal. Let us, for completeness, mention how to interpret such phase diagram. When for given N_B, the TM is far from the micelle we are to the right of the binodal, and the central minimum is the ground state. Upon reducing Δr we approach the binodal-curve at $\Delta r = \Delta r^*$. At this point we expect that the TM can thermodynamically reach the receptor 50% of the time, but this is an activated process as a barrier with height U^* needs to be overcome. When the receptor comes even closer to the micelle, the TM-R state is the ground state and the energy barrier is gradually reduced. When the dashed spinodal curve is crossed, at $\Delta r = \Delta r^{**}$, every attempt of the TM to reach the receptor is expected to be successful as the energy barrier is gone. The height of the energy barrier U^* at the binodal as a function of the chain length N_B^* at the binodal is additionally presented in panel b which accompanies the phase diagram, i.e., Fig. 5.6 (b). Here we have adopted to present the dependence with a solid curve when the TM is sufficiently short, so that in the absence of the receptor the TM is hidden inside the micelle corona. For longer chains this is no longer the case and part of the chain including the TM is outside the corona (dotted curves). In this regime we have used a dashed curve. As long as this energy barrier is sufficiently low, we choose a value of 3 k_BT, the binodal is the most relevant curve in the phase diagram, as it demarcates the point from whereon the translocation can effectively take place. However, when this energy barrier is much higher, a point closer to the spinodal is more relevant because of kinetic reasons the binodal is not noticed. At the spinodal translocation occurs spontaneously. In such cases we will present one extra curve in the phase diagram, namely the condition for which $U = 3\ k_BT$. We will use the dotted curve for this condition.

We start with a basic/default phase diagram shown in Fig. 5.6. Here we have opted for a TM which is 3 segments long and a relatively low value for the affinity for the receptor of χ_{TM-R} = –3. Again we have taken the situation that the minority chain has a vanishing affinity for the core. The current phase diagram is representative for all cases that the TM is repelled by the core or has a very negligible attraction. For a large affinity of the TM for the core the phase diagram alters dramatically (not shown). In this case the energy barrier at the binodal is very small and the $U = 3$-curve is not relevant. Inspection of the phase diagrams shows that with increasing length of the minority chain, the capture distances (binodal-solid

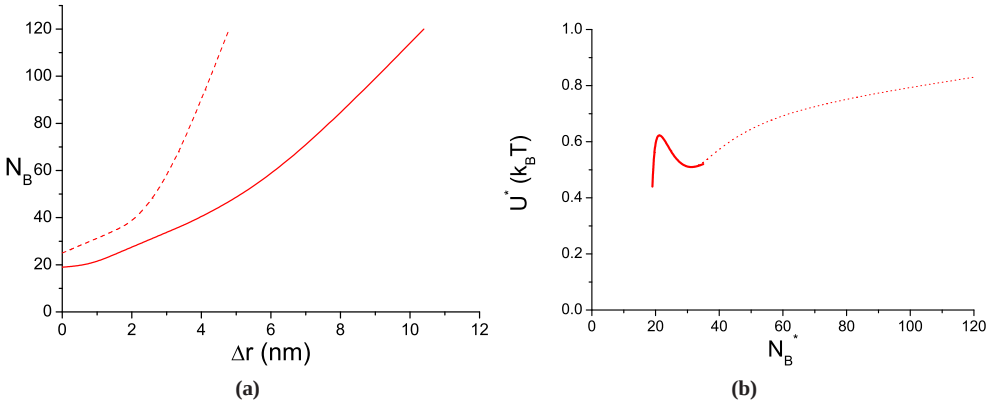

Figure 5.6: (a): Phase diagram in the (N_B, Δr) coordinates. The solid curve is the binodal condition and the dashed curve represents the spinodal. (b): The height of the energy barrier U^* at the binodal as a function of the chain length N_B^*. The solid curve in panel (b) indicate that the TM (in absence of a receptor) is within the hydrodynamic diameter and the dotted curve indicates that the TM is outside the hydrodynamic diameter. Affinity of the TM for the core: χ_{TM-LGA} = 1.0, for the receptor χ_{TM-R} = –3 and χ_{TM-H_2O} = 0.4, N_{TM} = 3. Other parameters: see section 5.2.3.

curve) Δr^* as well as the spinodal conditions Δr^{**} (dashed curves) increases. There exists a minimum value for N_B below which the binodal, and spinodal distances are becoming negative, meaning that the minority chain is too short and the receptor has to penetrate into the micelle before the TM can capture it. The binodal and spinodal curves are not plotted for longer chains than $N_B = 120$ either.

For large values of N_B the TM is outside the micelle (see dotted curve in Fig. 5.6 (b)). It this regime the minority chains have a flower-like conformation: they have a strongly stretched stem and a coil-like crown. The crown is outside the micelle and this crown can be used to stretch towards the receptor. For these long chain lengths the binodal and spinodal distances grow linearly with the length of the minority chain. This indicates that the chain has to stretch proportional to the chain length to reach the receptor. In this limit the stretching free energy (conformational entropy loss) is expected to be proportional to the chain length N_B as well and this is in good agreement with the result of Fig. 5.6 (b) for large values of N_B. Hence the barrier U^* has an entropic origin. When the TM extends towards the receptor the chain has a reduced conformational entropy. The position of the barrier is invariably close to the receptor surface, because when the TM is at this barrier position, there is already a first contact with the receptor surface (this causes the Landau energy to go down). This means that with increasing length of the TM moiety the barrier can be increasingly displaced from the receptor surface.

Arguably more relevant are the systems for which $N_B < 30$ as for these systems the TM remains inside the corona of the micelle when the receptor is far away. Now the minority chain is in a more or less homogeneously stretched conformation inside the corona region and the crown is missing. In this regime the binodal and spinodal distances grow also linearly with the chain length, albeit that the slope is less than for longer chain lengths. One possible reason for this is that when the minority chain is shorter than half the loop lengths of the corona

forming chains, the natural conformation of the minority chain is somewhat less stretched than the corona chains. These shorter chains therefore have to stretch comparatively stronger to reach the receptor surface. Hence the shorter chains are progressively less effective in capturing the receptor than longer ones.

The height of the energy barrier at the binodal (cf. Fig. 5.6 (b)) is very low in this case. These low values indicate that already at the binodal the capture efficiency of the TM for the receptor must be very high. Upon close inspection we see a rather complex behaviour for $N_B < 40$. Apparently, flower-like conformations ($N_B > 30$) have a relatively low value for the barrier height at the binodal. Chains that must capture the receptor from inside the corona ($N_B < 30$) have a relatively high energy barrier: these chains first have to stretch to get out of the corona and then have to stretch further to go to the receptor (adding up to a relatively high U^*). Apparently as a result, near $N_B \approx 30$, we find U^* to drop, but it must be kept in mind that the absolute value of the drop is small (just 0.1 k_BT). Indeed, we can see this non-monotonous behaviour of $U^*(N_B)$ because the absolute values of the barrier heights is small in this case. Below we find situations that the barrier height is significantly larger and then the irregularities for $U^*(N_B)$ near the value of the length of the minority chain for which flower-like conformations are found, are less visible.

5.3.1.1 Influence of the solvent quality χ_{TM-H_2O}

Obviously, we can construct many different phase diagrams and next, in Fig. 5.7, we will collect four different ones in a so-called collection of phase diagrams. The different colours represent different values for the solvent quality of the TM: χ_{TM-H_2O} ($= 0.1, 0.4, 1.0$ and 3.0). Meanwhile the values of the other parameters in the computations were maintained at: $\chi_{TM-R} = -3$, $\chi_{TM-LGA} = 1.0$, $N_{TM} = 3$ (as in the default phase diagram Fig. 5.6). With decreasing solvent quality, i.e. increasing χ_{TM-H_2O} the binodal shifts to higher Δr values, while the spinodal shifts to lower ones (Fig. 5.7 (a)). Meanwhile the height of the energy barrier at the binodal (Fig. 5.7 (b)) increases with decreasing solvent quality. Still the barrier height remains below the 3 k_BT value so that the kinetics for the TM-R formation is still expected to remain sufficiently fast. The shift of the binodal with decreasing solvent quality is attributed to the fact that the TM-R affinity also has a solvent quality induced part; the effective adsorption energy increases slightly. Below we will see that with increasing affinity between the TM and the receptor the binodal shifts dramatically to the right.

One clear consequence of the increasing repulsion between TM and water is an induced adsorption energy for the TM to the core. This is reflected in progressively longer minority chains that can maintain their TM within the hydrodynamic diameter (in the absence of a receptor), reflected in the length of the solid curves in Fig. 5.7 (b). In more detail, when the TM has an affinity for the hydrophobic core, the minority chain has a loop-like conformation, similarly as the corona forming chains. For very poor solvent conditions, $\chi_{TM-H_2O} = 3.0$, the local minimum of the Landau energy near the surface appears and this implies a finite energy barrier near the core (i.e., a barrier associated to the desorption transition) and therefore the spinodal curve suddenly drops to very negative Δr-values, see Fig. 5.7 (a). Fortunately, as the energy barriers still remain modest, the spinodal curves are not very relevant in this case; the key feature is the binodal.

The intricate behaviour found for the $U^*(N_B)$-curves in Fig. 5.7 (b) easily catches our attention. However, the energies involved in these irregularities are very small. On top of the

effect discussed above (the flower-like conformations having a lower barrier than internalized minority chains), we now also have an extra contribution to the desorption-transition of the TM from the core. Hence the extra energy needed to decouple the TM from the hydrophobic core and the stretching (unfolding) of the hydrophilic part of the diblock copolymer, may induce one extra maximum and/or minimum in $U^*(N_B)$, noticed for small values of N_B.

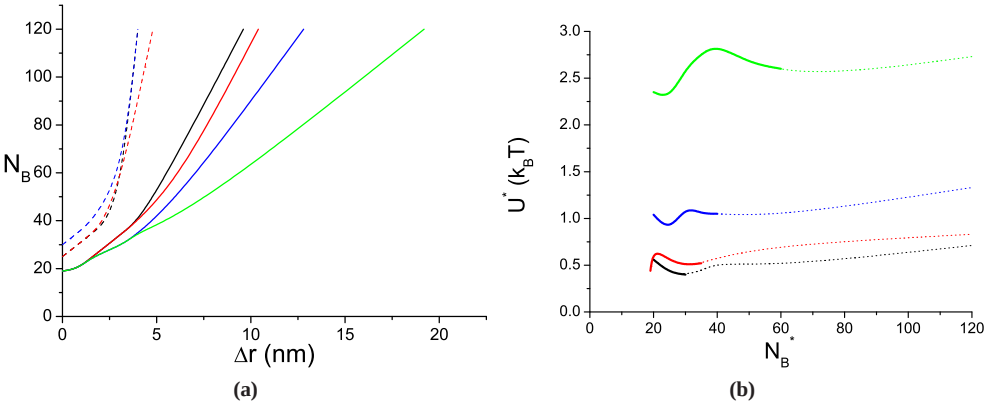

Figure 5.7: (a): Collection of phase diagrams in the N_B Δr coordinates. The solid curves are the binodal conditions and the dashed curves represents the spinodals. (b): The height of the energy barrier U^* at the binodal as a function of the chain length N_B^*. The solid curves in panel (b) indicate that the TM (in the absence of a receptor) is within the hydrodynamic diameter and the dotted curves indicate that the TM is outside the hydrodynamic diameter. The colours represent different parameters, namely black: χ_{TM-H_2O} = 0.1, red: χ_{TM-H_2O} = 0.4, blue: χ_{TM-H_2O} = 1.0 and green: χ_{TM-H_2O} = 3.0 (spinodal curve is for $\Delta r < 0$ and therefore not plotted). Other parameters as in Fig. 5.6.

5.3.1.2 Influence of N_{TM}

In this subsection the attention is drawn to the number of segments at the end of the minority chain. Changes in this value represent a larger/smaller targeting moiety. Alternatively, N_{TM} can be seen as a series of targeting moieties in a row. As an example, N_{TM}=10 and $\chi_{TM-R} = -3$ can be regarded either as a single targeting moiety of $\sim$ 1 kDa with a total $\chi_{TM-R} = -30$ (10×-3) or as 10 repetitive targeting moieties each with a $\chi_{TM-R} = -3$, the latter interpretation has our preference. The effect of the molar mass or repetition of targeting moiety (N_{TM}) units is collected in a collection of phase diagrams given in Fig. 5.8, lengths ranging from 1 to 10. Other parameters were the same as in the default phase diagram Fig. 5.6.

Inspection of Fig. 5.8 (a) and (b) reveals a clear trend that more repeating targeting moieties gives a shift of the binodal and spinodal curves to larger Δr values and an increase of the corresponding energy barrier at the binodal; again all energy barriers (U^*) remain below 3 k_BT. These trends may be explained by the fact that more repeating units of the targeting moiety effectively give a stronger TM-R interaction (see also results below). There may also be an entropic effect that as one particular TM-R contact is not realized there is in close vicinity another targeting moiety capable to connect to the receptor. There is a subtle

effect that the larger N_{TM} requires a shorter N_B block lengths to keep the TM within the hydrodynamic diameter, see Fig. 5.8 (b). This implies that larger N_{TM} for the same N_B block lengths establishes TM-R contact at higher Δr values. When we add the length of the TM and the spacer N_B we again see that the non-monotonous behaviour of $U^*(N_B)$ occurs at $N_B + N_{TM} \approx 30$, and thus should be attributed to the (undesired) formation of flower-like conformations of the minority chain (in the absence of the receptor).

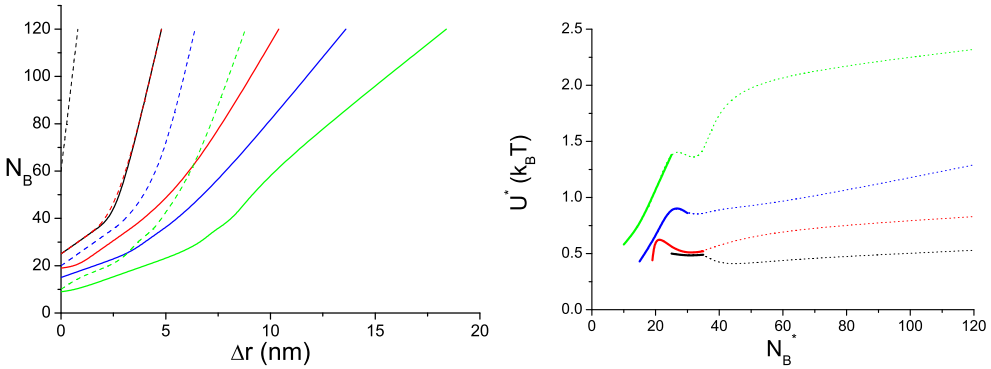

Figure 5.8: (a): Collection of phase diagrams in the N_B Δr coordinates. The solid curves are the binodal conditions and the dashed curves represent the spinodals (b): The height of the energy barrier U^* at the binodal as a function of the chain length N_B^*. The solid curves in panel (b) indicate that the TM is within the hydrodynamic diameter (when the receptor is absent) and the dotted curves indicate that the TM is outside the hydrodynamic diameter. The colours represent different lengths of the TM, namely black: N_{TM} = 1, red: N_{TM} = 3, blue: N_{TM} = 5 and green: N_{TM} = 10. Other parameters as in Fig. 5.6.

5.3.1.3 The influence of the affinity of the TM for the receptor χ_{TM-R}

We have already mentioned twice that when the TM has a higher affinity for the receptor, the translocation transition occurs at larger distances between the receptor and the TM. In this section we take a closer look to this TM-R affinity parameter. A collection of phase diagrams is presented in Fig. 5.9 for χ_{TM-R} (–3, –6, –12 and –18) while the remaining parameters were the same as the default phase diagram in Fig. 5.6. In line with expectations we observe that the binodal distance shifts strongly, and in a linear fashion, to larger distances with increasingly negative values of χ_{TM-R}. Remarkable, as can been seen in Fig. 5.9 (a), for this range of parameters the spinodals overlap within the accuracy of the lattice model and hence there is just one dashed red curve. The corresponding values of the energy barrier at the binodal Fig. 5.9 (b) is a linearly increasing function of the absolute value of χ_{TM-R}. As the barrier can easily become larger than the threshold value of 3 k_BT (for the χ_{TM-R} –3 and –6 values) we now also present for these cases the $U = 3$-curve in Fig. 5.9 (a) (dotted curves). Again, these 'practical spinodal' curves are given because we envision that an energy barrier of 3 k_BT can easily be passed and these practical spinodal values are more relevant than the true spinodal (and the binodal) curves. The practical spinodal distances increase slightly with stronger affinities between TM-R. In passing we note that with increasing affinity of the TM

for the receptor the irregularities in $U^*(N_B)$ still exist but become less clearly visible.

As long as $U^* < 3$ we take the binodal and above this value the $U = 3$-curve to estimate the relevant 'capture distance'. Inspection of Fig. 5.9 (a) then reveals that with increasing affinity of the TM for the receptor the 'capture distance' increases continuously, but does not easily go beyond the 10 nm (for $N_B < 30$) value.

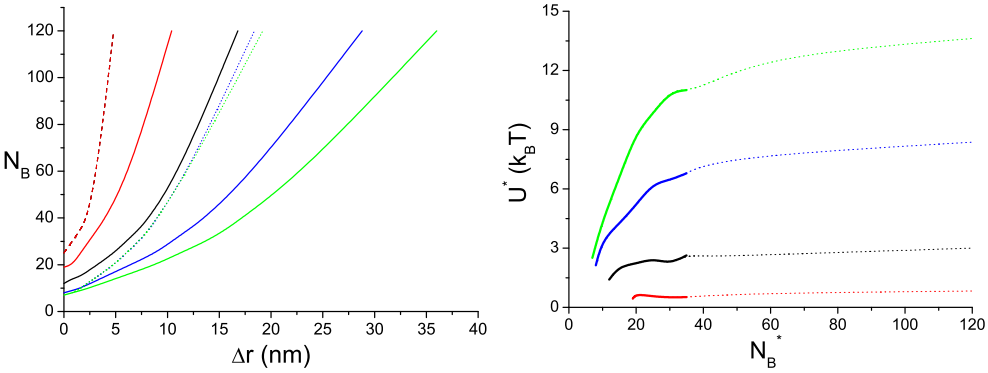

Figure 5.9: (a): Collection of phase diagrams in the N_B-Δr coordinates. The solid curves are the binodal conditions, the dashed curves represents the spinodals and the dotted curves are drawn for the $U = 3\ k_BT$ condition. (b): The height of the energy barrier U^* at the binodal as a function of the chain length N_B^*. The solid curves in panel (b) indicate that the TM is (when the receptor is absent) within the hydrodynamic diameter and the dotted curves indicate that the TM is outside the hydrodynamic diameter. The colours represent changes in TM-receptor affinity, namely red: χ_{TM-R} = –3, black: χ_{TM-R} = –6, blue: χ_{TM-R} = –12 and green: χ_{TM-R} = –18. Other parameters as in Fig. 5.6.

5.3.2 Optimization and discussion

Finally, after the assessment of the relevant modeling input parameters on the phase diagram and the free energy barrier U^* we will now zoom in onto systems with some preferred targeting design. The optimal design obeys to a set of conditions most of which we already encountered above. (i) The TM should not have a strong affinity for the core. As long as the affinity for the receptor exceeds that for the core, i.e. $\chi_{TM-R} < \chi_{TM-LGA}$, the translocation transition is still expected to occur. But, as soon as the affinity for the core is significant, the total free energy barrier, that is the desorption- plus translocation barrier, is expected to be correspondingly higher, so that the kinetics becomes progressively (exponentially) slower. (ii) There exists a minimum affinity of TM for R, $\chi_{TM-R} < -3$. When the affinity is too low the binding is not expected to take place in a significant fashion. (iii) The TM should not be too hydrophobic, that is, $\chi_{TM-H_2O} \lesssim 1$. Various complications are foreseen for hydrophobic TM. First of all, in the preparation the TM may be internalized inside the (glassy) core, and can then only be released when the core is degraded. Secondly, there is a solvent-induced affinity for the TM to adsorb onto the core. Then some extra energy is required to desorb the TM from the core. Thirdly, hydrophobic TMs are expected to have non-specific affinities for apolar substrates (molecules, receptors, tissues, membranes). Binding to these entities will

decrease the ultimate efficiency of the targeting micelle. (iv) The minority chain should be short enough so that the TM is kept inside the corona as long as the receptor surface is not in capturing distance. When the minority chain is too short, the translocation is impossible. Hence the longer the minority chain the better. As long as the TM is ideally repelled by the core, the maximum length of the minority chain is $N_{TM} + N_B \sim 30$. (v) The number of repeating TMs along the minority chain is preferably not very small. In the current system we have focused on linear chain architectures. We argue that it stands also model for the case that a minority chain has a branched or dendritic end fragment which features several TM to be coupled to one or more receptors, albeit that the details for this will be slightly different. Alternatively, one can include multiple minority chains inside a micelle to enhance the capturing efficiency.

We here like to argue that the capture distance, which is Δr^* when the energy barrier is low, and the distance Δr when $U = 3\ k_BT$, should be as large as possible. When this value is sufficiently large the minority chain can in practical situations circumvent obstacles and wonder around, which is important when the micelle is near the individual receptors (different from our modeling assumption that the receptor is around the micelle). The following results are presented with the idea in mind to maximize the capture distance.

From these requirements we have identified two parameters which deserve a closer investigation, namely the affinity of the TM with respect to the receptor χ_{TM-R} (we choose values –3, –6, –12 and –18) and the number of repeating units of TM in the minority chain. Larger values of these two parameters give larger capture distances. Other parameters are the same as for the default system (cf. Fig. 5.6). This means that we still ignore a significant affinity of the TM for the core and insist on good solvent conditions for the TM (χ_{TM-H_2O} = 0.4). The requirement to focus on the longest possible minority chain prompts us to fix the total length of the minority chain to $N_{TM} + N_B = 35$ (slightly larger than the value advised above to press our luck). In Fig. 5.10 we present a set of phase diagrams in the coordinates N_{TM} (longer values imply shorter spacer lengths N_B) versus the receptor distance Δr. As typically $U^* > 3$, we only present the spinodal curves (dashed) and the $U = 3\ k_BT$ curves (dotted).

It follows that for $N_B + N_{TM} = 35$ a wide array of spinodals and practical spinodals $U = 3\ k_BT$ can be realized. Let us first discuss the practical spinodals because these are of primary interest for the application. The practical spinodals (dotted curves) for $N_{TM} = 1$ (and $N_B = 34$) can be realized at Δr = 2 nm for $\chi_{TM-R} = -3$, $\Delta r = 4$ nm for $\chi_{TM-R} = -6$ and $\Delta r = 6$ nm for $\chi_{TM-R} = -12$ and –18 (the difference vanishes in the lattice approximations). The larger the N_{TM} value the larger Δr for the practical spinodals, although for the smaller χ_{TM-R} values (–3 and –6) the practical spinodals reach a plateau value at $\Delta r \approx 5$ nm for $\chi_{TM-R} = -3$ and at $\Delta r \approx 10$ nm for $\chi_{TM-R} = -6$. Meanwhile the practical spinodals for χ_{TM-R} = –12 and –18 still show a more or less linear growth of Δr with N_{TM}, enabling a record TM-R capturing distance $\Delta r \approx 6$ nm up to $\Delta r \approx 15$ nm for $N_{TM} = 20$. For the higher TM-R affinities the saturation of the 'capture distance' is expected to occur for even larger values of N_{TM}. Note that the practical spinodals for χ_{TM-R} = –12 and –18 (dotted blue and green curves) are close to each other. For small values of N_{TM} the practical spinodals for χ_{TM-R} = –12 and –18 effectively coincide, while for larger values of N_{TM} a constant difference of just ≈ 1 nm for Δr is maintained. This implies that the 'capture distance' is not easily increased by increasing the affinity χ_{TM-R} to even larger values. However, increasing N_{TM} remains effective as a means to increase the capture distance as mentioned already. We will elaborate on why this is the case below.

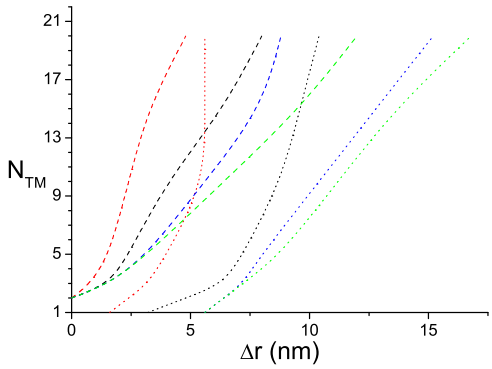

Figure 5.10: (a): Collection of phase diagrams in the N_{TM} Δr coordinates for TM situated within the hydrodynamic diameter. The dotted curves are the practical spinodals $U = 3\,k_BT$ and the dashed curves represents the spinodals. The colours represent different parameters, namely red: χ_{TM-R} = –3, black: χ_{TM-R} = –6, blue: χ_{TM-R} = –12 and green: χ_{TM-R} = –18. The other calculation parameters are similar to the default system (cf. Fig. 5.6). Here we have chosen for the longest possible minority chains, that is we have implemented the constraint $N_{TM} + N_B = 35$.

The difference between the spinodal (dashed curves) and the practical spinodals (dotted curve) is indicative for the height of the energy barrier at the binodal, i.e. U^*. When this difference is very small the value of U^* must be a bit larger than 3 k_BT, whereas when the difference is large, the barrier at the binodal is much larger than 3 k_BT, see also Figs 5.6 (a) and (b). With this information it is of interest to inspect the whereabouts of the spinodals. The spinodals (dashed curves) coincide at $\Delta r^{**} = 0$ nm for N_{TM} = 2 (and $N_B = 33$) for all χ_{TM-R} values. Within the accuracy of the lattice, the spinodal for $\chi_{TM-R} = -6$, –12 and –18 overlap until $N_{TM} = 3$ from this value the spinodal for $\chi_{TM-R} = -6$ splits off, while the spinodals for $\chi_{TM-R} = -12$ and –18 still overlap until $N_{TM} = 5$. The spinodals (dashed curves) in comparison to the practical spinodals (dotted curves) first seem to go in parallel where-after they achieve a maximum difference and from thereon they converge back to each other. Again, the latter implies that U^* increases with increasing N_{TM}. For the spinodals and practical spinodals of $\chi_{TM-R} = -3$ and –6 this behaviour can be completely monitored in Fig. 5.10. For the spinodal and practical spinodal of $\chi_{TM-R} = -12$ this behaviour can be seen until the maximum difference between the two spinodals (see blue curves). The spinodal and practical spinodal for $\chi_{TM-R} = -18$ (see green curves) only show the parallel part, and the other features are found for $N_{TM} > 20$ (not shown).

From this optimisation study we conclude that it is possible to increase the capture distance to at least 15 nm. This distance is significant as it is of the same order or a bit larger than the size of the corona. Apparently it is possible to stretch the minority chain by a factor of more than two to reach the receptor surface. Of course the relatively long series of TM contributes to this remarkable finding. A long sequence of TMs at the end of a relatively short spacer, allows the position of the barrier to be significantly displaced from the receptor surface. In a good approximation this distance scales linearly with N_{TM} (not shown). The further the barrier is displaced from the receptor the less the minority chain has to stretch to reach the barrier. That is why the overall barrier height can remain so low while the receptor is relatively far away.

Thus far we only focused on a single minority diblock copolymer per micelle. We note that while using the nanoprecipitation method the diblock copolymers are distributed randomly over the micelles and hence it is impossible to achieve exactly one diblock copolymer per micelle. This implies that some micelles certainly will contain more diblock copolymers, while others remain empty. In order to prevent that some micelles contain no diblock copolymers it is advised to aim at an average of e.g. ≈ 10 diblocks per micelle in order to achieve that at least the majority of all micelles contain at least one diblock per micelle. Also in order to increase the probability on TM-R contact we should incorporate more than one diblock copolymer per micelle. We recall that the corona is composed of over 200 tri-block copolymers and therefore having 10 minority chains is still expected to be only a slight perturbation. We have checked that his is indeed the case (not shown). In these cases we found that each minority chain behaves independently from all the others and therefore we simply can linearly add up the capture efficiency. In other words, the probability for a TM-R contact will increase linearly with the number of minority chains per micelle.

Here we only focused on repeating TM in a linear chain-architecture. Other architecture can still be handled by the SF-SCF machinery. It can be that other geometries (star-like or dendrimer-like) have even a more pronounced effect on TM-R contact and Δr. These could even be used with larger values for N_B while maintaining the TM within the hydrodynamic diameter and enabling TM-R contact at larger Δr. To study such modifications becomes appropriate when corresponding experimental systems become available.

There are several ways to check the viability of our SF-SCF modeling approach and we hope such experiments will be performed in the near future. One can, for instance, investigate the strength or possibility of a TM-R connection with atomic force microscopy to generate or validate the parameters needed. Another way of checking the efficiency of the hidden targeting moieties within the micellar corona and their receptor interaction is by exposing the micelles to specific antibodies for their targeting moieties. Comparing against micelles which do not contain targeting moieties with micelles that contain their targeting moieties beyond (flower-like conformations) and within the micellar corona (homogeneously stretched conformations). A similar experiment can also be performed with an immune response evoking targeting moiety. Again, when the TM is hidden inside the corona this should avoid an immune response, while a clear immune response is generated when the (too long) minority chains are in the flower-like conformation which exposes the TM.

5.4 Conclusions

Copolymer micelles are promising structures for passive and active drug delivery applications. Experimentally it is attractive to use the nanoprecipitation method to generate micelles with a well-defined structure and composition. This method can be adopted to include targeting moieties without the need to perform elaborate post-processing of the micelles. We have presented a modeling approach aimed at finding the best parameters for such composite micelles to perform as active delivery vehicles. We hope that this modeling study allows for a more efficient design of active drug delivery micelles in medical applications.

We have used the Scheutjens-Fleer Self-Consistent Field (SF-SCF) theory in a spherical coordinate system with concentration gradients in one direction, and implemented a coarse grained model with appropriate parameters that closely predict the micellar structure

when triblock copolymers with the PLGA-PEO-PLGA architecture self-assemble through the solvent-precipitation method. We postulated that it is possible to admix a small number of diblocks PLGA-PEO into these micelles without affecting the overall micelle structure. We reported an SF-SCF analysis to reveal which diblock copolymer molar masses/block lengths are beyond or hidden within the corona the micelles. We then focused on the hidden ones: these systems avoid the possible immune response upon their application in the human body. At the free end of the diblock copolymer we have attached a targeting moiety (TM) or a series of TMs and we have positioned in the cell-model a receptor surface around a (slightly simplified) composite micelle. A parameter search was executed to find the largest possible capture distance, that is, the distance between the receptor and the micelle at which the TM-R contact is efficiently established. We have introduced a Landau free energy as a function of the distance of the receptor (surface) to the micelle and identified the so-called translocation transition, wherein the TM jump-like goes from the hidden position inside the corona to the receptor which is outside the corona. Here we have taken the ad-hoc estimate that the free energy barrier (the minority chain has to stretch to reach the receptor) for the translocation transition should be about 3 k_BT to estimate the experimentally relevant capture distance. We have shown that it is possible to reach capture distances of at least 15 nm. This length corresponds to the size of the corona and implies that it should be possible to double the stretching of the minority chain in the process of capturing the receptor. On top of this we formulated a number of design rules. For example, we advised that the TM should not be too hydrophobic. It is also better to prevent specific adsorption of the TM on the core of the micelle. It is expected that the number of minority chains in the micelle can be larger than unity without adverse effects. More chains imply a higher capture efficiency, but increasing the value too much will perturb the micelle structure in unforeseen ways. We also speculated that a branching of the terminal end of the minority chain can be used to further improve the design.

Bibliography

[1] K.S. Soppimath, T.M. Aminabhavi, A.R. Kulkarni, W.E. Rudzinski, J. Control. Release, **70**, 1 - 20 (2001).
[2] J. Panyam, V. Labhasetwar, Adv. Drug Deliv. Rev., **55**, 329 - 347 (2003).
[3] N. Kamaly, Z. Xiao, P.M. Valencia, A.F.Radovc-Moreno and O.C. Farokhzad, Chem. Soc. Rev., **41**, 2971-3010 (2012).
[4] J.C. Wright and D.J. Burgess, Long acting injections and implants (Springer, 2012).
[5] R. Langer, Nature, **392**, 5-10 (1998).
[6] H. Maeda, G.Y. Bharate and J. Dauwalla, Eur. J. Pharm. Biopharm., **71**, 409-419 (2009).
[7] S.M. Mogihimi, A.C. Hunter and J.C. Murray, Pharmacol. Rev., **53**, 283-318 (2001).
[8] I. Brigger, C. Dubernet and P. Couvreur, Adv. Drug Deliv. Rev., **54**, 631-651 (2002).
[9] M.L. Hans and A.M. Lowman, Curr. Opin. Solid St. M., **6**, 319-327 (2002).
[10] G. Gaucher, M-H. Dufresne, V.P. Sant, N. Kang, D. Maysinger and J-C. Leroux, J. Control. Release, **109**, 169-188 (2005).
[11] J.D. Byrne, T. Betancourt and L. Brannon-Peppas, Adv. Drug Deliv. Rev., **60**, 1615-1626 (2008).
[12] D. Lembo and R. Cavalli, Antiviral Chemistry and Chemotherapy, **21**, 53-70 (2010).
[13] S. Prakash, M. Malhorta, W. Shao, C. Tomaro-Duchewneau and S. Abbasi, Adv. Drug Deliv. Rev., **63**, 1340-1351 (2011).
[14] K. Knop, R. Hoogenboom, D. Fisher, U.S. Schubert, Angew. Chem. Int. Ed., **49**, 6288 - 6308 (2010).
[15] Some commercially available FDA approved PLGA-based pharmaceutical applications, taken from reference [4]: PURASORB®, EXPANSORB®, RESOMER®, Absorv®; some FDA approved implants and drug delivery systems: Vicryl® degradable PLGA suture, Decapeptyl® and Lupron ® Depot both PLGA microparticles for the treatment of prostate cancer, Zoladex® a PLGA based implant for the treatment of prostate cancer, breast cancer and endometriosis, Risperdal® and Consta® PLGA microparticles for antipsychotic drug delivery and Eligard® PLGA based degradable drug depot system.
[16] J.M.H.M. Scheutjens, G.J. Fleer, *J. Phys. Chem.*, **83**, 1619 - 1635 (1979).
[17] J.M.H.M. Scheutjens, G.J. Fleer, *J. Phys. Chem.*, **84**, 178 - 190 (1980).
[18] J.M.H.M Scheutjens, G.J. Fleer and M.A. Cohen Stuart, Colloids and interfaces, **21**, 285-306 (1986).
[19] J.G.J.L. Lebouille, R. Tuinier, L.F.W. Vleugels, M.A. Cohen Stuart and F.A.M. Leermakers, Soft Matter, **9**, 7515-7525 (2013).
[20] J.G.J.L. Lebouille, L.F.W. Vleugels, A. Dias, F.A.M. Leermakers, M.A. Cohen Stuart and R. Tuinier, Eur. Phys. J. E, **36**, 107 (2013).
[21] J.G.J.L Lebouille, T. Kockelkoren, L.F.W. Vleugels and R. Tuinier, **US 0223206 A1** (2011).
[22] Y. Matsumura, H. Maeda, Cancer Res., **6**, 6387-6392 (1986).
[23] H. Maeda, J. Wu, T. Sawa, Y. Matsumura and K. Hori, J. Control. Release, **65**, 271-284 (2000)
[24] H. Maeda and Y. Matsumura, Crit. Rev. Ther. Drug, **6**, 193-210 (1989).
[25] H. Maeda and J. Fang, Adv. Polym. Sci., **193**,103 - 121 (2006).
[26] H. Maeda and J. Daruwalla, Eur. J. Pharm. Biopharm, **71**, 409 - 419 (2009).
[27] D.E. Owens and N.A. Peppas, Inter. J. Pharm., **307**, 93 - 102 (2006).

[28] B. Stella, S. Arpicco, M.T. Peracchia, D. Desmaëlle, J. Hoebeke, M. Renoir, J. D'Angelo, L.Gattel and P. Couvreur, J. Pharm. Sci., **89**, 1452-1464 (2000).
[29] J-C. Olivier, NeuroRx, **2**, 108-119 (2005).
[30] O.C. Farokhzad, J. Cheng, B.A. Teply, I. Sherifi, S. Jon, P.W. Kanthoff, J.P. Richie and R. Langer, PNAS, **103**, 6315-6320 (2006).
[31] A. Béduneau, P. Saulnier and J-P. Benoit, Biomaterials, **28**, 4947-4967 (2007).
[32] Y.B. Patil, U.S. Toti, A. Khdair, L. Ma and J. Panyam, Biomaterials, **30**, 859-866 (2009).
[33] F.A.M. Leermakers, J. Van Male and A.M. Skvortsov, Macromolecules, **34**, 8294-8302 (2001).
[34] A.M. Skvortsov, L.I. Klushin, J. Van Male and F.A.M. Leermakers, Journal of Chemical Physics, **115**, 1586-1595 (2001).
[35] A.M. Skvortsov, L.I. Klushin and F.A.M. Leermakers, Europhysics Letters, **58**, 292-298 (2002).

6

General discussion

In this thesis the focus is on rationalizing the size and loading of colloidal particles that are to be used as drug delivery vehicles, as obtained by using the nanoprecipitation process [1, 2]. In this chapter the implications and possibilities for further research and applications are discussed while the main findings of the previous chapters are briefly reviewed. Nanoprecipitation is an apparently simple process which was, however, still poorly understood [3].

When we started this work, nanoprecipitation had been studied experimentally quite thoroughly, but there was limited understanding of the underlying physics that determines the final particle size. A physical picture of the nanoprecipitation process of hydrophobic molecules in water and the role of stabilizing surfactants was described by Lannibois *et al.* [4], and was extended to high concentrations of polymeric hydrophobic compounds [5] and applied to obtain rather narrow size distributions [6]. Knowledge of the physics that governs the nanoprecipitation process could help to rationalize how various experimental parameters, such as mixing efficiency/time, surfactant and polymer concentration and molar masses, affect the final particle size. This tremendously facilitates the design of a smarter preparation protocol.

Especially the relation between the physical chemistry (polymer and surfactant size and concentration), the mixing efficiency of this process and the resulting particle sizes had been poorly investigated systematically and understood previously. Only advanced heavy computer simulations permitted to gain some understanding of the relation between the used chemistry, the present physical properties and the final result: the size and loading of colloidal particles [7, 8]. Other approaches were based on more or less design of experiment (DOE) research which fails to give an insight into how existing material and processing parameters influence the size obtained when using the nanoprecipitation process.

For many applications where compounds are encapsulated, simultaneous control over both size and loading is a prerequisite. Especially for drug delivery applications, more specifically in oncology, control over size and loading is of utmost importance [9–14]. A more thorough understanding of nanoprecipitation could give rise to a more general strategy to apply the resulting particles, for drug delivery applications in medicine. A key ingredient of drug delivery particles are biocompatible polymers and amphiphiles (surfactants and copolymers). The amphiphilic nature of surfactants or copolymers can be roughly divided into two separate categories. First, there are water soluble (polymeric) surfactants, which can be brought into solution by simply dissolving them into water, see Fig. 1.3 in the Chapter 1. Second, there are non-water soluble (polymeric) surfactants which can only be dispersed into water by special means. The nanoprecipitation technique allows to bring the latter in water where they will form colloids. During this process they undergo a transition from good to poor solvent conditions. Upon this solvent switch the polymers can form stable colloidal particles, see Fig. 1.4 in the Chapter 1. Both water soluble and non-water soluble surfactants can be used to make stable nanoparticulate suspensions of hydrophobic (co)polymers and/or active ingredients in aqueous environments.

For water soluble surfactants combined with hydrophobic polymers we tried to grasp the physics of the nanoprecipitation process into a simple theory resulting in simple analytical expressions [15] for the size dependence based on von Smoluckowski's theory [16, 17], as described in **Chapter 2**. The rapid switch from good solvent to poor solvent for the polymers results in a coalescence process which can be described by taking into account three differ-

ent time scales: mixing time, coalescence time and protection time. The end particle size is mainly dependent on the mixing time. The mixing time shows two regimes: the 'slow'- and the 'fast'-mixing regime. For the slow mixing regime the size is mainly dependent on the concentration and the viscosities of the solutions but is independent on the molar mass of the polymer. This dependency, which is linear in the polymer concentration, enables experimentalists to accurately target specific sizes. For the 'fast' mixing regime the end size is mainly dependent on the mixing time/speed, however, below a certain mixing time the size attains a plateau value and cannot be further reduced. Understanding of these two regimes enables the utilization of two approaches to generate particles of a certain desired size. First, the polymer concentration can be increased or decreased in order to obtain a desired bigger or smaller size in the 'slow' mixing regime. Second, if the polymer concentration does not permit to obtain smaller sizes the mixing time can be decreased by utilizing different techniques (e.g. using an impinging jet mixer).

The particles made with water soluble surfactants can be used in different applications where a more fine distribution, on a surface or in the bulk, plays a dominant role and where fast release is desired. For a fixed particle volume fraction small particles have a larger surface area and number density compared to big particles. This implies that the distribution of the encapsulated species is better. Especially particles which are stabilized with surfactants having a high critical micelle concentration (CMC) will exhibit a fast release. In the final application drug delivery systems are diluted to a high degree. Then the particles come into an environment where the surfactant concentration gets lower than the CMC which speeds up the release of the encapsulated compounds. Upon this dilution, below CMC, stabilizer molecules will desorb from the self-organized particles whereupon they can take along encapsulated molecules into the aqueous environment. Medical applications that require a fast release profile can benefit from this. Also for food applications (e.g. food preservatives) these systems could be useful since a better distribution will result in using less preservative while obtaining a higher efficacy. Slower release for these systems might be achieved in case of strong attractions between surfactant and encapsulated compound.

As non-water soluble surfactants we focused on triblock copolymers. These triblock copolymers were designed and synthesized in such a way that the middle block consisted of polyethylene oxide (PEO). The outer two blocks, equal in molar mass/size, were made of poly-(glycolic-co-lactic acid) (PLGA) or poly-(caprolactone) (PCL). The triblock copolymers were synthesized via the ring-opening polymerization method [18, 19]. PEO, PLGA and PCL were chosen because of their excellent biocompatibility [20–25] and vast usage in pharmaceutical applications. Rather than choosing diblock copolymers we opted for triblock copolymers. Because the (PEO) corona of these micelles is denser than the corona of diblock copolymer micelles. The higher the PEO corona density, the lower the mobility of water resulting in a slower drug release. Prolonged drug release profiles in time are more beneficial: (i) from a patient's point of view, because less treatments are needed, (ii) from an efficacy's point of view because long and preferably stable drug release profiles are often desired for better treatment results, and (iii) from an economic viewpoint because less frequent treatments and longer drug release also cut down costs.

In order to predetermine the relationship between chosen chemistry (PEO, PLGA and PCL), used molar masses and the size of the spherical micelles we employed Scheutjens-Fleer self-consistent field (SF-SCF) theory [26–29], see **Chapter 3**. In order to perform

SF-SCF computations, several important parameters are needed. First, the number of Kuhn segments and Kuhn length [30, 31] of the used (co)polymers are needed. The Kuhn segment can be found from literature data [32] and the molar mass, reflecting the polymer's chain length, then provides the number of Kuhn segments. Second, the Flory-Huggins interaction or χ-parameter [32] is needed. Although it is difficult to exactly measure this parameter it can often be rationalized from the hydrophobicity (in the case water is the poor solvent) of the polymer. It is possible to rank different polymers according to their hydrophobicity, deriving in such a way an estimated χ-parameter. Water-octanol partition coefficients and surface tension measurements can also aid in making a well-balanced educated guess for the χ-parameters. Moreover since SF-SCF calculations are fast ($10^4 - 10^5$ times faster than computer simulations) a certain interval for χ-parameters can be calculated in order to assess their influence. In this way it is possible to see which block lengths in relation to a χ-parameter range are capable of forming spherical micelles. For PEO the χ-parameter is known and for PLGA and PCL the χ-parameter can be derived from their hydrophobicity.

Chapter 3 explains in detail how SF-SCF for spherical triblock copolymer micelles is performed. We checked our theoretical predictions with experimental findings. To characterize the size we calculated the hydrodynamic diameter (D_h) from SF-SCF using Brinkman-Debye theory [33, 34] and compared this with hydrodynamic sizes measured by dynamic light scattering (DLS). We concluded from this comparison that given certain chemistry and molar masses SF-SCF can be used to design a predetermined size of spherical micelles. SF-SCF can be used as a tool to unravel the structure-function relationship between copolymer composition and micellar size and morphology [35]. Hence, SF-SCF predictions allow for more efficient experimentation. If some applications demand a specific chemistry together with a desired size, one can easily assess whether it is possible, by tuning the molar mass of the desired chemistry, to achieve this desired size by performing SF-SCF calculations.

In **Chapter 4** we studied the simultaneous tuning of size and loading. SF-SCF predictions of loading versus size were compared with experimental data revealing that SF-SCF is an excellent tool to predetermine the loading capacity of a certain copolymer composition and the influence of this loading on size. This approach enables the design of predetermined size and loading of spherical micelles. In **Chapter 4** we also checked the stability of these spherical micelle formulations in time. As expected once, hydrolytic, degradation of PLGA starts the stability of these micellar formulations only then is affected [22, 35]. Ostwald ripening [36] was not detected for these formulations indicating that the particles appear to be equilibrium structures. Our approach of loading block copolymer micelles with hydrophoic (co)polymers and/or active ingredients allowed to modify the size of polymeric nanoparticles [37].

However, these spherical micelles are not indefinitely stable in an aqueous environment. Since hydrolytically degradable (co)polymers are used, storing them in an aqueous suspensionshortens their shelf life, there is a need to find a way to prevent this. If the aqueous environment is removed (e.g. by evaporation or freeze drying) the micelles will collapse and then they are not resuspendable to their original size anymore. This collapse can be prevented by cross-linking the copolymers inside the micelles. Such an approach would demand an additional processing step after the nanoprecipitation process. This post processing step often demands the usage of cross-linking chemistry which can affect the encapsulated

cargo (by unwanted chemical reactions) and may need removal after cross-linking has been performed. Another option is to replace the aqueous environment with a hydrophilic and biocompatible (polymeric) liquid which does not promote hydrolytic degradation upon storage. Alternatively, it may be possible to perform the nanoprecipitation process in a hydrophilic (water soluble) and biocompatible polymeric melt which solidifies upon cooling. In the solid polymer matrix the micelles get embedded which may provide a solution for long term storage. This solid matrix can afterwards be turned into a powder, by e.g. milling, which reduces the solubility time and suspension of the micelles prior to application.

Besides using SF-SCF to study passive targeting micelles, by tuning size and loading, it can also be used to study active targeting by analyzing a targeting moiety (TM) into the micelles and study the possibility of linkage with the receptor (R). This is the subject of **Chapter 5**. Diblock copolymers with a targeting end group (targeting moiety), targeting diblock copolymers, were added to triblock copolymer based micelles. A theoretical study was performed using SF-SCF in which a micelle composed of mixed di- and triblock copolymers was brought closer to a surface with a receptor. From the SF-SCF calculations a maximum interaction distance could be derived. This defines the range over which a targeting moiety can jump to the receptor. The maximum interaction distance is the largest distance between micellar surface and receptor for which TM-R contacts are possible. TM-R contact is only possible after crossing an energy barrier. Interaction energies less than $< 3kT$ are considered to be spontaneous, enabling targeting moiety-receptor interaction. In general these targeting moieties are attached to the micelles after the formation of the micelles which implies that the reactants need to be removed from the system. We envision using the nanoprecipitation method to prepare these micelles to omit this post-processing step and incorporate the targeting diblock copolymers within the micelle upon nanoprecipitaion.

Since the synthesis of these targeting diblock copolymers is complicated and expensive, we strived to come to an optimized design using as little of these targeting diblock copolymers as possible, while maintaining targeting moiety receptor interaction. The optimized design takes into account the relevant interaction parameters of the whole system. In addition, we varied the lengths of the hydrophilic PEO block of the targeting diblock copolymer in order to assess the possibility that even when the targeting moiety is hidden within the micellar corona targeting moiety receptor interaction could still be achieved. Hiding the targeting moiety within the micellar corona, which is regarded as stealthy, may be beneficial in avoiding undesired immune responses possibly evoked by the targeting moiety. Our theoretical SF-SCF calculations show that it is indeed possible for a targeting moiety hidden within the micellar corona to maintain its receptor interaction. Another benefit of using short targeting diblock copolymers is that the solubility for copolymers having a smaller hydrophilic block is lower. This is beneficial for micellar stability and for the release of encapsulated compounds.

In **Chapter 3, 4 and 5** we used SF-SCF computations. The main advantages of performing SF-SCF calculations are: (i) they are faster than other computer based simulations (order of magnitude 10^4 to 10^5), (ii) before starting synthesis of copolymer surfactants one can calculate the desired polymer architecture for a desired chemistry in order to obtain desired size and loading, (iii) targeting moiety recpetor interactions can be modeled giving insight in maximum interaction distance and required interaction energy, (iv) it is a valuble toolbox for

the design of passive and active targeting micelles. The main disadvantage of SF-SCF is that for some desired chemistry the needed input parameters are not readily available. They have to be estimated, experimentally determined or calculated, which can be difficult.

In this last paragraph we would like to propose suggestions for future investigations as a follow-up of the research described in this thesis. The ability to design the proper polymers using theory for passive and active targeting offers a flexible toolbox to develop drug delivery applications. However, once an application is designed at a desired size, loading and envisioned receptor target, it needs to be assessed for its performance.

First, the micelles containing a targeting moiety should be experimentally made and characterized. The functionality of micelles with a targeting moiety can be studied using an animal study. There are mouse models which allow to monitor the accumulation of particles within tumor tissue due to the enhanced permeation and retention (EPR) effect for passive targeting. The EPR test will allow to practically confirm which micellar size(s) or size ranges result in an improved performance/higher accumulation of micelles in the tumor tissue without using the targeting moieties. Since tuning size and loading is easily performed utilizing SF-SCF one may find an optimal system using as little as possible of the active agents and enabling improved release profiles resulting in a more efficient, less repetitive medical treatment.

Second, the active targeting capabilities need to be confirmed in practice. *In vitro* cell testing can be performed revealing when an improved efficiency due to active targeting is achieved or not. One could easily compare similar sized micelles without targeting moieties, and with targeting moieties, both beyond and within the micellar corona. Adding these three systems to a cell culture which has an expressed receptor on the cellular surface can reveal the efficiencies of the systems after the cells are separated (by washing for instance) from non-bound micelles. An encapsulated fluorescent dye will quickly reveal the differences in active targeting capabilities by using different visualization techniques.

Thirdly, it is useful to study the maximum interaction distance. To validate the maximum interaction distance it is possible to deposit receptors at a surface surrounded by brushes which hold the micelles from the receptor at a distance larger, equal and smaller than the (modeled) maximum interaction distance resulting in a practical maximum interaction distance. In a biological system it might not be possible for a micelle to approach its target closer than a maximum interaction distance. It can very well be that other species present on a cellular surface (e.g. sugar chains; the so called polysaccharide trees or other molecules), by steric hindrance, depletion, repulsion or other reasons prevent the micelle to come close enough to the receptor to establish a bond. Therefore the practical maximum interaction distances still need to be assessed in a cell culture taking into account that the (biological) maximum interaction distance in a biological system might be smaller than the practical and modeled results.

Finally, it needs to be tested that hiding the targeting moieties within the stealthy micellar PEO corona will avoid immune response. The targeting moiety should be replaced with a known immunogen/antigen and exposed to a cell culture which contains immune cells for this specific antigen. The absence or presence of the antibodies, detected by appropiate techniques, for the specific antigen reveals whether immune response is avoided or not.

We envision that if all above mentioned tests give positive results one could tailor make micellar based active and passive targeting drug delivery applications for cancer treatments.

Since the detection of cancer is difficult in early stages, due to the small tumor sizes or wide distribution of tumor cells (metastasis) throughout the body, these passive and active targeting micelles could offer a solution. Due to their high efficiency they can be administered in low quantities and accumulate in high concentrations in the specific tumor tissue. Ultimately, they might even be used as preventive treatments for cancer, just like vaccination for flue.

Bibliography

[1] T. Niwa, H. Takeuchi, T. Hino, N. Kunou and Y. Kawashima, J. Control. Release, **25**, 89-98 (1993).
[2] H. Fessi, F. Puisieux, J.Ph. Devissaguet, N. Ammoury and S. Benita, Int. J. Pharm., **55**, R1-R4 (1989).
[3] J. Molpeceres, M. Guzman, M.R. Aberturas, M. Chacon and Y. Kawashima, J. Control. Release, **85**, 206-213 (1996).
[4] H. Lannibois, A. Hasmy, R. Botet, O.A. Chariol and B. Cabane, J. Phys. II France, **7**, 318-342 (1997).
[5] J. Aubry, F. Ganachaud, J.-P. Cohen Addad and B. Cabane, Langmuir, **25**, 1970-1979 (2009).
[6] K. Roger, R. Botet and B. Cabane, Langmuir, **29**, 5689-5700 (2013).
[7] T. Chen, A.-P. Hynninen, R.K. Prud'homme, I.G. Kevrekidis, and A.Z. Panagiotopoulos, J. Phys. Chem. B, **112**, 16357-16366 (2008).
[8] J.C. Cheng and R.O. Fox, Ind. Eng. Chem. Res., **49**, 10651-10662 (2010).
[9] L.H. Reddy, J. Pharm. Pharmacol., **57**, 1231-1242 (2005).
[10] H. Maeda, J. Wu, T. Sawa, Y. Matsumura and K. Hori, J. Control. Release, **65**, 271-284 (2000).
[11] H. Maeda and Y. Matsumura, Crit. Rev. Ther. Drug, **6**, 193-210 (1989).
[12] H. Maeda and J. Fang, Adv. Polym. Sci., **193**, 103-121 (2006).
[13] H. Maeda and J. Daruwalla, Eur. J. Pharm. Biopharm., **71**, 409-419 (2009).
[14] N. Kamaly, Z. Xiao, P.M. Valencia, A.F. Radovc-Moreno and O.C. Farokhzad, Chem. Soc. Rev., **41**, 2971-3010 (2012).
[15] R. Stepanyan, J.G.J.L. Lebouille, J.J.M. Slot, R. Tuinier and M.A. Cohen Stuart, Phys. Rev. Lett., **109**, 138301 (2012).
[16] M.v. Smoluchowski, Kolloid, **18**, 48-54 (1916).
[17] M.v. Smoluchowski, Kolloid, **21**, 98-104 (1917).
[18] S. Chen, R. Pieper, D.C. Webster and J. Singh, Int. J. Pharm., **288**, 207-218 (2005).
[19] G.M. Zentner, J. Control. Release, **1**, 203-215 (2001).
[20] R. Webster, E. Didier, P. Harris, N. Siegel, J. Stadler, L. Tilbury and D. Smith, Drug Metab. Dispos., **35**, 9-16 (2007).
[21] K. Knop, R. Hoogenboom, D. Fisher and U.S. Schubert, Angew. Chem. Int. Edit., **49**, 6288-6308 (2010).
[22] R. Peters, J.G.J.L. Lebouille, B. Plum, P. Schoenmakers and S. van de Wal, Pol. Degrad. Stabil., **96**, 1589-1601 (2011).
[23] A. Sodergard and M. Stolt, Prog. Polym. Sci., **27**, 1123-1163 (2002).
[24] T. Nie, Y. Zhao, Z. Xie and C. Wu Macromolecules, **36**, 8825-8829 (2003).
[25] Y. Hu, L. Zhang, Y. Cao, H. Ge, X. Jiang and C. Yang, Biomacromolecules, **5**, 1756-1762 (2004).
[26] P.N. Hurter, J.M.H.M. Scheutjens and T.A. Hatton, Macromolecules, **26**, 5592-5601 (1993).
[27] J.M.H.M. Scheutjens and G.J. Fleer, J. Phys. Chem., **83**, 1619-1635 (1979).
[28] J.M.H.M. Scheutjens and G.J. Fleer, J. Phys. Chem., **84**, 178-190 (1980).
[29] G.J. Fleer, M.A. Cohen Stuart, J.M.H.M. Scheutjens, T. Cosgrove, and B. Vincent, *Polymers at Interfaces* (Chapman and Hall, London, first edition, 1993).

[30] P.J. Flory, *Principles of Polymer Chemistry* (Cornell University Press, Ithaca, New York, 1953).
[31] B. Vincent, Colloids and Surfaces, **50**, 241-249 (1990).
[32] J. Brandrup, E.H. Immergut, E.A. Grulke, A. Abe and D.R. Bloch, *Polymer Handbook* (John Wiley and Sons,4th Edition, 2005).
[33] M.A. Cohen Stuart, F.H.W.H. Waaijen, T. Cosgrove, B. Vincent and T.L. Crowley, Macromolecules, **17**, 1825-1830 (1984).
[34] J.M.H.M Scheutjens, G.J. Fleer and M.A. Cohen Stuart, Colloids and Surfaces, **21**, 285-306 (1986).
[35] J.G.J.L. Lebouille, R. Tuinier, L.F.W. Vleugels, M.A. Cohen Stuart and F.A.M. Leermakers, Soft Matter, **9**, 7515-7525 (2013).
[36] Y. Liu, K. Kathan, W. Saad and R.K. Prud'homme, Phys. Rev. Lett., **98**, 036102 (2007).
[37] J.G.J.L. Lebouille, L.F.W. Vleugels, A. Dias, F.A.M. Leermakers, M.A. Cohen Stuart and R. Tuinier, Eur. Phys. J. E, **36**, 107 (2013).

Summary

Many active ingredients like drugs, preservatives and vitamins are hydrophobic. In most applications for food and pharma, however, they need to be functional in aqueous environments. In order to facilitate their usage in aqueous environments one needs a way to enable the dispersion of hydrophobic compounds into submicron particles in water in a controlled manner. We investigated the stabilization by surfactants and encapsulation into micelles of hydrophobic compounds using the nanoprecipitation method. The research described in this thesis is about building more understanding of the nanoprecipitation method in relation to the relevant physical chemical parameters. The theoretical results led to predictions that were compared to experimental data. For water-soluble surfactants as stabilizers in the nanoprecipitation process a new theory was developed to relate the process parameters to the final particle size. For non-water-soluble surfactants self-consistent field theory was used in order to unravel the structure-function relationship between used copolymer chemistry and the form and morphology of the obtained particles, spherical micelles and their size.

In Chapter 2 we analyzed new and existing experiments on the nanoprecipitation method using water-soluble surfactants as stabilizers in a systematic manner. These were interpreted in terms of a new theory that links the process and material properties to the final particle size. The nanoprecipitation procedure consists of quenching a polymer solution from a good to a poor solvent containing surfactant solution. Three characteristic time scales can be identified which affect the final particle size, see Fig. 1. First, the mixing time (τ_{mix}) was identified; the time needed to mix the polymer solution (polymer in good solvent) into the surfactant solution (poor solvent). Second, the coalescence time (τ_{cls}) was identified; the time needed for the collapsed polymer chains to coalesce into bigger droplets and subsequently to harden out into particles with long term storage stability. Last, the protection time (τ_{pro}) was identified; the time that the surfactant molecules need to completely cover the coalescing droplets and by this stop the coalescence of the collapsed polymer chains/droplets. The two latter characteristic times are intrinsic properties of the used solvents, surfactants and polymers and cannot be changed without addition of extra/new molecules. However, the mixing time is the only parameter which can be changed without modifying the material properties of the system. The mixing time can be easily varied by the method of mixing the good and the poor solvent. Using a pipette to mix the two solutions will result in a 'slow' mixing time regime and utilizing for instance an impingent jet mixer can result in a 'fast' mixing regime. For both mixing regimes a clear analytical expression could be derived enabling more efficient experimentation in order to obtain a specific final particle size. For the 'slow' mixing regime the relation between final particle size (R_p^{end}) was found

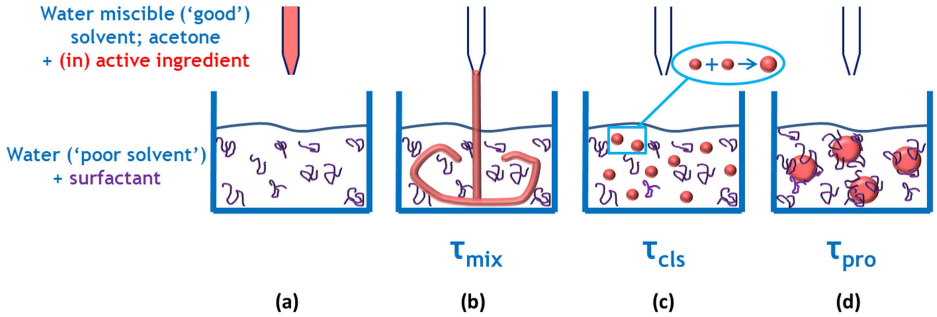

Figure 1: Different stages of a nanoprecipitation experiment: (a) typically 1 mL of a 10 mg/mL of polymer solution in good solvent is added to 10 mL of 1 wt% surfactant solution in water; (b) the macroscopic mixing step; (c) the initial state of the system considered: polymer spheres are homogeneously distributed within the experimental volume; (d) end of the experiment: polymer spheres have coalesced until a protective layer of surfactant protects the individual spheres against coalescence.

only to be dependent of the used polymer concentration (c_{mp}) as $R_p^{\text{end}} \sim c_{mp}$. The practical interpretation of this analytical expression is rather simple; an eight times higher polymer concentration will result in a two times bigger final particle size. For the 'fast' mixing regime the analytical expression can be interpreted also in an easy way; the faster the mixing the smaller the final particle size. Below a certain value for the mixing time the final particle size attains a plateau value; even faster mixing will not further decrease the final particle size. When using water-soluble surfactants the release of the cargo, which in practice often takes place after significant dilution, is expected to be fast. In order to increase the release of the encapsulated compound(s) in time we incorporated the surfactant functionality into a non-water soluble triblock copolymer (in Chapter 3 and 4). This results, even upon huge dilution, in an extended release profile in time.

In Chapter 3 we employed self-consistent field theory for non-water-soluble surfactants in order to relate the (block copolymer) surfactant chemistry to the size and composition of the resulting spherical equilibrium micelles. The surfactants, triblock copolymers synthesized via ring-opening polymerization, were employed in the nanoprecipitation process in order to make spherical micelles, see Fig. 2. The theoretical predictions were compared to the experimental results and it was concluded that self-consistent field theory is an accurate theoretical tool to predict the size of spherical micelles given a certain chemistry and composition of the copolymers and the conditions required to form these micelles.

In Chapter 4 we experimentally studied whether hydrophobic compounds (polymers, different active ingredients or a mixture of the two) were added in order to verify whether these spherical micelles could be loaded by these compounds. We investigated the encapsulation behavior of these micelles for hydrophobic compounds both theoretically and experimentally and considered the influence of the size for the micelles. From both the

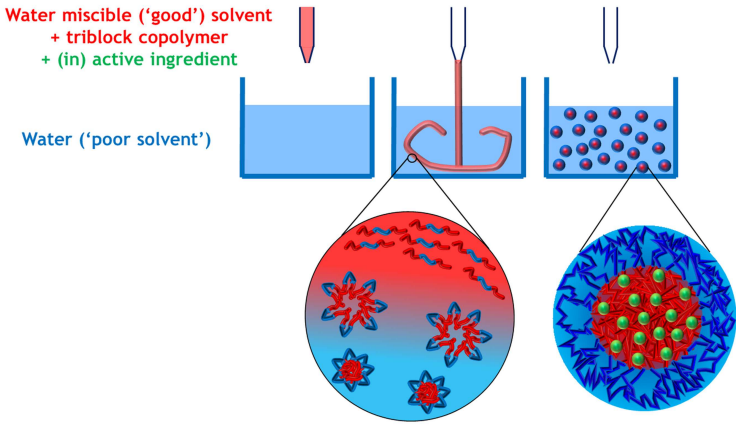

Figure 2: Cartoon of the nanoprecipitation process for triblock copolymer micelles. Typically 0.4 mL of a 45 mg/mL of copolymer solution in good solvent is added to 10 mL water. Upon this mixing the copolymer shifts from a good solvent to a poor solvent evoking the formation of micelles. If an (in)active ingredient (which is hydrophobic) is added together with the copolymer to the good solvent it accumulates upon solvent switch within the hydrophobic micellar core resulting in micelles encapsulating the (in)active ingredient.

theoretical predictions and the experimentally obtained data it followed that these micelles can be used for encapsulation of hydrophobic compounds. Moreover, the theoretical predictions matched with the experimentally obtained data. It was concluded that self-consistent field predictions can be used to predict the size and stability of spherical micelles with encapsulated hydrophobic compounds.

Tuning size and loading is mandatory for passive targeting applications because the particle size mainly determines the biologic faith. In order to enable active targeting, utilizing a targeting moiety and (specific) receptor interaction is needed while maintaining the stealthy nature of the spherical particles developed in Chapter 3 and 4. In Chapter 5 we performed a theoretical self-consistent field study on spherical block copolymer micelles to investigate whether it is feasible to hide the targeting moiety within the micellar corona while maintaining receptor interaction. We determined the maximum interaction distance wherefrom targeting moiety receptor connection can be established and the required energy barrier at different distances. The outcome of these calculations was used to design a (theoretical) optimized system for active targeting.

We used self-consistent field theory to calculate the size, loading and targeting capability of triblock copolymer based micelles enabling both passive and active targeting and verified our calculation results experimentally. Although the active targeting predictions were not verified experimentally we established a design for passive and active targeting micellar applications for, for instance, drug delivery applications while maintaining the stealthy nature of these micelles.

Samenvatting

Actieve ingrediënten zoals medicijnen, conserveermiddelen en vitaminen zijn vaak onoplosbaar in water. In de meeste toepassingen voor voeding en farmacologie is het echter nuttig wanneer zulke ingrediënten fijn verdeeld worden in een waterige omgeving. Om hun gebruik in een waterige omgeving te vergemakkelijken is er een manier nodig om deze ingrediënten op een gecontroleerde manier te dispergeren in water. In dit proefschrift staat onderzoek beschreven naar de stabilisatie door middel van oppervlakteactieve stoffen en de incapsulatie in micellen (deeltjes bestaande uit oppervlakteactieve stoffen). Deze stabilisatie en incapsulatie van niet-wateroplosbare stoffen werd gerealiseerd door gebruik te maken van de nanoprecipitatie methode.

Het onderzoek beschreven in dit proefschrift handelt over het begrip van de nanoprecipitatie methode in relatie tot de relevante fysisch-chemische parameters. De theoretische begripsvorming werd aan de hand van experimentele data getoetst. Om in staat te zijn deeltjes met een *a priori* gewenste uiteindelijke grootte te maken met wateroplosbare oppervlakteactieve stoffen werden verschillende parameters gecombineerd tot een elegante begrijpelijke analytische uitdrukking in hoofdstuk 2. Tijdens de nanoprecipitatie methode worden, in aanwezigheid van oppervlakte actieve stoffen, polymeren van een goed oplosmiddel naar een slecht oplosmiddel gebracht. Bij deze overgang van goed naar slecht oplosmiddel werden drie verschillende tijdsschalen geïdentificeerd, zie Fig. 1. De grootte van deze drie tijdsschalen bepalen de uiteindelijke deeltjesgrootte. Als eerste werd de mengtijd geïdentificeerd; de tijd die nodig is om de polymeeroplossing (polymeer in goed oplosmiddel) te mengen met de oplossing van de oppervlakteactieve stof (slecht oplosmiddel). De tweede tijdschaal is de coalescentietijd; de tijd die de gekrompen polymeerketens nodig hebben om zich samen te voegen tot grotere polymeerdruppeltjes om vervolgens uit te harden tot deeltjes met een lange opslag stabiliteit. Als laatste werd de beschermingstijd geïdentificeerd; de tijd die oppervlakteactieve stof moleculen nodig hebben om het hele oppervlak van de polymeerdruppels te bedekken waardoor het coalesceren van de polymeerdruppels tot een einde komt. De twee laatstgenoemde tijden zijn intrinsieke eigenschappen van de gebruikte chemie (oplosmiddel, polymeer en oppervlakteactieve stof) en kan niet worden veranderd zonder toevoeging van extra of nieuwe moleculen. De mengtijd daarentegen is de enige parameter die veranderd kan worden zonder enige verandering van de materiaaleigenschappen. De mengtijd kan eenvoudig worden veranderd door een andere mengmethode te gebruiken. Gebruik van een pipet om de twee oplossingen te mengen zal resulteren in een langzaam mengregime. Door een speciaal mengapparaat te gebruiken kan de mengsnelheid worden gevarieerd. Voor beide mengregimes (langzaam en

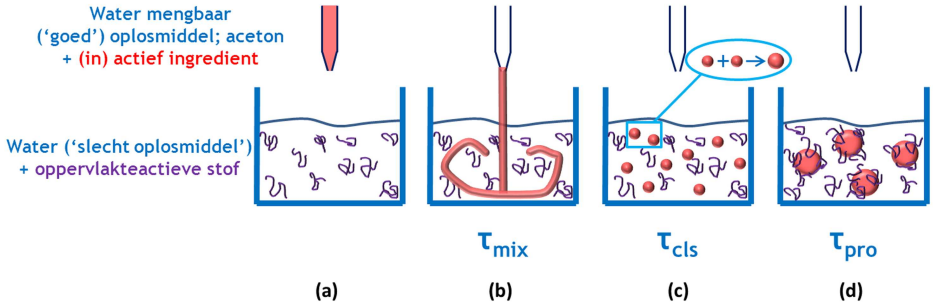

Figuur 1: Verschillende stadia van een nanoprecipitatie experiment: (a) gewoonlijk wordt 1 mL van een 10 mg/mL polymeeroplossing ('goed' oplosmiddel) bij 10 mL van een 1 gew% (gewichtsprocent) oppervlakteactieve stof oplossing toegevoegd ('slecht' oplosmiddel); (b) de macroscopische meng stap; (c) de initiële staat van het systeem beschouwd: polymeerdruppels zijn homogeen verdeeld in het experimentele volume; (d) einde van het experiment: polymeerdruppels zijn gecoalesceerd totdat het gehele oppervlak bedekt is met een beschermende laag van oppervlakteactieve stoffen die de individuele druppels beschermd tegen verdere coalescentie.

snel) kon een analytische uitdrukking afgeleid worden. De analytische vergelijkingen stellen experimentatoren in staat om efficiëntere experimenten uit te voeren met als doel om deeltjes met een specifieke uiteindelijke deeltjesgrootte te maken. Voor het langzame mengregime werd gevonden dat de (uiteindelijke) grootte deeltjesgrootte (R_p^{end}) enkel afhankelijk is van de gebruikte polymeer concentratie (c_{mp}) in het goede oplosmiddel $R_p^{\text{end}} \sim c_{mp}$. De praktische interpretatie van de analytische uitdrukking is vrij simpel; een acht keer hogere polymeer concentratie resulteert in een twee keer grotere deeltjesgrootte. Voor het snelle mengregime kan de analytische uitdrukking ook op een simpele manier geïnterpreteerd worden; sneller mengen leidt tot kleinere deeltjes. Onder een bepaalde mengsnelheid bereikt de deeltjesgrootte een plateau waarde; sneller mengen zal de deeltjesgrootte niet meer beïnvloeden. Wanneer wateroplosbare oppervlakteactieve stoffen gebruikt worden om niet-wateroplosbare stoffen (actieve ingrediënten) te incapsuleren wordt verwacht dat het vrijkomen van deze stoffen snel is. om dit vrijkomen te vertragen is de oppervlakteactieve functie geïncorporeerd in niet-wateroplosbare triblok copolymeren. Dit resulteert, zelf tijdens significant verdunnen, in een vertraagd vrijkomen van de actieve ingrediënten. Voor wateroplosbare oppervlakteactieve stoffen werd een nieuwe theorie ontwikkeld om het verband tussen proces parameters en de deeltjesgrootte te kunnen begrijpen.

In hoofdstuk 3 werd voor niet-wateroplosbare oppervlakteactieve stoffen, de reeds bestaande, Scheutjens-Fleer zelf consistente veld theorie (SF-SCF; Scheutjens-Fleer self-consistent field) gebruikt. De SF-SCF theorie maakte het mogelijk om de structuur-functie relatie tussen de gebruikte blok copolymeer (oppervlakteactieve stof) chemie en de vorm, morfologie en grootte van de verkregen deeltjes, bolvormige micellen, te ontrafelen.
Voor niet-wateroplosbare oppervlakteactieve stoffen werd SF-SCF theorie gebruikt om een relatie te verkrijgen tussen (blok copolymeer) oppervlakteactieve stof chemie, fysische kenmerken en de grootte van de bolvormige micellen. De oppervlakteactieve stoffen,

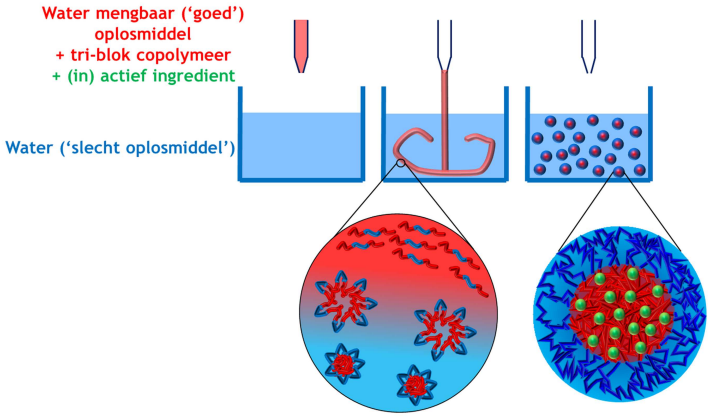

Figuur 2: Voorstelling van het nanoprecipitatie proces voor micellen gemaakt van tri-blok copolymeren. Gebruikelijk wordt 0.4 mL van een 45 mg/mL copolymeer oplossing, in goed oplosmiddel, toegevoegd aan 10 mL water, slecht oplosmiddel. Tijdens het mengen van beide oplossingen ondergaat het copolymeer een overgang van goed naar slecht oplosmiddel wat de vorming van micellen veroorzaakt. Indien een (in)actief ingrediënt (dat niet wateroplosbaar is) wordt toegevoegd bij het copolymeer in het goede oplosmiddel dan zal het zich tijdens de overgang van goed naar slecht oplosmiddel ophopen in de niet-wateroplosbare kern van de micel. Dit resulteert in de incapsulatie van de (in)actieve ingrediënten in de micel.

tri-blok copolymeer gesynthetiseerd via ring-opening polymerisatie, werden toegepast in de nanoprecipitatie methode om bolvormige micellen mee te maken, zie Fig. 2. De theoretische SF-SCF voorspellingen werden vergeleken met de experimentele resultaten. Hieruit bleek dat SF-SCF een nauwkeurige theoretische methode is om de grootte van bolvormige micellen te voorspellen met een gegeven compositie van de blok copolymeren om deze micellen te vormen.

In hoofdstuk 4 werden vervolgens, niet-wateroplosbare stoffen (polymeren, verschillende actieve ingrediënten of een combinatie ervan), toegevoegd om te controleren of deze bolvormige micellen geladen konden worden met deze niet-wateroplosbare stoffen. Wij bestudeerden het incapsulatie gedrag van deze micellen voor niet-wateroplosbare stoffen zowel theoretisch als experimenteel en onderzochten de invloed op de grootte voor deze micellen. Uit zowel de SF-SCF voorspellingen als de experimentele data volgde dat deze micellen gebruikt kunnen worden voor de incapsulatie van niet-wateroplosbare stoffen en dat deeltjes kunnen worden gemaakt van elke gewenste grootte tussen enkele nanometers en een paar honderd nanometer. Bovendien kwamen de SF-SCF voorspellingen overeen met de experimenteel verkregen data.

De grootte van de deeltjes is van groot belang aangezien dit bepalend is voor hun biologische ”bestemming”. Indien micellen een bepaalde grootte hebben zijn ze in staat om zich op te hopen in specifieke weefsels (bijvoorbeeld tumor weefsels). Dit leidt tot

passief behandelen van (ziek) weefsel. Indien gebruik wordt gemaakt van moleculen die een interactie/binding aangaan met specifieke aangrijpingspunten, bijvoorbeeld receptoren op een cel, dan wordt van actief richten gesproken. Om actief richten mogelijk te maken voor micellen moeten aan de micel 'richt'-moleculen gekoppeld worden die het mogelijk maken om met receptoren een binding aan te gaan. In hoofdstuk 5 is theoretisch bestudeerd of micellen gemaakt kunnen worden die zich actief op bepaalde receptoren kunnen richten. De uitkomst van deze berekeningen laat zien dat het mogelijk is om deze 'richt'-moleculen in een micel te verstoppen terwijl ze toch nog kunnen binden met de recpetor als de micel in de buurt komt. Deze resultaten werden gebruikt om een optimaal systeem te ontwerpen om tot actieve micellen te komen.

Wij gebruikten SF-SCF berekeningen om de grootte, incapsulatie van niet-wateroplosbare ingrediënten en het actief richtvermogen van micellen, gebaseerd op tri-blok copolymeren, te voorspellen. Voor passieve micellen werden de berekeningen experimenteel bevestigd. Hoewel het actief richtvermogen van de micellen niet experimenteel werd onderzocht zou het mogelijk moeten zijn om voor farmaceutische toepassingen micellen te ontwerpen die zowel passief en actief gericht kunnen worden op specifiek weefsel.

Educational activities

Overview of completed training activities:

Discipline specific activities:

Courses:

- PRA radiation curing course (London); 2008.
- Surfaces: Interaction forces and engineering (COST school; TU Delft); 2010.
- International Granulation Workshop (University of Sheffield); 2011.
- Optimization in emulsion technology using SAD approach (DSM; Geleen); 2011.
- Surfactants and polymers in aqueous solution (MPI; Potsdam/Golm); 2011.
- Emulsions-formulation and properties (YKI; Stockholm) 2012.
- Colloids and medical applications (Sofia University; Sofia); 2013.

Congresses and conferences:

- European Colloid and Interface Society (ECIS) conference (Berlin); 2011.
- Nanoformulation (Barcelona); 2012.
- European Colloid and Interface Society (ECIS) conference (Malmö); 2012.
- Jülich soft matter days (Bad Honnef); 2012.
- European Colloid and Interface Society (ECIS) conference (Sofia); 2013.

Presentations and posters:

- World Biomaterial Congress (Amsterdam), poster; 2008.
- European Colloid and Interface Society (ECIS) conference (Malmö), poster; 2012.
- Jülich Soft Matter days, poster; 2012.
- DSM Advanced Chemical Engineering Solutions Symposium, presentation; 2012.

- DSM Process Technology Symposium, poster; 2012.
- European Colloid and Interface Society (ECIS) conference (Sofia), presentation; 2013.

General courses:

- Basic Intellectual Property course; Patents, trade marks and trade secrets; 2010.
- Design of experiments (DSM; Geleen); 2010.
- Advanced Intellectual Property course; 2011.
- Dupont safety course (DSM; Geleen); 2012.
- Basic safety course level 1 and 2 (DSM; Geleen); 2010-2013.
- Code of business conduct; 2013.
- DSM life saving rules; 2013.
- Document classification; 2013.

Optional courses and activities:

- Preparation of project proposal; 2010.
- Biweekly Biomedical drug delivery meeting (DSM; Geleen); 2010-2011.
- Biweekly C&I meeting (DSM; Geleen); 2010-2014.
- Biweekly particle technology meeting (DSM; Geleen); 2011-2014.
- DSM Advanced Chemical Engineering Solutions colloqia; 2011-2014.
- DSM Process Technology symposium; 2012.
- DSM Advanced Chemical Engineering Solutions Symposium; 2012.

Acknowledgements

In my educational, professional and private life I was lucky to meet many chimneys, people who kept my fire (passion) burning, for chemistry, technology, science overall and daily life. A lot of people have given me a great deal of their time, patience, professional and personal help. These people triggered me to get more out myself and other people. I am extremely grateful for the time they invested in me.

I would like to thank Martien Cohen Stuart and Frans Leermakers for accepting me in Wageningen and giving me the opportunity to accept me as your Ph.D. student. Without your supervision, scientific support, stimulating discussions and ideas I would never have been able to finish my research and thesis. Every visit to Wageningen, the Physical Chemistry and Colloid Science group, was always something to look forward to. I am enormously proud to have you as my promoters; thanks for all the time that I could spend with you.

Remco Tuinier, I owe you a lot of gratitude, your guidance was impeccable. I enjoyed our interaction enormously and wish it will never end. I learned a lot from you and hope that I still can keep on learning from you. I am extremely proud that you are my promoter, your first Ph.D. student but certainly many others will follow. You taught me to do things according to two triples: Triple M: Model, Make and Measure; the basis of this thesis, in the beginning you modeled, I made and we measured. Triple P: do things with Passion, Persistence and Pleasure. You taught me to focus and finish, which was hard for me because many ideas and little time asks to prioritize; focus and finish. Our visits to the ECIS and other conferences are truly unforgettable, you gave me the opportunity to meet many inspiring people. Your passion, scientific knowledge and your didactic skills are without any limit. I also hope our friendship will continue for a long time no matter how much distance is between us. Thank you for letting me be your ”padawan”, which I will remain to be until I truly master ”the force”!

I am indebted to DSM for allowing and supporting me to do my Ph.D. research in Geleen and Wageningen. I especially like to thank Jos Put and Marcel Wubbolts (former and current CTO of DSM) for their personal approval and support of doing my Ph.D. in Wageningen. I would also like to thank the managing board of DSM whom succeeded to create a company where it is possible to do this. A special thanks to Aylvin Dias and Remco Tuinier who were crucial in starting this Ph.D., you are great initiators. I thank the management of DSM Biomedical, Marc Hendriks, and DSM ChemTech R&D, Peter Jansens, Jeroen Kluytmans, Jan Geerts and Rob Geertman, for the support and trust.

There are many DSM colleagues to thank. Ron Peters: next to your daily job at DSM you succeeded in obtaining a Ph.D. which inspired me to do the same. Pascale Vandevijver you challenged our micelle idea in such a way that you enabled to write a patent with a strong composition of matter parameter. Your support was essential for writing the patent. Also your interest in my progress and the chats we had were always extremely stimulating for me, thanks. Roman Stepanyan and Han Slot, you amazed me by your ability to transform findings in experiments/experimental data to comprehensive elegant physical formulas. Bart Plum and Mark Boerakker both of you introduced me within the DSM research environment. All DSM Biomedical (Drug Delivery and Medical coatings) colleagues thank you for your support, interest and pleasant work environment. Nina Woike, thanks for your excellent support in the DSM Biomedical project which initiated this research and thesis.
Thanks to all my DSM ACES colleagues for your genuine interest in the subject, progress and support. I would like to mention and thank three ACES colleagues in particular: Patrick Wenmakers, for his LateX support, Feng Li, for his assistance with eps files and Jan Oversier, for being a comprehensive, listening and pleasant office mate. Of course a big thanks to the C&I group where I could discuss all aspects of the research performed resulting in this thesis.

My two paranymphs: Tessa Kockelkoren and Leo Vleugels, our early collaboration on this subject was crucial for this thesis. Tessa your synthesis skills enabled making the triblock copolymers used for micellar suspensions described in this thesis which were the foundation of all the research that followed. Leo your creativity, measurement support and introduction to Remco Tuinier made the circle round. Both of you had an enormous catalytic effect on the chain of events yet to be started for me; my research and thesis, thank you!

I acknowledge Josie Zeevat for all the support at Wageningen University, you made a key contribution by helping me filling out the right forms at the right time. Also Marielle Keulen and Misha Schepers, the ACES support office, thank you for assisting me with planning my conference visits, enrolment in trainings and courses, you truly supported me in getting things arranged in a fast and pleasant way.

Magda van Montfort, thank you for your guidance and patience in my early life, in my opinion essential for the rest of my life.

Ms. Timmermans, Kees and Van Assche, you kept me going doing my B.Sc. in chemistry, always answering my questions, challenging me sharing your passion for chemistry and science, you are really inspirational and really teach!

Chris and Annie, beloved parents in law and family in law, Kevin en Elke, a special thanks to you when Ilse had to cope with things herself, your help was more than welcome and gave me a piece of mind to do what I needed and wanted to do.

Francine and Teun, my sister and godchild, Jean-Louis and George(ke), my two brothers, you were always able to get my mind of things so that I was able to relax and reload my batteries in a nice familiar environment. Also your help, at home and with the kids, was well

appreciated! I enjoyed our childhood and admire you for the talents I lack, I still learn a lot from you and I always enjoy our get togethers.

My parents, thank you for letting me make my own choices, your support and love. You needed a lot of patience with me, thank you for that. You always stimulated my curiosity, challenged my stubbornness and encouraged me to develop myself which I consider to be essential for scientific research and life. You laid the first stones for the person I am today, something I can only (try to) learn from now that I am raising my own children. To you I also dedicate this thesis.

The three people that always supported me in good and bad times to you I dedicate this work. Lyzl and Lien, my precious two girls, the time I spent with you the past years was less than I wanted, however, I made sure it was well spent. The time we had and have together is always of intense quality, pleasure and love, let us do this for many years to come! I hope for the two of you that in the future you can do what you are both good at and what you love to do. This will enable you, no matter what, to truly enjoy your lives.
Ilse the love of my life, without you I was certainly not able to bring this to a good end as for many things the past 15 years. You supported, stimulated and inspired me constantly to pursue what I (you will say we) wanted, knowing very well that our time spent together decreased and that you had to cope with certain things yourself. Especially in difficult periods you were able to get me back on track. The sacrifices you made are amazing, I am forever grateful to you. You were able to handle me at my worst, so you deserve me at my best. If you consider this as my achievement it is actually all yours, thanks a lot my love!

Jérôme G.J.L. Lebouille

May 2014